THESIS

Three Dimensional Cell Culture Using Nanopillar Plate

Ryosuke Takahashi

Publication list

This thesis is based on the following publications.

R. Takahashi, H. Sonoda, Y. Tabata, A. Hisada.
"Formation of hepatocyte spheroids with structural polarity and functional bile canaliculi using nanopillar sheets."
Tissue Eng. Part A., 16:1983 (2010).
doi: 10.1089/ten.tea.2009.0662

R. Takahashi, H. Sonoda, A. Hisada.
"Higher Expressions of Cytochrome P450, UDP-Glucuronosyltransferase, and Transporter Genes in Nanopillar-Cultured Rat Hepatocyte Spheroids"
Journal of Drug Metabolism and Toxicology, 4: article number 146 (p pages) (2013)
doi: 10.4172/2157-7609.1000146

R. Takahashi, Y. Zhou, Y. Horiguchi, H. Shiku, H. Sonoda, N. Itabashi, J. Yamamoto, T. Saito, T. Matsue, A. Hisada
"Noninvasively measuring respiratory activity of rat primary hepatocyte spheroids by scanning electrochemical microscopy"
Journal of Bioscience and Bioengineering, in press (2013)

Abstract

In the course of drug development today, whole animals are used to evaluate drug metabolism and toxicity in preclinical stages. However, studies using animals are not always successful in predicting the metabolic fates of drug candidates in the human body. In recent years, only a small fraction (~11%) of drug candidates that were selected for clinical trials has reached markets. It is hoped that alternative assay models using human cells *in vitro* will be better able to predict *in vivo* pharmacokinetics and help reduce this high attrition rate. Cells in such models must maintain their differentiated functions and viability, and, hence, cell culture methods that can fulfill this requirement are being sought. This study tested and showed the utility of nano-scaled pillars (nanopillars) in culturing hepatocytes, cells of the primary organ of drug metabolism, the liver. Primary hepatocytes cultured in nanopillar plates, cell culture plates with nanopillars in wells, formed three-dimensional aggregates, or spheroids, with a structural polarity and functional bile canaliculi. They were more similar to freshly isolated hepatocytes than those cultured in monolayer with respect to gene expression. This study also showed that scanning electrochemical microscopy can non-invasively evaluate the respiratory activity of the cultured cells and thus has a potential in validating the quality of cultured cells and in measuring the responses of the cells to drugs.

Hepatocytes in the liver have a cuboidal shape with two or three basal surfaces facing the sinusoid and adjacent cells form bile canaliculi. Primary hepatocytes cultured in monolayer lose their structural and functional characteristics and are no longer suitable as a cell model of the liver. In contrast, hepatocytes induced to form spheroids maintain the characteristics and have promise for drug screening. I envisaged that nanopillars would be a suitable substratum for formation of hepatocyte spheroids, as HeLa cells had been shown to weakly adhere to the substratum and to take a round shape, when cultured in plates with nanopillars. When rat hepatocytes were cultured on

nanopillar substratum, they did form spheroids. A nanopillar diameter of 2.0 μm was found to be optimal in that the number of obtained spheroids with diameter of 50-100 μm in which cells located centrally is not necrotic, starting from the same number of cells, was the largest. Plates pre-coated with type I collagen at 100 ng/mL yielded better results than uncoated plates or those coated at 10 μg/mL. The spheroids resembled hepatocytes in the liver, when immune-stained for actin and E-cadherin and observed under a fluorescence microscope. Transmission electron microscopy showed that the spheroids had bile canaliculi, some with well-developed microvilli. The well-developed microvilli had not been observed for hepatocytes grown in sandwich culture systems, which have been used to evaluate hepatocyte functions. The functionality of the bile canaliculi such as biliary excretion was confirmed microscopically with CDFDA in the spheroid. These results established histological and functional similarity of the spheroid in nanopillar plates to the liver.

Semi-quantitative real-time PCR showed that expression of Abcc2 (ATP-binding cassette transporter, superfamily C, member 2), albumin, and Cyp3a23/3a1 (cytochrome P450-3a23/3a1) genes, which are known to be highly expressed in the liver, was higher in the spheroids than in hepatocytes cultured in monolayer. In order to comprehensively examine gene expression, DNA microarray analysis using Agilent Whole Rat Genome Microarray 4x44 K was carried out for hepatocytes cultured in nanopillar plates, in a sandwich system, and in monolayer, and for freshly isolated hepatocytes. Principal component analysis of all valid data showed that gene expression was similar in hepatocytes cultured in nanopillar plates and in those in a sandwich system. The cells in these two systems were closer to freshly isolated hepatocytes along the primary component axis than those in monolayer. Expression of genes related to drug metabolism and pharmacokinetics, especially those coding for cytochromes P450, UDP-glucuronosyltransferase, and transporters, showed the same trend: the expression was highest in freshly isolated hepatocytes and lowest in monolayer hepatocytes; it was intermediate and similar in hepatocytes in nanopillar plates and those in a sandwich system. Thus, the spheroids obtained with nanopillar plates were shown to resemble freshly isolated hepatocytes more than the monolayer culture of hepatocytes with respect to gene expression as well.

Scanning electrochemical microscopy was tested for its utility in non-invasive evaluation of the quality of each spheroid through measuring their respiratory activity. In order to obtain smaller spheroids for this purpose, nanopillar culture plates of a new design were tested, in which each macroscopic culture well had microscopic hollows

with a diameter of 200 μm and a depth of 80 μm and each microscopic hollow had a round nanopillar area with a diameter of 80 μm in the middle. With the new design, called hollow nanopillar plate, smaller spheroids with less size heterogeneity were obtained. Each spheroid was moved to cone-shaped microwells and the oxygen concentration was measured along the vertical axis in the vicinity of each spheroid using platinum microelectrode. The oxygen consumption rate derived from the measurement showed an abrupt increase in variability for spheroids larger than 70 μm in diameter, suggesting that the larger spheroids contained cells performing anaerobic respiration. This interpretation was supported by the results of semi-quantitative real-time PCR showing that expression of the gene for lactose dehydrogenase A, an indicator of anaerobic respiration, was higher in larger spheroids. Real-time PCR also showed that expression of hepatocyte nuclear factor 4α, which is essential for the expression of liver functions, was higher in smaller spheroids and that smaller spheroids were more likely to resemble hepatocytes in the liver. Thus, the results showed that scanning electrochemical microscopy can be used to evaluate individual hepatocyte spheroids prior to drug screening and to continuously monitor their responses to drugs.

In conclusion, cell culture in microscopic compartments with nanopillars, combined with continuous monitoring with scanning electrochemical microscopy, has a great promise as a much sought cell-based *in vitro* screening system and also as a well-controlled system for cell biology in general.

Contents

Chapter 1

Introduction

1.1 Background

Drug development is a long process that generally spans 10 to 15 years. The standard process of new drug development generally consists of the following stages (Figure 1.1). At the first stage, desired pharmaceutical candidates are screened. In other words, the target disease for drug development is selected after having investigated pharmaceutical needs and effective lead candidates for the disease are optimized. At the second and third stages, efficacy and safety of a pharmaceutical candidate in the body are proved through non-clinical and clinical trial successively. And the manufacturer files a new drug application based on the evaluation results of these studies to acquire the approval of the country at the fourth stage. Following acceptance, the manufacturer can be requested to conduct additional post-marketing study (1,2).

In recent years, the cost of new drug development is significantly increasing (Figure 1.2) (1,3). The reasons for the increasing cost could be accounted for by a number of explanation: the pharmaceutical industry is currently attacking disease of great complexity; the entry bar for new drugs is higher because they are often competing with enhanced standard of care; and/or the regulatory authorities are more demanding (3). However, the main reason for the escalating developmental cost is low clinical success rate (~11%) (3) because of unacceptable clinical efficacy (56%) and hepatocellular toxicity (28%) (Figure 1.3) (4), which suggests pre-clinical animal pharmacokinetics (PK) study may not be sufficient for predicting the fate of drug candidate in human (5,6). In other words, great number of attrition of pre-clinical and clinical tests are conducted, as a result, brings escalating developmental cost. For this reason, the alternative *in vitro*

cell-based assay models using human cells that can predict *in vivo* PK are intensively required from pharmaceutical companies in recent years (6).

Today, most pharmaceutical companies try to use a set of specific *in vitro* assays using human cells as the initial step in drug lead discovery. Numerous cell-based assays have been established over the past 5 to 10 years, incorporating a broad range of technological and instrument advances. This promising process is still ongoing, but the value of any individual cell-based assay to predict *in vivo* efficacy has not been firmly established in the drug discovery process (7).

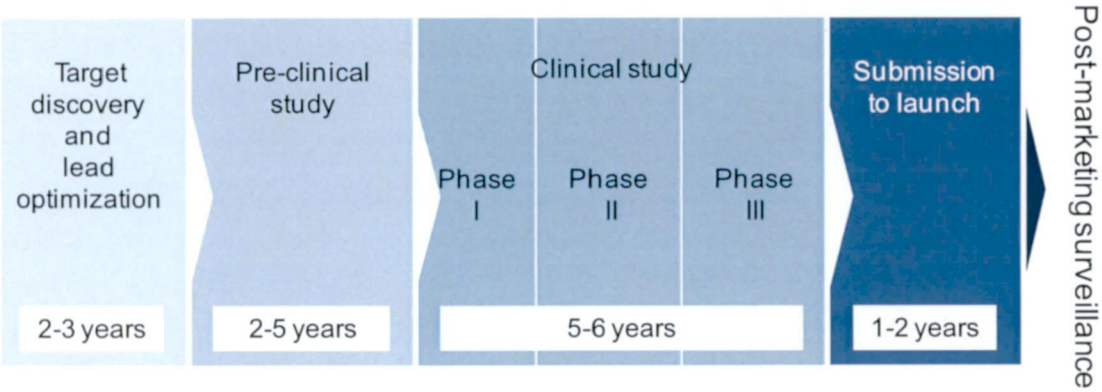

Figure 1.1 New drug development process (reproduced from reference1 and 2).

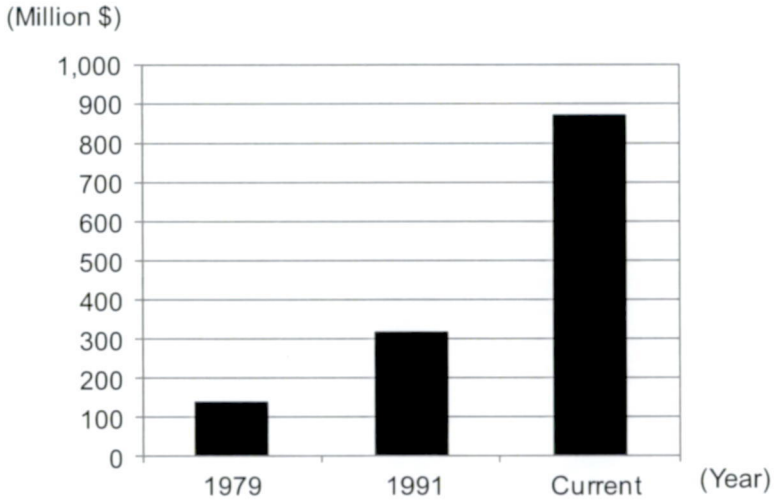

Figure 1.2 Temporal increase in developmental cost per approved new drug (reproduced from reference 1 and 3).

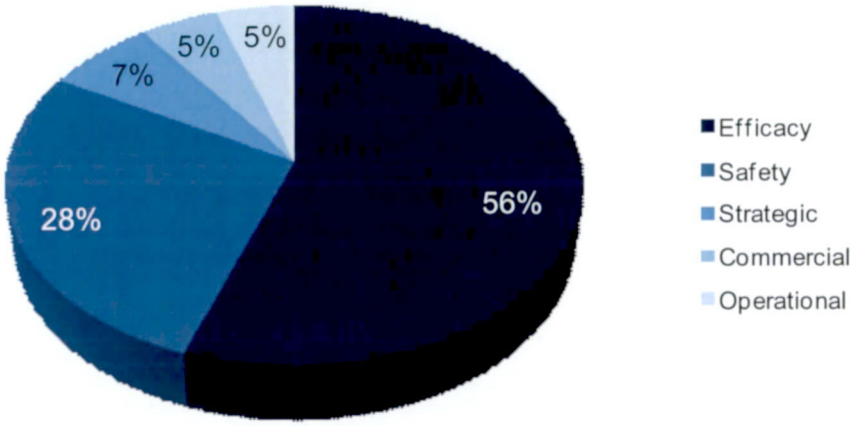

Figure 1.3 Cause of failure. The majority of failure s were due to lack of efficacy (56%) or to safety issues (28%) in Phase I/II studies (reproduced from reference 4).

1.2 3-D spheroid culture of hepatocytes

To replace the *in vivo* screening system with an *in vitro* high-throughput one, primary hepatocytes are particularly interested as the cell source because the hepatocytes are metabolic fundamental elements in the body. They play critical roles in synthesizing molecules that are utilized elsewhere to support homeostasis, and in converting molecules of one type to another.

The lack of predictability of *in vivo* efficacy are reported to attribute to commonly employed two-dimensional (2-D) cell culture system which does not mimic the response of cell of *in vivo* microenvironment (7). Traditional 2-D monolayer culture of primary hepatocytes on tissue culture plastic dish is problematic and has been associated with a rapid loss of differentiated function (8). Therefore, novel culture systems are needed to facilitate short and long-term culture of hepatocyte for diagnostic, therapeutic, and drug discovery applications.

In order to overcome this drawback, three-dimensional (3-D) multicellular aggregates, spheroids, have been focused on. Original observations of tissue-like aggregate formation from isolated cells was reported by Moscona in 1961, using fetal liver cells and a rotational technique (9). The descriptive term "spheroid" was coined years later by Landry in 1985 when multicellular aggregates were formed from isolated rat hepatocytes after 2-5 days of culture on non-adherent plastic surfaces precoated with

poly(2-hydroxyethyl methacrylate) (poly-HEMA) (Figure 1.4A) (10). Since then, a great number of 3-D spheroid culture methods or devices other than those above have been developed such as proteoglycan (11), alginate scaffold (12,13), titanium dioxide(14), hollow fibers (15), polyurethane form (16), and spinner flask (17,18).

Reports of structural polarity and bile canaliculi formation by primary hepatocytes in spheroid aggregate provide further evidence that hepatic spheroids mimic the hepatocellular microanatomy of the liver (Figure 1.4B) (12). Moreover, the spheroid allows recapitulation of the cuboidal geometry of primary hepatocytes with relatively stable long-term differentiated function such as albumin secretion (Figure 1.4C) (14). The spheroid culture system is accordingly an alternative culturing technique for evaluating drug metabolism and toxicity in the new drug development. In response to these issues, we have been studied culture device to construct 3-D tissue *in vitro*. We therefore made a start on developing a novel culture device with aiming at controlling spheroid formation by optimizing the local geometric architecture of the substratum, which is the "Nanopillar Cell Culture Plate (NP plate)".

1.3 Nanopillar cell culture plate (NP plate)

Ingber's group originally reported that mechanical forces serve as important regulators at the cell and molecular levels, and that they are equally potent as chemical cues in 1991 (19). Physiologist and clinician have been recognizing the importance of this mechanobiology for the development and function of the cell over the past two decades (20). Now that, the geometric architecture of the culture substratum that brings cellular proliferation, motility to tissue morphogenesis reaches nanoscale level.

Nanotechnology has attracted the much interest of researchers not only in the field of material science but also in that of molecular and cellular biology. In order to fabricate nanostructures or nanoscale pattern for culture device efficiently and highly throughput, nanoimprinting is the key technology (21). Conventional nanostructures have been fabricated using large-scale integration (LSI) processes by photolithography with materials limited to silicon (Si)-based. However, Kuwabara *et al.* have been succeeded in forming nano-scaled structures (nanopillars) with diameters of 80-1,000 nm and heights of 1-3 μm using nanoimprinting technology, which is nano-scaled 3-D culture device (22). The examples are shown in Figure 1.5.

A

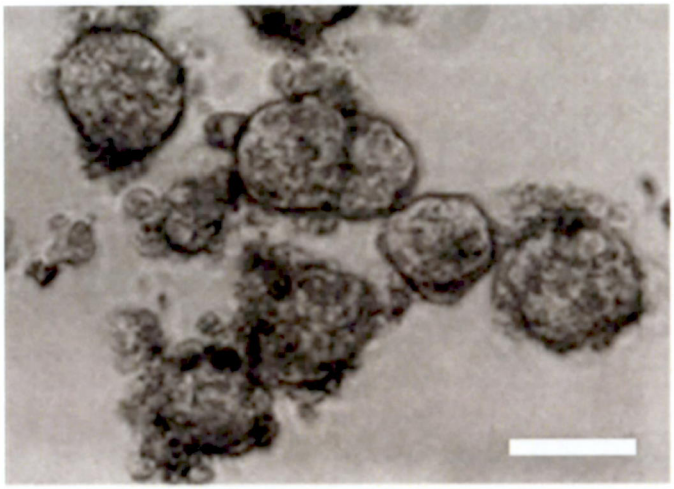

B

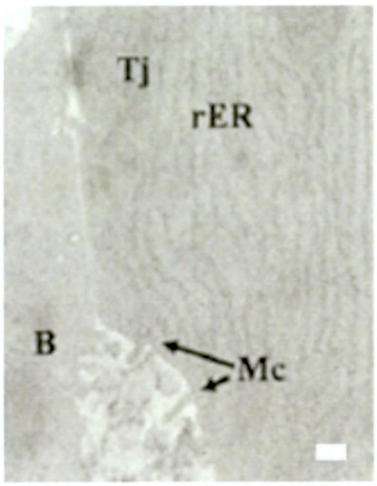

C

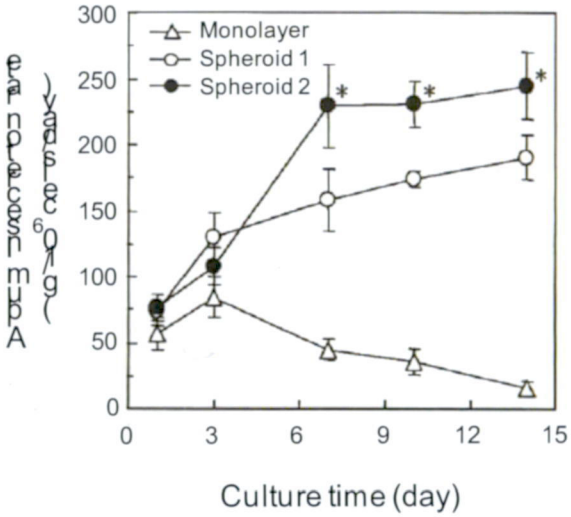

Figure 1.4 (A) Phase-contrast photograph of the hepatocyte spheroid on day 2. Bar, 50 μm (reproduced from reference 10). (B) Ultrastructural feature of the hepatocyte spheroid by transmission electron microscopy (TEM) on day 3. The spheroid exhibits tight junction (Tj) between adjacent cells. Rough endothelial reticulum (rER) indicates hepatic metabolism in active. Microvillus-lined channels (Mc) and Bile canaliculi (B) show structural polarity. Bar, 200 nm (reproduces from reference 13). (C) Time course of albumin secretion rate (reproduced from reference 15).

Balaban *et al.* reported the elastic micropatterned substrates with nanopillar structures was applied as a measurement tool of local force added by cells to the substrates (23). Nomura *et al.* has reported the possible application of a nanopillar device as a new type of cell culture dish (24). In these studies, they reported using HeLa cells that the localization of cell adhesion-related molecule such as actin and vinculin commonly limited to the top of the nanopillars. This phenomenon means the adhesion to the substratum is weaker than that to the conventional flat cell culture dish. They also reported that the cell morphology on the nanopillar device was round-shape, however, that on the conventional flat petri dish were flattened 2-D manner.

From this point of view, we considered practical use of the nanopillar culture device, NP plate, for 3-D spheroid formation with aiming at utilization in the course of new drug development.

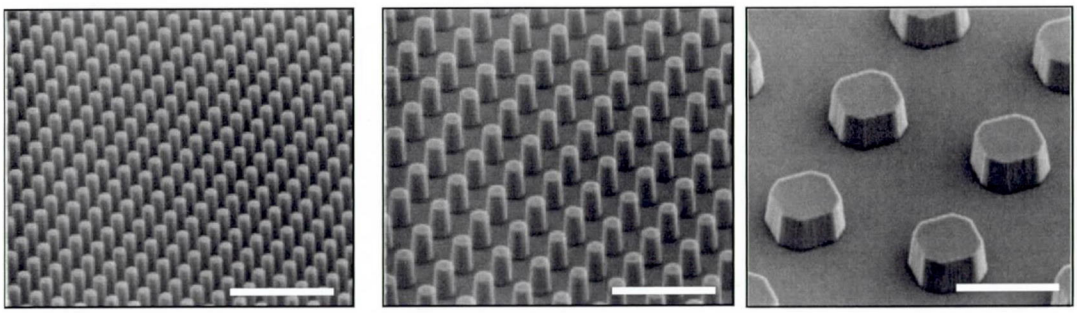

Figure 1.5 Scanning electron microscope (SEM) images of the NP plate surface structure. Bars, 3.0 μm.

1.4 Scanning electrochemical microscopy

When we apply 3-D spheroids as *in vitro* cell-based assay models for preclinical testing in the new drug development process, we need to establish noninvasive measuring method that can evaluate the cellular activity and viability. Noninvasive analysis is essential requirement in order to make use of spheroid itself which will be tested. Furthermore, noninvasive measurement provides a benefit that the drug response or metabolic process can be monitored continuously using the same spheroid throughout evaluating. Based on this background, we focused attention on scanning electrochemical microscopy (SECM). SECM is ideally noninvasive; oxygen consumption around cells can be monitored continuously.

SECM was originally developed in 1986 (25), which is the technology that the current that flows through the very small electrode tip (generally an ultramicroelectrode with a tip diameter of 10 μm or less) can be measured near a conductive, semi-conductive, or insulating substrate immersed in solution (26). The features of the SECM are the ability to induce a chemical reaction in the local region and to measure *in situ* the chemical reaction quantitatively in the local area of biological sample.

Application to the biological sample was firstly reported in 1990 in which the oxygen reduction current of leaves produced by photosynthesis was measured (27). Then, the target object has been moved to mammalian cells. SECM was applied to measure the oxygen consumption of single bovine embryos to evaluate the viability for an effective artificial insemination (28,29). In this case, microelectrode measures the reduction current with a negative charge that flows when the dissolved oxygen in the medium is reduced to water (Figure 1.6). The amount of reduction current is proportional to the amount of dissolved oxygen. In the very close region of the cell surface, the amount of reduction current is small because of low concentration of dissolved oxygen due to vigorous cellular respiration. However, at the bulk, a point away from the cell surface, the amount of reduction current increases because of high concentration of dissolved oxygen (Figure 1.6). By scanning the microelectrode along vertical direction, we measure the oxygen concentration difference (ΔC) between the cell surface and the bulk, and calculate the oxygen consumption rate of sample.

By applying this measuring principle, we challenged to measure the respiratory activity of single spheroids, which were formed on a NP plate in this study.

1.5 Organization of this thesis

As described in Section 1.1, most pharmaceutical companies demand a set of specific *in vitro* high-throughput cell-based screening system that can predict the fate of drug candidates in human. Primary hepatocytes would firstly be favored candidates for the cell source. However, traditional 2-D monolayer culture has a problem of rapid loss of differentiated function. Therefore, novel 3-D culture systems are needed for diagnostic, therapeutic, and drug discovery applications. In addition, a noninvasive measuring system that can evaluate the cellular activity and viability is also needed. Noninvasive measurement provides a benefit that the cellular viability, drug response or metabolic process can be monitored continuously. The objective of this study is to establish

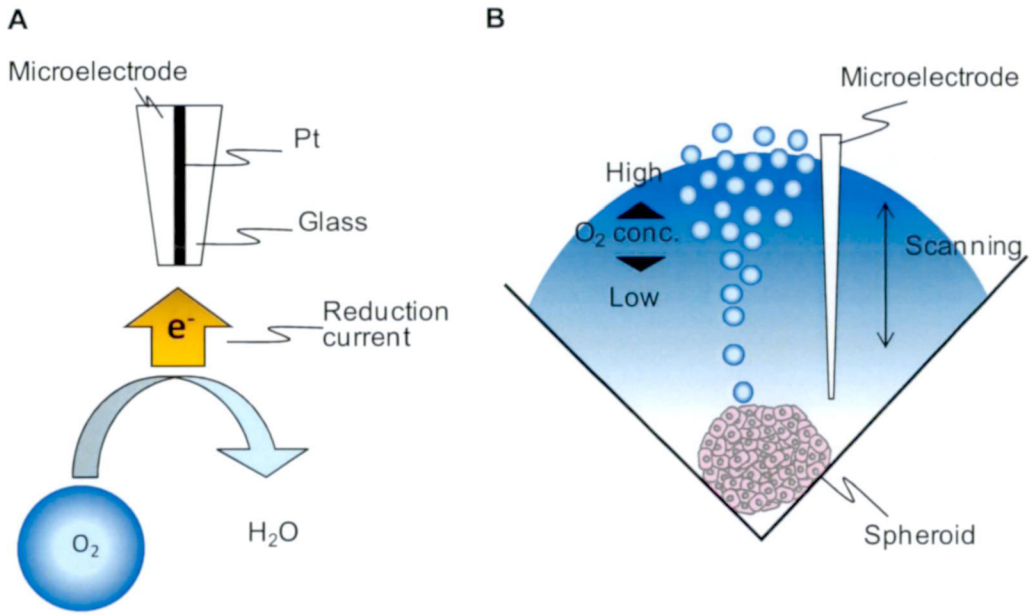

Figure 1.6 Measuring principle of SECM. (A) Microelectrode measures the reduction current with a negative charge that flows when the dissolved oxygen in the medium is reduced to water. The amount of reduction current is proportional to the amount of dissolved oxygen. (B) In the very close region of the spheroid surface, the amount of reduction current is small because of low concentration of dissolved oxygen due to the cellular respiration. However, at the bulk, a point away from the cell surface, the amount of reduction current increases because of high concentration of dissolved oxygen. By scanning the microelectrode along vertical direction, we measure the oxygen concentration difference (ΔC) between the cell surface and the bulk, and calculate the oxygen consumption rate of sample.

a culturing method for 3-D spheroid formation using NP plate and a non-invasive cellular activity measuring method by applying the scanning electrochemical microscopy. Furthermore, we analyze the mechanism the 3-D spheroid formation on the pillar structure, and the way of cellular respiration of spheroid depended on the spheroid size. In this study, we used rat primary hepatocytes as basic study before applying human ones.

Chapter 2 describes the 3-D spheroid culture with higher structural polarity and hepatic functions using NP plate that was developed in Hitachi. Chapter 3 describes the comprehensive increase in the drug metabolism and pharmacokinetics (DMPK)-related gene expression of NP-cultured 3-D spheroid using global gene expression analysis.

Chapter 4 describes the noninvasive measuring of cellular respiratory activity using SECM and offers the new numerical insight into the way of cellular respiration of spheroid. Finally, the thesis is summarized in chapter 5

Chapter 2

Higher Structural Polarity and Hepatic Functions of Nanopillar-Cultured Spheroids

2.1 Introduction

Most methodologies used to evaluate drug metabolism and toxicity in the drug development process are performed using animals and animal body parts. However, it is difficult to fully predict how drug candidates work in human body with this *in vivo* animal model (5,6). To replace the *in vivo* screening system with an *in vitro* one, primary hepatocytes must first be explored as the cell source. Additionally, culture conditions for hepatocytes must be identified that maintain the structural and functional polarity of the hepatocytes after isolation from the liver (12). Hepatocytes in their native environment have a structural polarity. They have a cuboidal shape with two to three basal surfaces facing the sinusoid while adjacent cells that form the bile canaliculi (12,17). After isolation from the liver, hepatocytes rapidly lose their polarized structure and their differentiated functions, such as albumin secretion, urea synthesis, and cytochrome P450 (Cyp) activity (12,17).

Conventionally cultured hepatocytes have a flat, monolayer morphology on extracellular matrix (ECM)-coated surfaces with a rare, short-lived bile canalicular structure, and their structure and function are lost or decreased and cannot be recovered under such monolayer culture conditions (11,14,18,30). Among such 2-D monolayer culture conditions, "sandwich (SW)" culture systems (Figure 2.1) have been reported to support differentiated functions and polarity of adult rat hepatocytes (31,32). In this

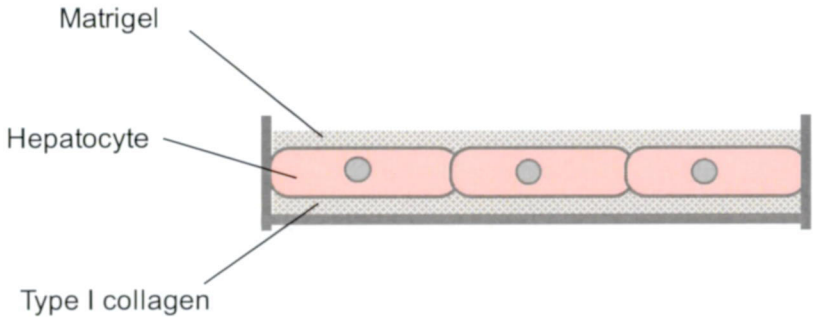

Figure 2.1 Schematic view of sandwich (SW) culture. Hepatocytes are cultured on a thin layer of type I collagen and then overlaid with Matrigel.

system, hepatocytes are cultured on a thin layer of type I collagen and then overlaid with Matrigel, a basement membrane extract from Engelbreth-Holm-Swarm (EHS) mouse sarcoma (33). This system is used to evaluate hepatocyte function such as biliary excretion activity *in vitro* (34).

In contrast, primary hepatocytes maintain differentiated hepatocellular functions when they are induced to self-assemble into 3-D aggregates, spheroids by culturing on an extracellular matrix or substrate such as proteoglycan (11), alginate scaffold (12), poly (2-hydroxymethyl methacrylate) (poly-HEMA) (10), titanium dioxide (14), hollow fibers (15), polyurethane foam (PUF) (16), and spinner flask (35). Several investigators have reported that hepatocyte spheroids possess structural polarity and transporters similar to those of the bile canaliculi in the native tissue, which explains the enhanced hepatocellular activities of spheroids (12,17,18). Accordingly, the spheroid culture system is expected to be an alternative culturing technique for evaluating drug metabolism and toxicity in the course of drug screening (12,13). A great number of cell culture devices have been developed for forming three-dimensional structures (such as spheroids), including NP plate (14,24,36-38). In one case, NP plates were fabricated with high aspect ratio structures with a pillar diameter of 160–1,000 nm and a height of 280–1,000 nm using nanoimprinting technology (24).

In the previous research on the effect of ECM patterns in the micrometer range during the initial phases of cell adhesion and spreading, Ingber's group found that the long-term effect of cell shape on growth and viability depends on the local geometric architecture of the substratum, synergistically with a consequence of the type of matrix

protein (39,40). Bastmeryer and co-workers analyzed the effect of ECM patterns in the micrometer range by controlling the size of ECM squares (dots) and the distance between them. They found that a dot distance of around 2–5 μm affected the cellular shape and functions (41).

On the basis of these findings, we envisaged the 3-D spheroid would be formed on the NP plate (Figure 2.2), and investigated how the NP surface structure affects cell adhesion, migration, and consequent spheroid formation. We used the NP plates with pillar diameters of 0.18, 0.5, 1.0, 2.0, and 5.0 μm and with pillar pitches (pillar center-to-center distance) that were twice the pillar diameter (Figure 2.3). The adhesion area of cells cultured on the NP plates was reported to be restricted to the top of the pillars (24). Accordingly, the mode of cell migration and the resultant morphology of tissues on the NP plate should differ from those on a conventional culture dish. From this point of view, our objective is to identify the optimal pillar diameters for spheroid formation in terms of cell adhesion and migration. We examined the structural polarity and biological functions of spheroids formed on the NP plates and investigated the effects of Matrigel-overlaying on the hepatocellular functions.

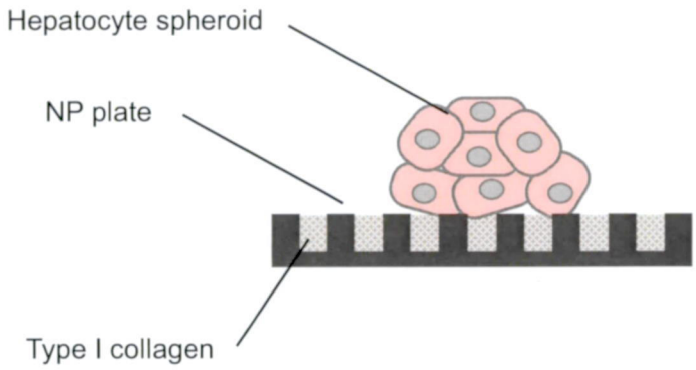

Figure 2.2 Schematic view of 3-D spheroid cultured by NP plate.

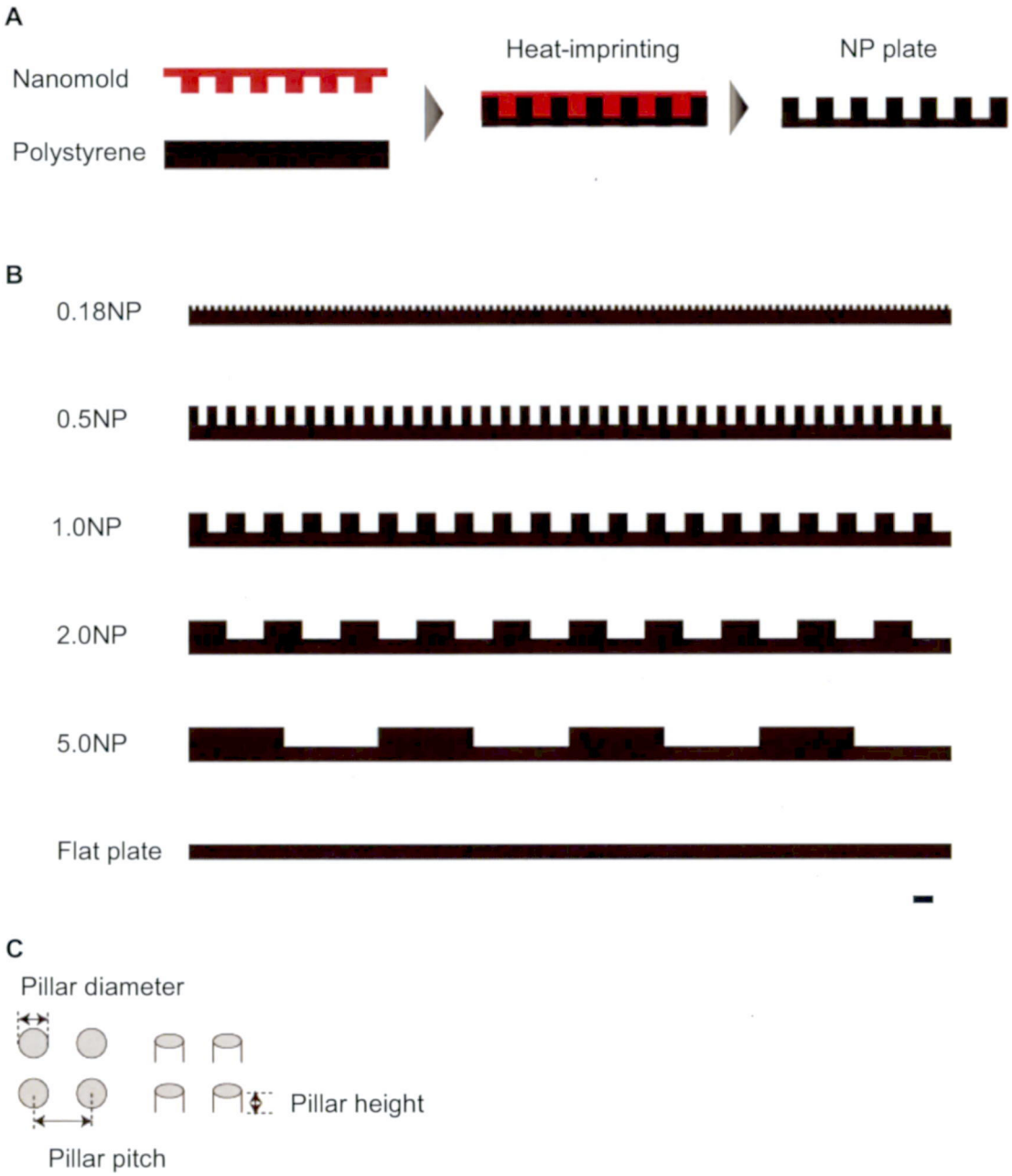

Figure 2.3 (A) Fabrication process of the NP plate. Nanomold is made of silicon wafer and fabricated using photolithography. By heat-imprinting the nanomold onto the polystyrene film, nanopillar sheet is made. (B) A side views of surface patterns of NP plates used in this study. Bar, 1 μm. (C) Definitions of pillar diameter, pillar pitch and pillar height.

2.2 Materials and Methods

2.2.1 Nanopillar plate preparation

Polystyrene film with a thickness of 1.0 mm was spin-coated onto a glass substrate. A nanomold was made of silicon wafer and fabricated using photolithography. An NP structure was formed by pressing the mold onto the film at 423.K and then releasing it at room temperature (RT) (24). The surface patterns of the fabricated NP plates are illustrated in Figure 2.3.

2.2.2 Hepatocyte culture

Hepatocytes were isolated from 6- to 8-week-old male specific viral pathogen free Wister rats (Charles River Japan Inc., Japan) weighing about 150-250 g by using a modified two-step in situ collagenase perfusion method (42) and purified by isodensity Percoll centrifugation (43). The viability of the hepatocytes was determined by trypan blue exclusion, and hepatocytes with over 85% viability were used for culturing.

The hepatocytes were resuspended in William's E medium containing 10% fetal bovine serum, supplemented with 8.6 nM insulin (Sigma-Aldrich Corp., MO), 255 nM dexamethasone (Nacalai Tesque, Inc., Japan), 50 ng/ml epidermal growth factor (Sigma-Aldrich Corp.), 5 KIU/ml aprotinin (Wako Pure Chemical Industries, Ltd., Japan) and were seeded at a density of 1×10^5 cells/cm^2 onto prepared NP plates and into a 35-mm-diameter culture dish. The plates were precoated with a solution containing 10 μg or 100 ng/ml of type I collagen. The dish that type I collagen were precoated was purchased from AGC Techno Glass Co., Ltd. (Japan). The procedure for the NP, SW, and conventional monolayer (ML) cultures is described below.

NP culture: after 24 hours of post-seeding, the medium was replaced with serum-free William's E medium containing the same supplements described above. After 48 hours of post-seeding, the medium was replaced with a serum-free medium containing Matrigel™ (BD Bioscience, MA) with the same supplements described above. Subsequently, the culture medium was changed daily. Hepatocytes were cultured in total for 96 hours.

SW culture (31,32): after 24 hours of post-seeding, the culture medium was replaced with serum-free William's E medium containing Matrigel (BD) with the same supplements described above. Subsequently, the culture medium without Matrigel was

changed daily. Hepatocytes were cultured in total for 96 hours.

ML culture: the culture medium was replaced with serum-free William's E medium every 24 hours. Hepatocytes were cultured in total for 96 hours.

2.2.3 Immunohistochemistry

After a total of 96 h of culturing, the spheroids cultured on the NP plates and the hepatocytes cultured in the dish were washed with phosphate buffered saline (-) (PBS(-)) after removing the culture medium, and then fixed in 4% paraformaldehyde in PBS(-) and permeabilized in 0.05% Triton-X in PBS(-). After blocking by FBS in PBS(-), the samples were incubated in rabbit anti-human E-cadherin polyclonal antibody in a 100-fold dilution (SC-7870; Santa Cruz Biotechnology, Inc., CA), washed with 0.05% Tween 20 in PBS(-), and incubated in biotinylated anti-rabbit IgG antibody (BA-1000; Vector Laboratories, CA). The samples were then washed with 0.05% Tween 20 in PBS(-) and incubated in Streptavidin-Fluorescein (NEL720; PerkinElmer Life Science, Inc., MA). They were then washed again with 0.05% Tween 20 in PBS(-) and incubated in rhodamine phalloidin (R415; Invitrogen Corp., CA). After that, the samples were washed with PBS(-) and incubated in Hoechst 33258. After a final washing in deionized water (DW), the samples were embedded in glass slides. Fluorescence images were taken with an optical microscope (AX70; Olympus Optical, Japan).

2.2.4 Resin embedding and microscopy

Rat hepatocytes cultured on the NP plates were fixed with 2.5% glutaraldehyde in 0.1 M phosphate buffer, pH 7.4, incubated overnight at 4°C, and rinsed with 0.1 M phosphate buffer. Post-fixation was performed with 1% osmium tetroxide in 0.1 M phosphate buffer, pH 7.4. After being washed with 0.1 M phosphate buffer and DW, the hepatocytes on the NP plates were embedded in 1.5% SeaPlaque® agarose (Lonza Ltd., Switzerland). Agar-containing hepatocytes was dehydrated with a serial dilution of ethanol, treated with propylene oxide, and embedded in epon-araldite mixed resin. Vertical sections of the samples were prepared using an ultramicrotome (Sorvall MT-6000; Du Pont Company, DE). Semi-thin sections (500 nm) were stained with toluidine blue and viewed with an optical microscope (AX70; Olympus Optical, Japan). Ultrathin sections (60 nm) were stained with uranyl acetate and lead citrate and examined with a transmission electron microscope (H-7100; Hitachi Ltd., Japan).

2.2.5 Semi-quantitative gene expression analysis

Total RNA was extracted using an RNeasy Tissue Kit (Qiagen GmbH, Germany) every 24 h from rat hepatocytes cultured on the NP plates with and without Matrigel, from ones conventionally cultured as a monolayer, and from ones SW cultured. 2.0 μg of the total RNA was reverse transcribed, and quantitative real-time PCR was conducted in a Thermal Cycler Dice Real Time System (TaKaRa Bio Inc., Japan) using a final reaction mixture of the RT product, TaqMan Gene Expression Assay (Applied Biosystems, CA), Premix Ex Taq™ (Takara Bio Inc.), and DW. The $2^{-\Delta\Delta Ct}$ method was used to calculate the relative change in the gene expression (44); TATA-binding protein (TBP) was used as an endogenous control. The relative changes in expression were determined toward the control sample that freshly isolated (time 0).

2.2.6 Biliary excretion analysis

Every 24 h after cell culture started, biliary excretion assay was performed. Before each assay, the medium was washed by Hanks' Balanced Salt Solution (HBSS; Sigma-Aldrich Corp.) with calcium and magnesium. After that, it was replaced with a medium containing 5-carboxy-2', 7'-dichlorofluorescein diacetate (CDFDA; Molecular Probes, Inc., OR). After incubation at 37°C, the extracellular CDFDA was rinsed out by HBSS with calcium and magnesium. Fluorescence and phase-contrast images of the samples were acquired using an optical microscope (Axiovert 200; Carl Zeiss GmbH, Germany)

2.3 Results

2.3.1 Formation of rat hepatocyte spheroids on NP plates

To examine the effect of the NP diameter on spheroid formation, hepatocytes were seeded on NP plates with a pillar diameter of 0.18, 0.5, 1.0, 2.0, or 5.0 μm, which are referred to as 0.18NP, 0.5NP, 1.0NP, 2.0NP, and 5.0NP, respectively (Figure 2.3B). A culture dish without NP (flat plate) was used as a control (Figure 2.3B). The pillar diameter, pitch, and height were defined as shown in Figure 2.3C, and the dimensions are summarized in Table 2.1. To examine the effect of the amount of type I collagen in

the coating solution on spheroid formation, we observed spheroid morphology at 96 h post-seeding. Since hepatocytes are conventionally cultured in a culture dish precoated with a solution containing 1–1.5 mg/mL of type I collagen (33,34), we tested a sequential 100-fold dilution series: 1 ng, 100 ng, 10 μg, and 1 mg/ml. We show here the results of culture using 100 ng/ml and 10 μg/ml of type I collagen. In experiments using six different kinds of NP plates including flat plate and solutions with different concentrations of type I collagen, we observed spheroids with a compact morphology in which individual cells constituting spheroid could barely be distinguished on the 0.18NP, 2.0NP, 5.0NP, and flat plates coated with a solution containing 100 ng/ml type I collagen (Figure 2.4B, K, N, and Q). Intermingled monolayer hepatocytes and spheroids were observed on the 0.5NP and 1.0NP with the same concentration of type I collagen (Figure 2.4E and H). Similar results were observed for the uncoated NP and flat plates. However, unlike the spheroids on the NP plates coated with 100 ng/ml collagen solution, the spheroids on the uncoated 0.18NP, 2.0NP, 5.0NP, and flat plates (Figure 2.4A, J, M, and P) had weak adhesion to the substrate. The number of spheroids decreased over time due to the changing of the culture medium. Rat hepatocytes were spread on the NP plates and flat plate coated with 10 μg/ml of type I collagen solution in monolayer configuration for all pillar diameters (Figure 2.4C, F, I, L, O, and R). This revealed that the hepatocyte and spheroid morphologies depended on the pillar diameter and/or the concentration of type I collagen. Spheroids with a compact morphology adhered to the substratum were accomplished on 0.18NP, 2.0NP, 5.0NP, and flat plates coated with a solution containing 100 ng/ml of type I collagen.

Table 2.1 Pillar diameter, pitch, and height of the NP plate

	0.18NP	0.5NP	1.0NP	2.0NP	5.0NP
Diameter (μm)	0.18	0.5	1.0	2.0	5.0
Pitch (μm)	0.36	1.0	2.0	4.0	10.0
Height (μm)	0.2	1.0	1.0	1.0	1.0

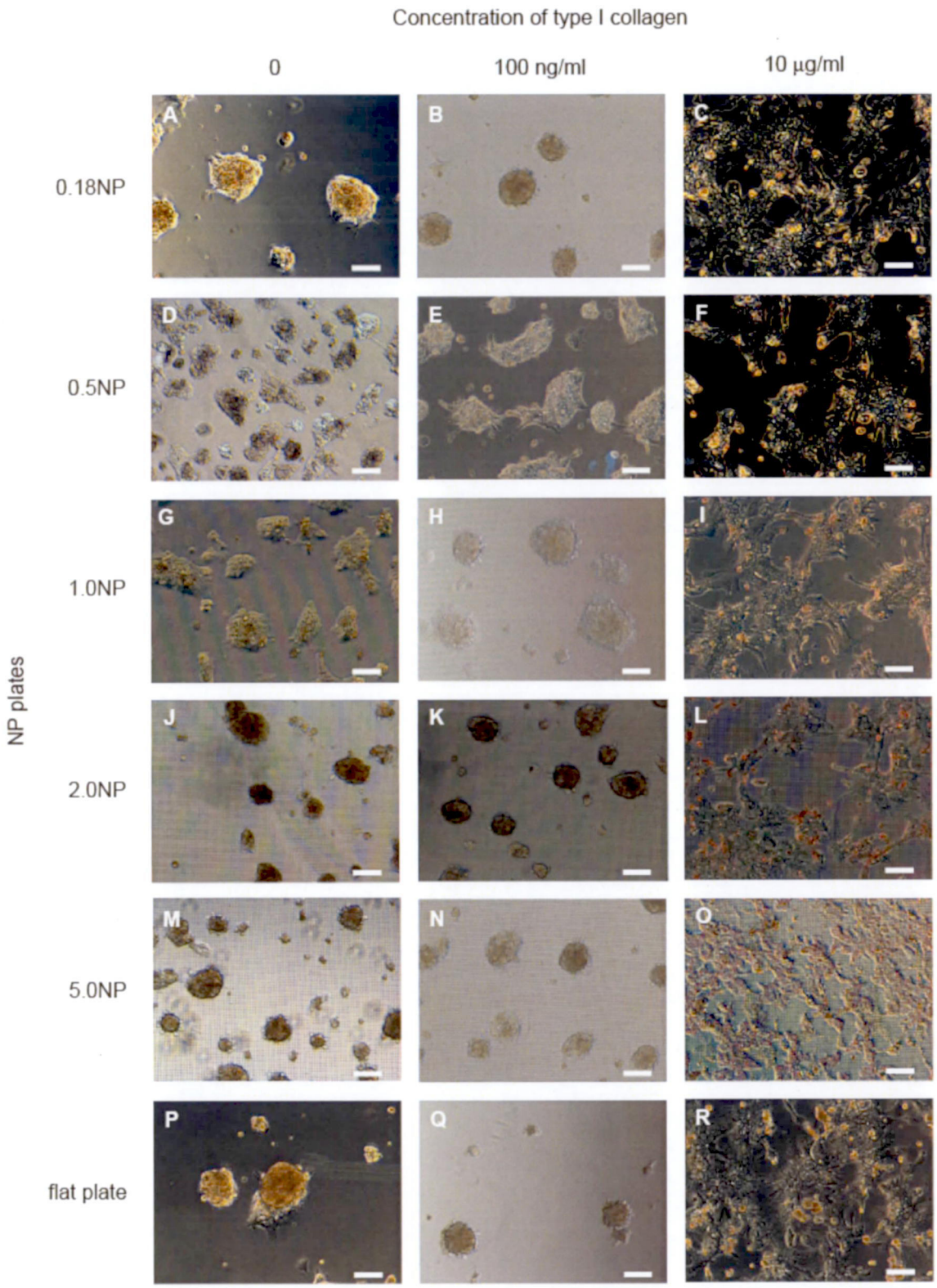

Figure 2.4 Phase-contrast micrographs of hepatocyte cultures on the NP plates 96 hr after seeding. Hepatocytes were cultured on 0.18, 0.5, 1.0, 2.0, and 5.0NP and on a flat plate. NP plates were coated with a solution containing 100 ng/ml or 10 mg/ml of type I collagen solution. Uncoated NP plates and flat plate were used as a control (-). Bars, 100 μm.

To determine the optimal size of pillar diameter for spheroid formation, we calculated the number of spheroids and the distribution of their diameters on the basis of micrograph data for spheroids that formed on the NP plates coated with a solution containing 100 ng/ml of type I collagen. Most of the spheroids on the 0.18NP, 2.0NP, and flat plates were 50–100 μm in size, and most of those on the other NP plates were 100-150 μm in size (Figure 2.5). As shown in Table 2.2, the 2.0NP had the most spheroids (153.6) and the smallest standard deviation (±5.3), indicating that a number of spheroids of relatively uniform size formed on the 2.0NP. Since spheroids up to 100 μm in diameter have higher viability or effective cellular function (45), 2.0NP is suitable for formation of spheroids because both the number (58.1±13.3) and ratio (37.8%) of spheroids on the 2.0NP ranging in size from 50-100 μm were the highest among the NP plates (Figure 2.5) and because the number of 1-100 μm spheroids on the 2.0NP versus the other NP plates was consistently larger with statistically significant differences ($p<0.05$) (Table 2.3). Consequently, 2.0NP coated with a solution containing 100 ng/ml of type I collagen were used in the subsequent experiments.

The recruitment of E-cadherin and actin to regions of intercellular contact is essential for the formation and stabilization of adherens junctions, resulting in appropriate tissue structure (46). Accordingly, the localizations of E-cadherin and actin were investigated using immunohistochemistry to compare the structure of hepatocyte spheroids with native liver tissue. Figure 2.6 shows double staining images for a frozen section of rat native liver, an NP-cultured spheroid, and monolayer-cultured hepatocytes. Rhodamine-phalloidin was used to stain the actin (red), and anti E-cadherin antibody was used to stain the E-cadherin (green). The E-cadherin of the rat liver and the spheroids formed on the NP plate were highly concentrated at the cell-cell junction (Figure 2.6D and E) as was the actin (Figure 2.6A and B). In contrast, the E-cadherin of the conventional monolayer culture was below the limit of detection (Figure 2.6F), and actin stress fibers were observed (Figure 2.6C).

Table 2.2 Total number of spheroids formed on the nanopillar and flat plates; mean±SD.

0.18NP	0.5NP	1.0NP	2.0NP	5.0NP	flat sheet
120±21.3	120.4±13.8	105.6±25	153.6±5.3	123.2±17.6	39.2±16.8

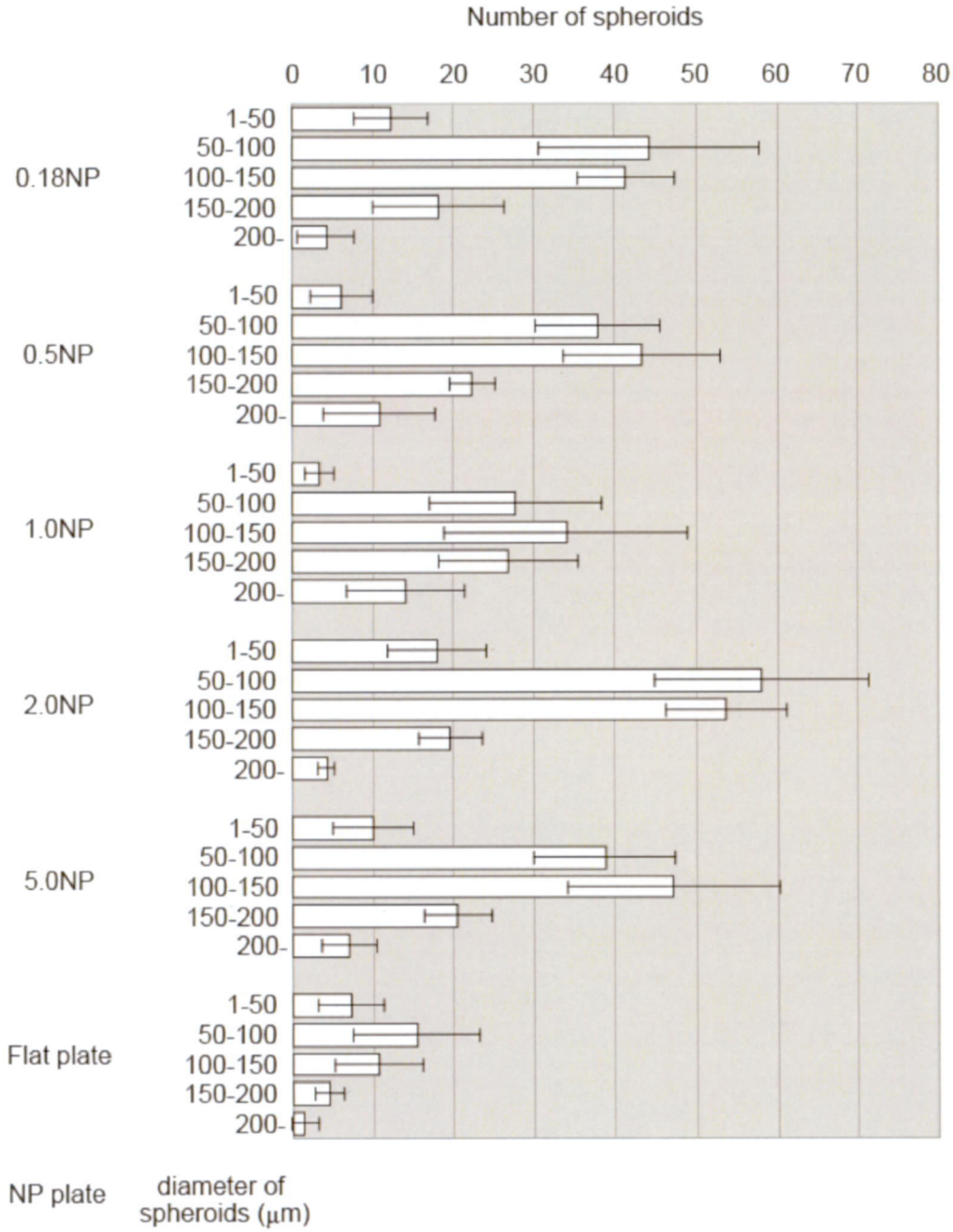

Figure 2.5 Size distributions of hepatocyte spheroids. Hepatocytes were cultured on 0.18, 0.5, 1.0, 2.0, and 5.0NP and on a flat plate coated with a solution containing 100 ng/ml of type I collagen solution. Spheroids were counted 96 h post-seeding.

Table 2.3 Number of 1-100 μm spheroids and p-value

	2.0NP	0.18NP	0.5NP	1.0NP	5.0NP	flat sheet
n=1	65	59	56	14	53	14
n=2	99	40	50	27	56	37
n=3	86	77	40	31	61	38
n=4	60	45	4	44	37	13
n=5	65	61	32	39	36	21
p-value versus 2.0NP	-	<0.05	<0.01	<0.01	<0.01	<0.01

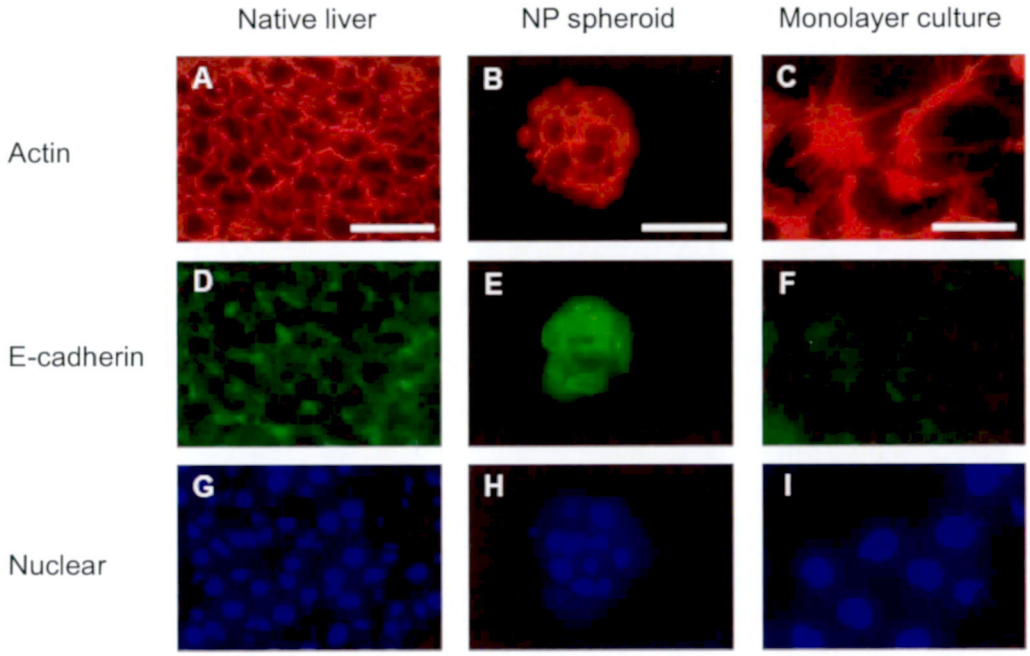

Figure 2.6 Immunohistological staining of actin and E-cadherin for hepatocytes cultured on 2.0NP and in conventional collagen-coated dish for 96 h. Frozen section of rat native liver, hepatocyte spheroids on the NP plates and hepatocyte monolayer cultured in dish were stained with rhodamine-phalloidin (red: A-C) and anti-E-cadherin antibody (green: D-F). Hoechst 33258 was used for nuclear counterstaining (blue: G-I). Bars, 50 μm.

2.3.2 Effects of Matrigel overlay on hepatocyte spheroids

Structural analysis. It is well established that an ECM can modulate gene expression in many biological systems, and it has been suggested that a complex ECM, but not its purified components, is needed to maintain differentiated hepatocytes *in vitro* for a long period (47). Accordingly, we expect the effect of extracellular matrix, which simulates the environment of a living organism by surrounding the cells, and overlaid Matrigel which includes complex basement membrane extract but not purified components on the spheroids formed by NP culturing.

To observe the morphology and examine cellular viability before and after overlaying the Matrigel, we cultured rat hepatocytes on the 2.0NP coated with a solution containing 100 ng/ml of type I collagen. Semi-thin sections of reconstituted spheroids were stained with toluidine blue. Rat native liver tissue and SW-cultured hepatocytes were also examined for comparison. In the SW culture system, monolayer-cultured hepatocytes are held between two kinds of thin-layered ECM components In the NP culture system with Matrigel, it is overlaid on spheroids formed on the NP plates. The hepatocytes cultured without the Matrigel overlay had a variety of shapes but were spheroidal overall (Figure 2.7A and B) while those cultured with Matrigel were individually round polygons (Figure 2.7C), much like those of native liver (Figure 2.7E). The SW-cultured hepatocytes were uniformly flat (Figure 2.7D). These results indicate that the use of the Matrigel overlaying onto spheroids is more effective than the use of monolayer culturing for recovering the native morphology. The viability of the hepatocytes was then examined. The ratio of dead hepatocytes represented by asterisks in the Figure 2.7 was increased time dependently under the condition of without the Matrigel overlay 48 h and 96 h post-seeding (Figure 2.7A and B). Almost all the hepatocytes of spheroids cultured with the Matrigel overlaid at 48 h were still alive at 96 h (Figure 2.7C). The viability of the hepatocytes was thus improved by the Matrigel overlay (Figure 2.7A-C).

To investigate the bile canaliculi structures and their peripheral parts in more detail, we used a transmission electron microscope (TEM; H-7100; Hitachi Ltd., Japan). We found that bile canaliculi divided by a tight junction formed in all the reconfigured structures: NP-cultured spheroids (Figure 2.8A-C) and SW-cultured tissues (Figure 2.8D). Bile canaliculi with well-developed microvilli those were in native tissue (Figure 2.8E) were observed in spheroids cultured with and without Matrigel (Figure 2.8A and C). Bile canaliculi with and without well-developed microvilli were observed in

spheroids cultured with Matrigel (Figure 2.8B and C), but only bile canaliculi without well-developed microvilli could be observed in SW-cultured (Figure 2.8D).

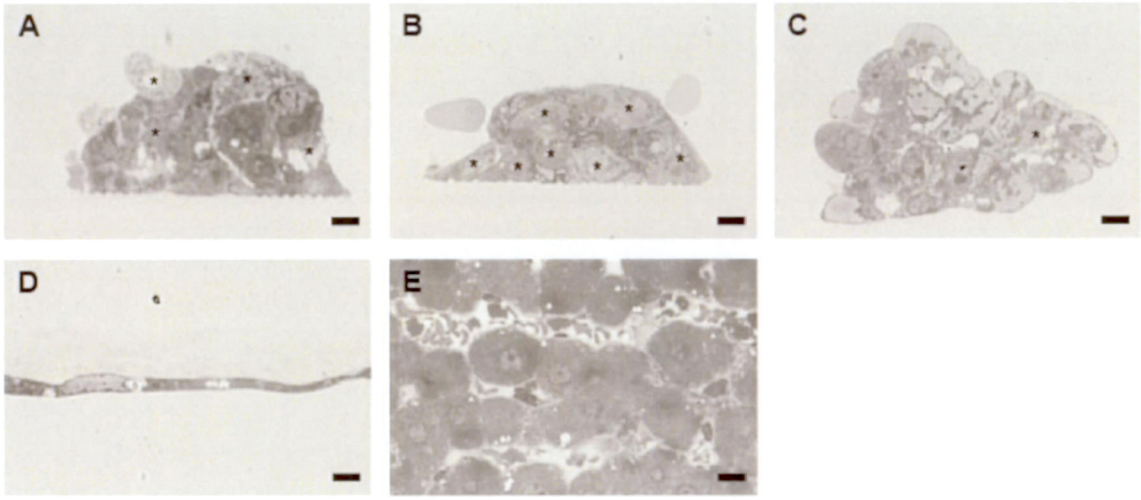

Figure 2.7 Toluidine blue staining of hepatocyte spheroid sections on 2.0NP (A-C), sandwich-cultured hepatocytes (D), and liver tissue (E). A: 48 h, B: 96 h, C: 48 h after Matrigel overlay at 48 h (total 96 h culture), D: 72 h of sandwich culture (total 96 h culture), E: rat liver tissue. Dead hepatocytes indicated by asterisks. Bars, 10 μm.

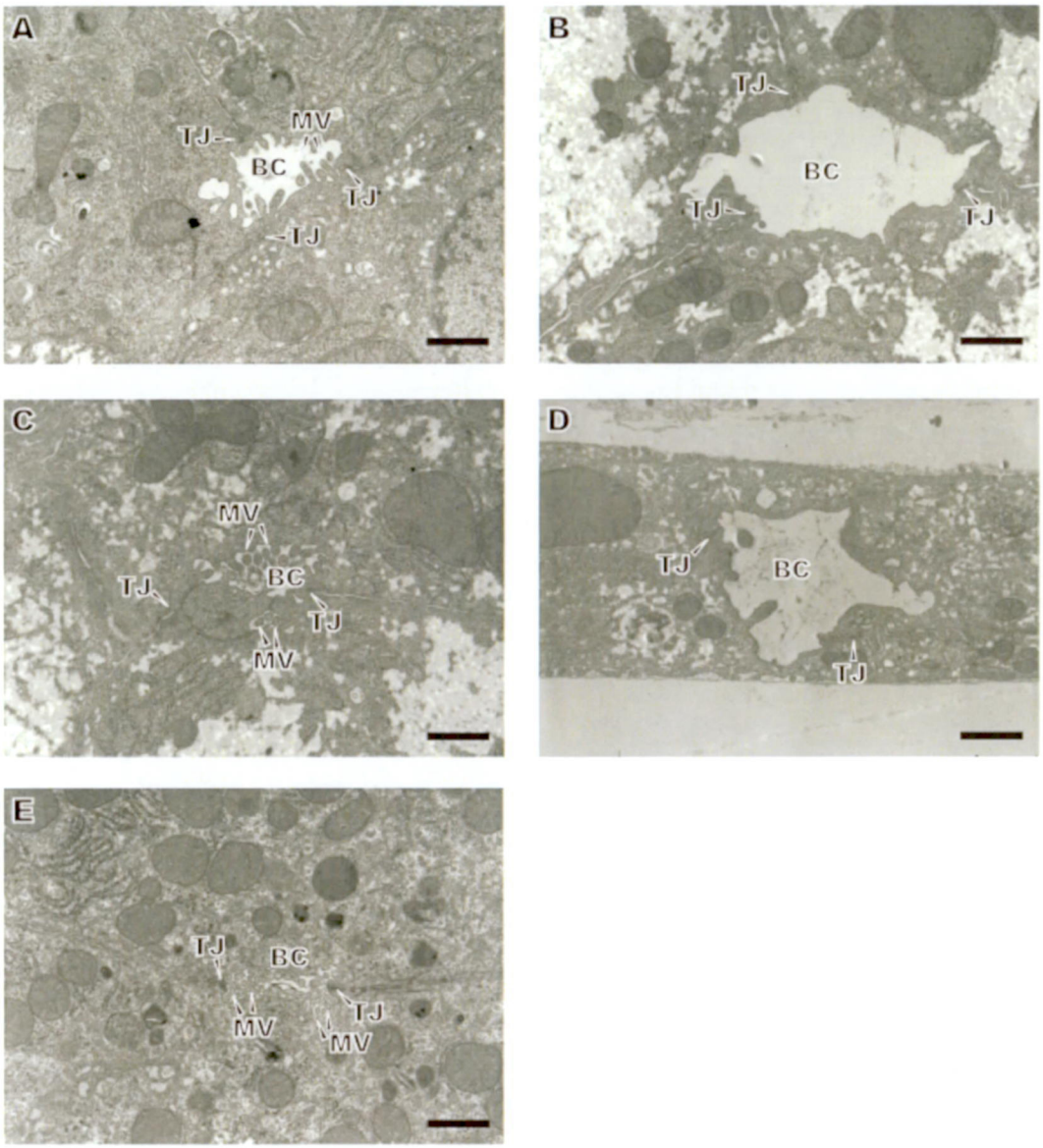

Figure 2.8 Transmission electron microscope (TEM) images of ultrathin section of hepatocyte spheroids cultured on 2.0NP for 96h without Matrigel overlay (A), hepatocyte spheroids cultured on 2.0NP for 96h with Matrigel overlay at 48 h post-seeding (B,C), sandwich-cultured hepatocytes for 96h (D), and rat liver tissue (E). Tight junctions (TJ), bile canaliculus (BC), and microvilli (MV) are indicated. Bars, 1 μm

Semi-quantitative gene expression analysis. The real-time PCR was performed to measure the relative amounts of gene expression among four kinds of culture conditions. Freshly isolated hepatocytes were used as the calibrator sample, which is indicated as time 0 in Figure 2.9. The expression of Abcc2 (ATP-binding cassette transporters superfamily C, member 2) tended to increase with time except for the ML culture, and those at 96 h for spheroids cultured on the NP plates with and without Matrigel were higher than those for the SW- and ML-cultured hepatocytes ($p<0.05$) (Figure 2.9A). The expression at 72 h for spheroids cultured on the NP plate with Matrigel overlay at 48 h was substantially higher than that for those cultured without Matrigel. However, the final values for these expressions at 96 h were virtually the same and were close to the initial level at time 0 (Figure 2.9A). While a substantial increase was also observed during the next 24 h after Matrigel overlay for the SW culture, a further increase over time was not observed.

Under all conditions except for the monolayer culture, the expression level of Cyp3a23/3a1 (cytochrome P450-3a23/3a1) increased over time (Figure 2.9B). Although the expression level for spheroids cultured on the NP plate with Matrigel overlay took 24 h after the overlay to substantially increase, that for the SW culture took 48 h. That is, there was a time lag between these two culture conditions. Comparison of the expressions at 96 h revealed that the one for spheroids cultured on the NP plate with Matrigel was much higher than the others ($p<0.05$).

While the albumin expressions for spheroids cultured on the NP plates and the ML-cultured hepatocytes tended to decrease during the first 48 h, that for spheroids cultured on the NP plate with Matrigel increased after Matrigel overlay at 48 h (Figure 2.9C). The expression for the SW-cultured hepatocytes trended upward for the first 72 h and then turned downward. Comparison of the expressions at 96 h showed that the one for spheroids cultured on the NP plate with Matrigel was much higher than that for the others ($p<0.05$). However, the expressions at 96 h were at most around 60% of the initial level.

The expression patterns for talin differed from those for the three other genes. The expression for the ML-cultured hepatocytes increased over time, resulting in a 2.5-fold higher level at 96 h than the initial level (Figure 2.9D). In contrast, for the other three conditions, the expression levels remained fairly constant, and the levels at 96 h were substantially lower than that for the ML culture ($p<0.05$).

The expression patterns for E-cadherin for spheroids cultured on the NP plate with Matrigel showed a substantial increase in a 24 h period after Matrigel overlay at 48 h

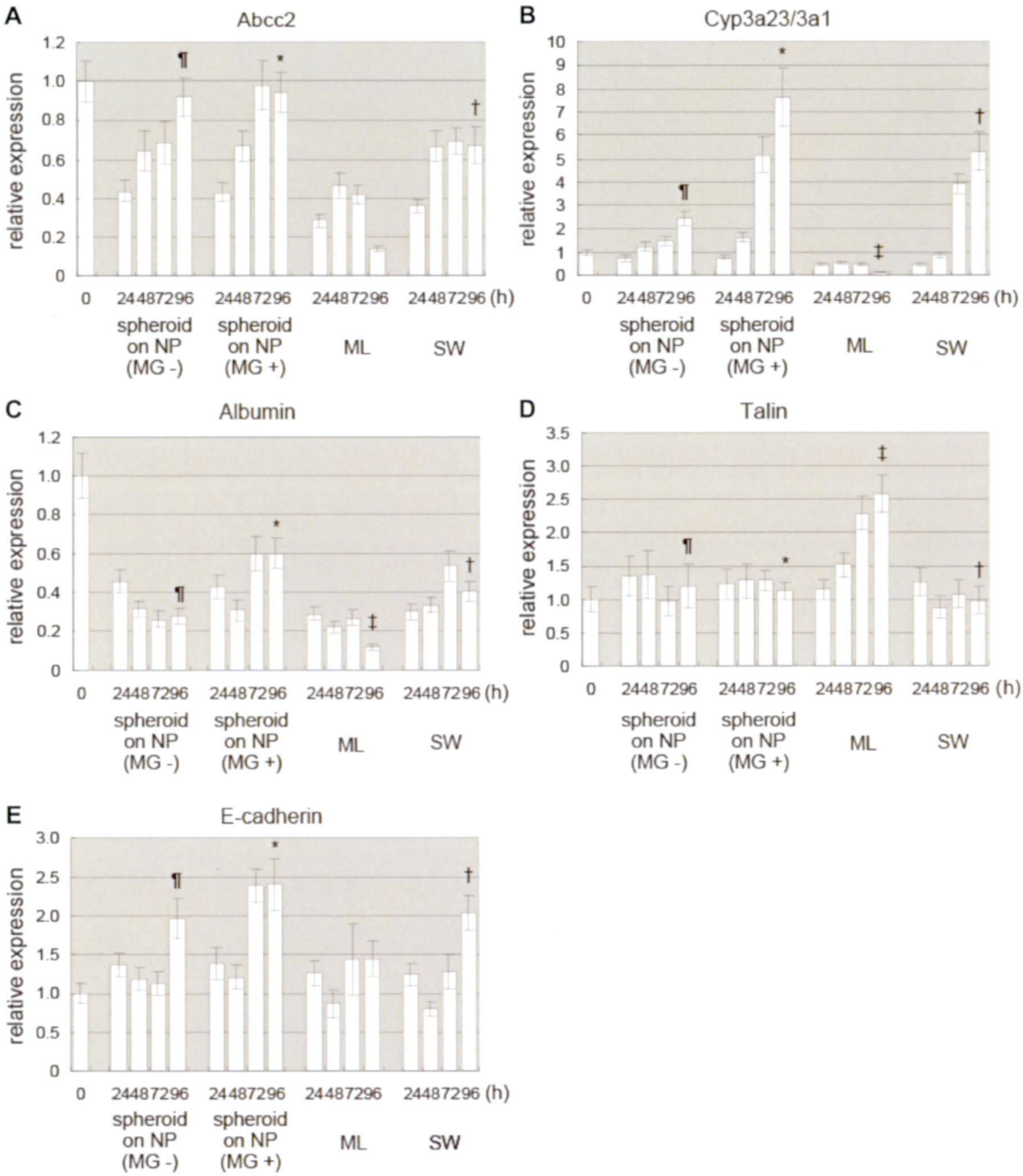

Figure 2.9 Semi-quantitative real-time PCR. Relative amounts of mRNA expression of Abcc2, Cyp3a23/3a1, albumin, talin, and E-cadherin were measured every 24 h under four culture conditions: culture on 2.0NP without Matrigel (MG -), culture on 2.0NP with Matrigel overlaid at 48 h post-seeding (MG +), monolayer culture in collagen-coat dish (ML culture), and sandwich culture (SW). Expression values of each gene were compared to freshly isolated hepatocytes (time 0, before seeding). Statistical comparison was performed for 96 h samples for each culture condition. A: $p<0.05$ for MG - (¶) or MG + (*) versus SW (†). B: $p<0.05$ for MG + (*) versus MG - (¶), ML (‡), or SW (†). C: $p<0.05$ for MG + (*) versus MG - (¶), ML (‡), or SW (†). D: $p<0.05$ for ML (‡) versus MG - (¶), MG + (*), or SW (†). E: Expressional levels have no statistically significant differences at $p<0.05$ for MG + (*) versus MG - (¶) or SW (†). The results are averages of three repetitions.

(Figure 2.9E). For the SW-cultured hepatocytes, expressional induction caused by Matrigel overlay was not showed within a 24 h. While the expression level for spheroids cultured on the NP plate with Matrigel at 72 h was higher than that for spheroids cultured on the one without Matrigel and the SW-cultured hepatocytes, the expressions at 96 h were not significantly different at $p<0.05$ for all conditions except ML culture.

2.3.3 Higher functional nanopillar 3-D spheroid

To examine MRP2 (multidrug resistance associated protein 2) (48,49), a translated product of Abcc2, works as a hepatocyte efflux transporter, a capability revealed in a previous gene expression study (Figure 2.10), a biliary excretion assay was conducted under two culture conditions: NP and SW. CDFDA, a substrate of MRP2 (50), was used to visualize the canalicular uptake and efflux. Fluorescence and phase-contrast micrographs were taken with an optical microscope every 24 h (Figure 2.10). Analysis of the micrographs revealed that CDFDA had accumulated inside both the NP-cultured spheroids and SW-cultured hepatocytes for 24 h (Figure 2.10A and C). Subsequently, CDF gradually accumulated inside both types of cells, and bile canaliculi formed in a time-dependent fashion (Figure 2.10E and G). Almost all the CDF were excreted into the canalicular networks in the final 48 h (Figure 2.10I, K, M, O, and Q). In comparison to those in the spheroids formed by culturing without Matrigel (Figure 2.10Q), the bile canaliculi that reconstituted in the spheroids formed by culturing with Matrigel (Figure 2.10M) were longer and more numerous.

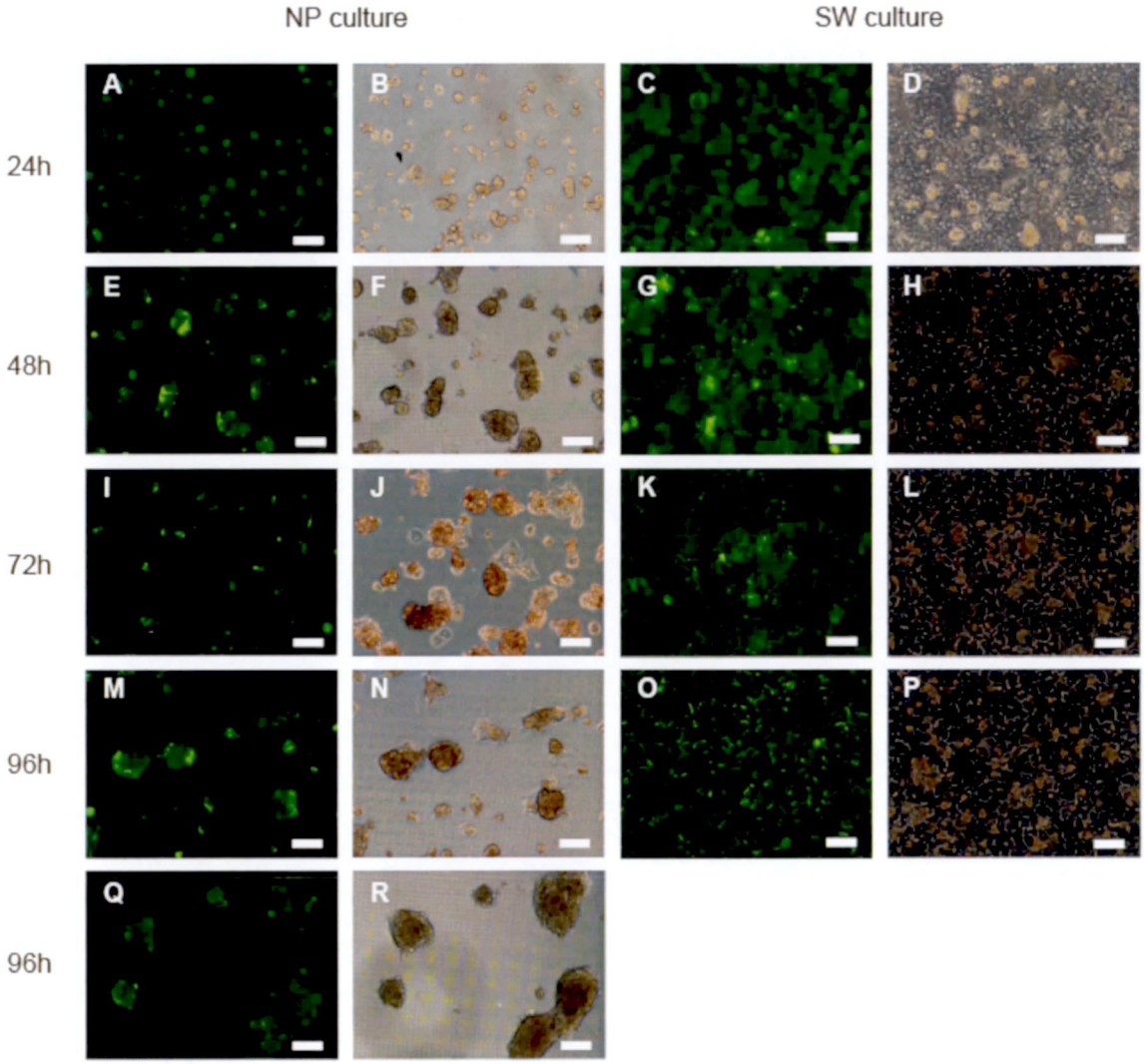

Figure 2.10 Biliary excretion assay. Hepatocytes were cultured on 2.0NP with or without Matrigel and in SW configuration. CDFDA was used to enable canalicular uptake and efflux to be visualized. Phase-contrast micrographs and fluorescent micrographs were taken every 24 h. Matrigel for NP spheroid was overlaid at 48 h post-seeding. A, E, I, M: fluorescent micrographs of NP-cultured spheroid with Matrigel; B, F, J, N: phase-contrast images of NP-cultured spheroid with Matrigel; C, G, K, O: fluorescent micrographs of SW culture; D, H, L, P: phase-contrast images of SW culture; Q: fluorescent micrographs at 96 h of NP-cultured spheroid without Matrigel; R: phase-contrast images at 96 h of NP-cultured spheroid without Matrigel. Bars, 100 μm

2.4 Discussion

In this study, hepatocyte spheroids with a compact and homogenous morphology in which the hepatocytes were individually round polygons, a configuration close to those of native liver, were formed by culturing with the NP plates. This spheroid formation could be controlled simply by altering the pillar diameter and pitch (Figure 2.4). As a result, a nanopillar diameter of 2.0 μm was found to be optimal in that the number of obtained spheroids with diameter of 50-100 μm. The downregulation of cell-substratum adhesion molecules of talin, a cytoskeletal protein, concentrated in the region of cell-substratum contact; focal adhesion and is capable of linking integrins to the actin cytoskeleton (51), were observed to form spheroids (Figure 2.9). It is conceivable that the pillar diameter modifies the cell-cell or cell-substratum adhesion force and thus the extent of cell migration, resulting in enhanced spheroid formation. Further study is needed to clarify the relationship among the pillar diameter, the expression and localization of cell-cell and cell-substratum adhesion molecules, and the signal transductions mediated by cellular adhesion and small GTPase such (52) for detailed understanding about the mechanism of pillar diameter-dependent spheroid formation.

Controlling the spheroid diameter is another critical issue to avoid the decrease of cellular viability or metabolic activity in terms of oxygen limitation at the center of spheroid. It is reported that the no oxygen limitation will take place in spheroids up to 100 μm in diameter (25). Culturing using microimprinting technology (38) or a two-dimensional multiarray technique (36) is more effective because spheroids are immobilized at a defined location and their diameter can be controlled by defining cell adhesion and non-adhesion areas. On the other hand, while it was also observed in the NP culture system that the number of hepatocytes or spheroids gradually decreased as the medium was changed because of weak adhesiveness to the substratum, this was improved by optimizing the pillar diameter in our experiments (Figure 2.4 and 2.5). In this experiment, 2.0NP had relatively uniform-sized spheroids ranging in 50-100 μm (Figure 2.5) and its ratio is 37.8% which is apparently higher than other four kinds of NP plate (Figure 2.5). Moreover, there is no need to immerse them in a chemical solution such as polyethylene glycol (PEG) (36,38) to define cell adhesion and non-adhesion area.

The hepatocytes of spheroids cultured on the NP plate with Matrigel were round polygons, morphology close to that of those in native liver (Figure 2.7). This is because the hepatocytes were surrounded by the extracellular matrix of the Matrigel, resulting in

the recovery of primary polarity by simulation of the native environment. One of the representative molecules indicating recovery is MRP2, which is a canalicular multispecific organic anion transporter and located exclusively in the canalicular membrane (53).The upregulation of the Abcc2 of the NP spheroids with Matrigel supports the positive effect of Matrigel on the recovery of primary hepatocellular polarity. Interestingly, the cells that did not contact the Matrigel directly showed a polygonal morphology (Figure 2.7). This indicates that intracellular signals were transmitted to all the hepatocytes constituting the spheroid. This phenomenon is considered to reflect the native structure, which supports a cuboidal cell shape, distinct polarity, and a three-dimensional cellular communication system (38). A polygonal morphology was not observed for the hepatocytes by SW culture. This may be because the hepatocytes were cultured in higher concentrations of type I collagen than those cultured on the NP plate. As a result, the cell-substrate adhesion force was stronger, causing the hepatocytes to be uniformly flat rather than polygonal. The use of a Matrigel overlay is thus effective for reconstituting morphologies similar to that of hepatocytes in native liver. It is effective when overlaid on spheroids and not on structures with a flat morphology like those formed by SW culturing.

The bile canaliculi of the spheroids cultured on the NP plate with a Matrigel overlay and of the SW-cultured hepatocytes with a Matrigel overlay tended to be larger (Figure 2.8). The presence of large-bore bile canaliculi in spheroids formed using Matrigel was confirmed by the results of biliary excretion assay (Figure 2.10). This is because reconstituted *in vitro* bile canaliculi were the closed structure where the excreted metabolites were accumulated. The uptake and efflux of the metabolites became even more active due to the Matrigel overlay, and eventually the closed bile canaliculi became larger. Since accumulated metabolites harm the hepatocytes and decrease cell viability (12,54), a method is needed to prevent this accumulation in order to obtain a more effective system for evaluating drug metabolism and toxicity.

The use of real-time PCR enabled us to quantitate the amount of expressed gene. The Abcc2 expressions of the spheroids cultured on the NP plates with and without Matrigel were higher than for those of the SW- and ML-cultured structures (Figure 2.9A). This indicates that spheroid formation on the NP plate is effective for Abcc2 expression. Cyps are ubiquitous superfamily of heme-containing monooxygenase enzymes that play a fundamental role in the metabolism of chemically diverse compounds, including endogenous chemicals and pharmaceutical agents (55,56). Serum albumin is a major protein synthesized almost exclusively by liver cells in animals, and

its concentration increases from low levels early in fetal development to a high plateau level in adults (57). Both Cyps and serum albumin are major indicators of hepatocellular function. The expression levels of these two genes were the highest for the spheroids cultured with Matrigel (Figure 2.9B, C), suggesting that overlaying Matrigel on 3-D structure, spheroids, is more effective on transcription level of the two genes than overlaying that merely on 2-D hepatocytes such as SW culture. In contrast, the expression level of talin was the highest for the monolayer-cultured hepatocytes (Figure 2.9D). These findings are consistent with those of the immunohistochemical analysis (Figure 2.6), which showed that the actin stress fibers were formed with ML culturing, unlike spheroids cultured on the NP plate. This means the talin was overexpressed with ML culture (58) which was consistent with the result revealed by real-time PCR (Figure 2.9D). The expression of E-cadherin of the spheroids cultured with Matrigel at 72 h was higher than other culturing conditions at 72 h (Figure 2.9E). This indicates that Matrigel-overlaying has a faster effect on E-cadherin expression than on flat structures such as SW culture. There was no particular culture condition showing a particularly high expression of E-cadherin at 96 h among the NP culturing with, without Matrigel, and SW culturing (Figure 2.9E). It has been reported that E-cadherin expression needs to form 3-D structures such as spheroids (59,60), which is consistent with our findings (Figure 2.9).

2.5 Conclusion

In conclusion, the present results suggest that the spheroid formation of rat primary hepatocytes was controlled by optimizing the pillar diameters of NP plate and that the combination of spheroid formation and Matrigel overlaying have positive effects on hepatocyte viability, polarity, and functions. The present study demonstrates that it is practically possible to control the formation of spheroid only by optimizing the physical property of substrate surface. The mechanism of spheroid formation on the NP plate was speculated to be correlated with less-expression of cell-matrix related protein such as Talin by immunohistochemical and gene expression analysis. Our next challenge is to examine the 3-D spheroid cultured by the NP plate has hepatocellular functions related to drug metabolism and pharmacokinetics (DMPK) comprehensively. This verification will contribute to establish an *in vitro* drug screening method that reflects a drug's DMPK properties within the body.

Chapter 3

Global Gene Expression Analysis of Nanopillar-Cultured Spheroids

3.1 Introduction

In the preclinical stage of drug discovery, evaluating drug metabolism and pharmacokinetics (DMPK) is essential (61). To determine the DMPK properties of drug candidates, it is necessary to evaluate the process of absorption, distribution, metabolism, and excretion (ADME) within the body (61). Most of these evaluations are currently performed using a whole animal (13). Unfortunately, only a small fraction (~11%) of drug candidates that were selected for clinical development eventually have become marketed drugs in recent years (3,6). The failure rate of drugs in clinical trials could be attributed to poor DMPK and low bioavailability (4,61). This situation explains the fact that animal study may not be sufficient for predicting the fate of drug candidates in humans (5,6). Accordingly, there is a growing need for an *in vitro* cell-based assay method for evaluating DMPK properties that can extrapolate to human very early in the drug discovery process. This makes a contribution to reduction of the attrition during development instead of using the conventional *in vivo* preclinical test that uses animals (5). Suitable DMPK features of a drug are essential in regard to the reliable selection of effective drug candidates in the clinical development stage and successful progression of those candidates without attrition through clinical evaluation (61).

To date, primary hepatocytes have been extensively used as a cell source for studying *in vitro* drug metabolism and excretion. Hepatocytes in their native

environment possess a structural polarity and liver-specific functions such as drug metabolizing or albumin secretion (17,18). Conventionally cultured hepatocytes have a spreading-monolayer morphology on an extracellular matrix (ECM)-coated culture surface (11,30,62). The intrinsic differentiated structure and function of hepatocytes rapidly deteriorate or are lost and cannot be recovered under such monolayer culture conditions (12,17). Accordingly, this 2-D monolayer culture system has difficulty in predicting such a metabolic process as DMPK in all native environments. This difficulty is one of the potential limiting factors in establishing an *in vitro* assay system.

In comparison, 3-D hepatocyte spheroids sustain viability for extended culture periods and higher liver-specific functions (10,17,63-66). A spheroid culture system is thus an alternative culture technique for evaluating drug metabolism in the course of drug screening (12,13). The authors previously developed culture devices for forming 3-D spheroids, namely, nanopillar (NP) plate, and reported that the spheroid formation of rat primary hepatocytes was controlled by optimizing the pillar diameters and pillar pitch (pillar center-to-center distance) of the NP plate (64). In the report, the NP-cultured spheroids possessed higher viability and polarity, and liver-specific functions related to metabolism and excretion were also induced by overlaying Matrigel on the spheroids. These hepatocellular functions were assessed by using a gene-expression analysis of the Cyp3a23/3a1 and Abcc2 genes with a real-time polymerase chain reaction (PCR) and by using a CDFDA excretion assay. In addition, the NP plate has an advantage in that it can be used to set up more reproducible culture conditions because its surface geometry can be designed artificially (64). These advantages of the NP culture will contribute to acquiring stable and reproducible data at early stage and establishing an alternative culturing technique for evaluating metabolism and toxicity in future drug screening processes.

Toward establishing an *in vitro* drug screening method that reflects a drug's DMPK properties within the body, the objective of the current study is to elucidate that the expression levels of Cyp (cytochrome P450), Ugt (UDP-glucuronosyltransferase), and transporter genes are higher overall in the NP-cultured 3-D spheroids than in the conventional 2-D tissue. Taking particular note of these DMPK-related genes, we therefore performed a genome-wide gene-expression analysis by using a DNA microarray to assess the gene expression profiles of four different conditions, namely, NP, sandwich (SW), and monolayer (ML) cultures and freshly isolated hepatocytes. The DNA microarray analysis could show an entire image of the gene expression profile that cannot be read in the real-time PCR that focuses on individual genes. Moreover,

pathway analysis based on the altered gene expression reveals the expressional dynamics. In this chapter, we describe the 3-D spheroids formed by the NP culture possess a higher ability of metabolism and excretion than does 2-D tissue formed by the conventional monolayer culture. The result suggests that the NP culture is valuable for evaluating metabolism and toxicity toward new drug development.

3.2 Materials and Methods

3.2.1 Nanopillar plate preparation

Preparation of the NP plate was described in chapter 1 (Figure 2.3A) (64). In brief, a 1.0-mm-thick polystyrene film was spin-coated onto a glass substrate. A nanomold was made of silicon wafer and fabricated by photolithography. The NP plate with a 2.0-μm pillar diameter and with pitches twice the pillar diameter were formed by pressing the mold onto the film at 423 K and then releasing it at room temperature. The NP plate was precoated with a solution containing 100 ng/ml of type-I collagen.

3.2.2 Hepatocyte culture

Hepatocytes were isolated from six- to eight-week-old specific viral-pathogen-free male Fisher rats weighing about 150-250 g (Charles River Japan Inc., Japan) by modified two-step *in situ* collagenase perfusion (42) and purified by Percoll gradient separation (43). The viability of the hepatocytes was determined by trypan blue exclusion, and hepatocytes with over 85% viability were used for the following culture.

The hepatocytes were resuspended in William's E medium containing 10% fetal bovine serum supplemented with 8.6 nM of insulin (Sigma-Aldrich Corp., MO), 255 nM of dexamethasone (Nacalai Tesque, Inc., Japan), 50 ng/ml of epidermal growth factor (Sigma-Aldrich Corp.), and 5 KIU/ml of aprotinin (Wako Pure Chemical Industries, Ltd., Japan). The cells were seeded at a density of 1×10^5 cells/cm^2 onto prepared NP plates or into a 35-mm-diameter culture dish (AGC Techno Glass Co., Ltd., Japan) in which type-I collagen was pre-coated. The seeded hepatocytes were incubated in a humidified chamber with 5% CO_2 at 37°C. The procedure for the NP, SW, and ML cultures is described below.

NP culture (64): after 24 hours of post-seeding, the medium was replaced with

serum-free William's E medium containing the same supplements described above. After 48 hours of post-seeding, the medium was replaced with a serum-free medium containing Matrigel™ (BD Bioscience, MA) with the same supplements described above. Subsequently, the culture medium was changed daily. Hepatocytes were cultured in total for 96 hours.

SW culture (31,32): after 24 hours of post-seeding, the culture medium was replaced with serum-free William's E medium containing Matrigel (BD) with the same supplements described above. Subsequently, the culture medium without Matrigel was changed daily. Hepatocytes were cultured in total for 96 hours.

ML culture: the culture medium was replaced with serum-free William's E medium every 24 hours. Hepatocytes were cultured in total for 96 hours.

3.2.3 DNA microarray analysis

Total RNA was extracted from the four kinds of samples mentioned above by using an RNeasy Plus Micro Kit (Qiagen GmbH, Germany) according to the manufacturer's instructions. The quantity and quality of the RNA were determined with a Nanodrop ND-1000 spectrophotometer (Thermo Fisher Scientific Inc., Waltham, MA) and an Agilent Bioanalyzer (Agilent Technologies, Palo Alto, CA), as recommended.

Total RNA was amplified and labeled with Cy3 (Cyanine 3) by using an Agilent Low Input Quick Amp Labeling Kit, one-color (Agilent Technologies, Palo Alto, CA) following the manufacturer's instructions. Briefly, 100 ng of total RNA was reverse-transcribed to double-strand cDNA by using a poly dT-T7 promoter primer. The primer, template RNA, and quality-control transcripts of the known concentration and quality were first denatured at 65°C for 10 min and incubated for two hours at 40°C with 5X first-strand buffer, 0.1-M DTT, 10-mM dNTP mix, and AffinityScript RNase Block Mix. The AffinityScript enzyme was inactivated at 70°C for 15 min. cDNA products were then used as templates for *in vitro* transcription to generate fluorescent cRNA. The cDNA products were mixed with a transcription master mix in the presence of T7 RNA polymerase and Cy3 labeled-CTP and incubated at 40°C for two hours. The labeled cRNAs were purified by using Qiagen's RNeasy mini spin columns and eluted in 30 μl of nuclease-free water. Subsequently, the amplified cRNA quantity and labeled cyanine incorporation were determined by using the Nanodrop ND-1000 spectrophotometer and the Agilent bioanalyzer (67). 1.65 μg of Cy3-labeled cRNA was fragmented and hybridized at 65°C for 17 hours to an Agilent Whole Rat Genome Microarrays 4×44K

(Design ID: 014879). Finally, microarrays were scanned by using an Agilent DNA microarray scanner.

The microarray data were analyzed by using a GeneSpring GX 10.0.2. (Agilent Technologies) at DNA Chip Research Inc. (Kanagawa, Japan). The raw microarray data are available in the GEOarchive file format in the Gene Expression Omnibus with accession number GSE38950 at http://www.ncbi.nlm.gov/geo/. The intensity values of each scanned feature were quantified by using an Agilent Feature Extraction Software version 10.5.1.1, which performs background subtractions. Only features that were flagged as not errors (present flags) were used, and features that were not positive, not significant, not uniform, not above the background, saturated, and population outliers (marginal and absent flags) were excluded. Normalization was performed by using the Agilent GeneSpring GX version 10.0.2. (per chip: normalization to 75-percentile shift; per gene: normalization to median of all samples) (67). There are a total of 41,012 probes on the Agilent Whole Rat Genome Microarray 4x44K (Design ID: 014879), and there are no control probes. Data filtration was performed, and we eventually acquired a valid 22,596 probe set, where at least four out of a total of twelve samples had had the present flag for further analysis. The altered transcripts were quantified by using the comparative method. To identify significant differences in gene expression between samples, False Discovery Rate (FDR)-corrected p-value <= 0.01 combined with >= 2 to 10-fold change in signal intensity was applied in this study. Hierarchical clustering analysis (HCA) (68) and principal component analysis (PCA) (69) were performed by using the GeneSpring GX 10.0.2.

Gene expression data were mapped to rat pathways of GenMAPP 2.1, and MAPPFinder 2.0 was used to find significant pathways in which a relative amount of genes satisfy the following several-fold-change criteria: 4.0 < [ML/NP] < 8.0, 2.0 < [ML/NP] < 4.0, -4.0 < [ML/NP] < -2.0, -8.0 < [ML/NP] <-4.0, 4.0 < [SW/NP] < 8.0, 2.0 < [SW/NP] < 4.0, -4.0 < [SW/NP] < -2.0, and -8.0 < [SW/NP] <-4.0.

3.3 Results

3.3.1 Tissue morphology under three different culture conditions: NP, SW, and ML cultures

Rat primary hepatocytes were cultured to compare tissue morphologies produced under three different culture conditions, namely, NP, SW, and conventional ML cultures. Phase-contrast micrographs of the cultures at 96 hours of post-seeding are shown in Figure 3.1. Spheroids with diameters of 50 to 100 μm and a compact morphology in which individual cells can barely be distinguished on the NP plate were observed (Figure 3.1A). Clear bile canaliculi were observed at cell-cell adhesion sites in the SW culture, meaning that each cell had a higher structural polarity (Figure 3.1B, arrow heads). Individual cells strongly adhered to the substrate and spread in the ML culture (Figure 3.1C).

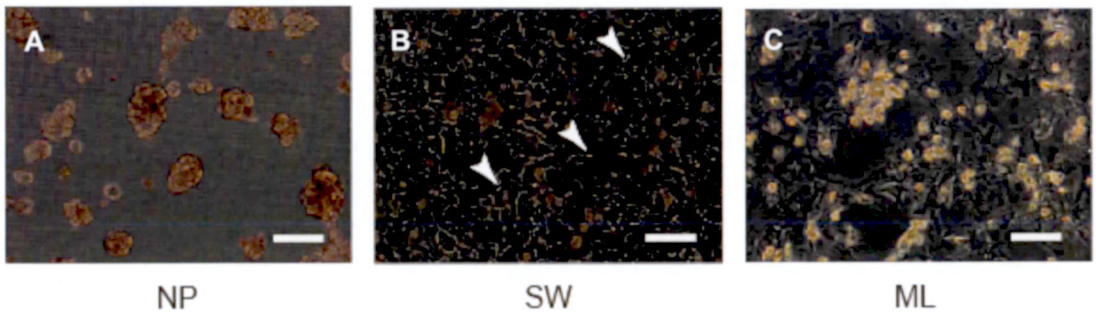

Figure 3.1 Phase-contrast micrographs of (A) nanopillar (NP)-, (B) sandwich (SW)-, and (C) monolayer (ML)-cultured hepatocytes. Micrographs were taken at 96-h post-seeding. Bars: 100 mm.

3.3.2 Determination of individual variability by hierarchical clustering analysis (HCA)

To investigate the expressional change of DMPK-related genes in these three kinds of cultured tissue and freshly isolated hepatocytes that resemble native liver parenchymal cells, DNA microarray analysis was conducted. To visualize possible similarities and differences between gene expression profiles, hierarchical clustering analysis (HCA) was performed after whole genome gene expression profiles of four groups were generated by using the Agilent Whole Rat Genome Microarrays 4×44K.

Hierarchical clustering of gene expressional data is an intuitive way to analyze the

expressional trends of differentially expressed genes and the relationships between different groups of gene expression patterns. HCA of all 22,596 probes was performed by using the GeneSpring software to examine the similarity of gene expressional profiles of four groups, namely, NP, SW, ML cultures and freshly isolated hepatocytes. The number of samples in each group was three, which are from three different rats (biological replicates). A hierarchical cluster diagram of these 12 samples (freshly isolated hepatocytes-1, -2, and -3; ML-1, -2, and -3; SW-1, -2, and -3; and NP-1, -2, and -3) based on the HCA results is shown in Figure 3.2. The diagram showed that the 12 samples were divided into four clusters according to the four groups. This result indicates that the individual variability in each expressional profile was little. NP and SW belonged to the same cluster by clustering with higher hierarchy. This result means that the expression profile of the NP culture is related more closely to that of the SW culture that was reported to reflect the native environment rather than to that of the ML culture. The freshly isolated hepatocytes had longer clustering distances to all the other groups.

3.3.3 Close association between NP and freshly isolated hepatocytes investigated by principal component analysis (PCA)

The similarity and differences between the genome-wide gene expressions of the NP, SW, and ML cultures and freshly isolated hepatocytes (the number of samples in each group is three of biological replicates) were further investigated by principal component analysis (PCA). PCA allows correlations in datasets to be visualized by compressing information in a low number of dimensions. The method is very flexible, and large datasets can be handled easily. An important step in PCA is determining the number of latent variables, which contain relevant information (69). PCA with all 22,596 probe sets was performed by using the GeneSpring software. The three most variable principal components (PC1, PC2, and PC3) are plotted in three dimensions in Figure 3.3. In the graph, freshly isolated hepatocytes and ML are plotted widely apart, and NP and SW are plotted closely between freshly isolated hepatocytes and ML in PC1 (63.3%). NP is plotted slightly closer to the freshly isolated hepatocytes than is SW in PC1, which means that the expressional profile of NP is more similar to that of the freshly isolated hepatocytes than that of SW. NP and SW are plotted closely, as well as the freshly isolated hepatocytes and ML, in PC2 (26.8%). However, these two groups are plotted widely apart in PC2, respectively.

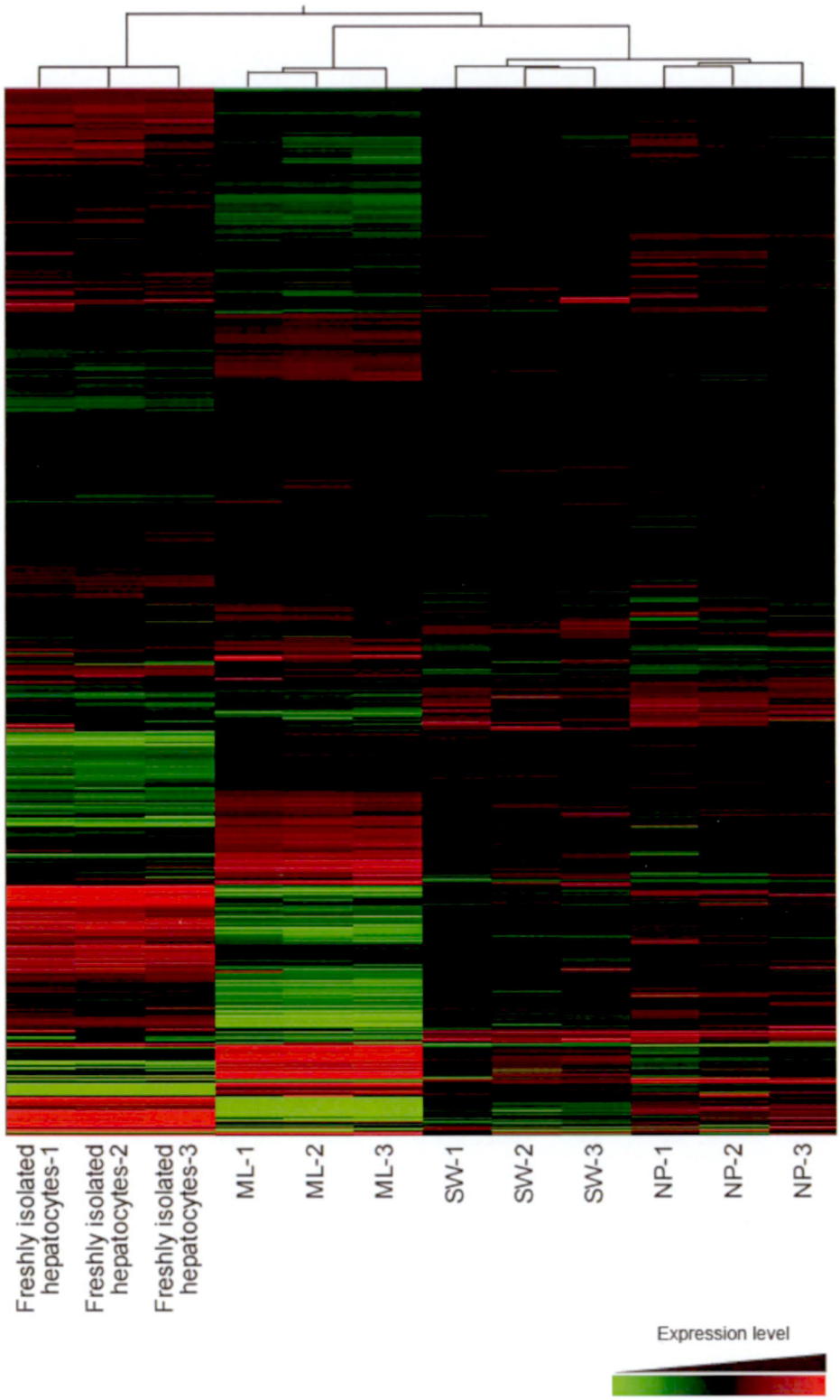

Figure 3.2 Hierarchical clustering analysis of gene expression of freshly isolated hepatocytes-1, -2, and -3, ML-1, -2, and -3, SW-1, -2, and -3, and NP-1, -2, and -3. The clustering is based on all the 22,596 probes that passed quality filtering. Data were subjected to HCA by using a Euclidian-distance calculation based on the centroid-linkage rule.

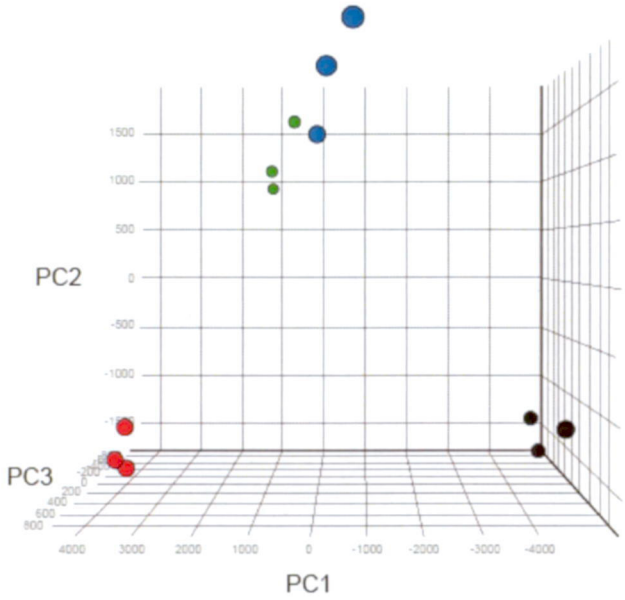

Figure 3.3 Principal component analysis of gene expression of freshly isolated hepatocytes-1, -2, and -3, ML-1, -2, and -3, SW-1, -2, and -3, and NP-1, -2, and -3. For the 22,596 probes that passed quality filtering, the relative contribution of the variance is shown by three major principal components plotted in three dimensions.

3.3.4 Higher hepatocellular functions related to drug metabolism and excretion in the NP-cultured 3-D spheroid

To assess the expressional changes of DMPK-related genes under four different conditions, the genes of the following three kinds were analyzed: 1) Cyps, which encode a ubiquitous superfamily of heme-containing monooxygenase enzymes that plays a fundamental role in the metabolism of chemically diverse compounds such as endogenous chemicals and pharmaceutical agents (55), 2) Ugts, which encode catalyze enzymes whose role is to add a glycosyl group from a UTP-sugar to a small hydrophobic molecule (70), and 3) Slcos (solute-carrier organic anion transporters) and Abccs, which encode uptake and excretion transporters, respectively (71). The expressional ratios of NP/ML, NP/SW, and NP/freshly isolated hepatocytes are

represented from top down for each gene in Figure 3.4. In the case that the expression level in the denominator is higher than that in the numerator, the expressional ratio will converge at 0 to 1. To avoid the graphs becoming illegible, the horizontal axis in Figure 3.4 is the exponent.

First, the gene expressions of Cyps were analyzed (Table 3.1). The translation products of Cyps, which are called "phase I metabolic enzymes", metabolize approximately 70% of drugs in clinical use, and these Cyps belong to Cyp families 1 to 3 (72). In this case, of the valid results for 66 genes belonging to all Cyp families, the results of 14 genes belonging to Cyp 1 to 3 are described (Figure 3.4). The results showed that the Cyps expression level of NP was higher than that of ML in all 12 genes. Furthermore, that of NP was higher than that of SW in the 10 genes not including Cyp1a2 and 2j4. These results mean that the Cyps expression level of the 3-D NP culture was higher than that of a conventional 2-D culture such as SW and ML, which indicates that the 3-D NP culture exhibited better performance closer to an *in vivo* environment than did the conventional 2-D culture. When the NP culture was compared with freshly isolated hepatocytes, the expression levels of Cyp1a1 and 3a23/3a1 in the NP culture were significantly higher.

Next, the gene expressions of Ugts were analyzed (Table 3.1). The translation products, which are called "phase II metabolic enzymes", metabolize about 30-40% of drugs in clinical use (72), and these expressions were analyzed. As a result, the expression level of the NP was higher than that of ML and SW in all genes except for Ugt1a2 (Figure 3.4). This result indicates that the expression levels of the phase II genes were increased more in the 3-D spheroid by the NP culture than in the 2-D tissue by the conventional ML culture. The expression level of Ugt1a1, one of the key conjugation enzymes whose substrate is a bilirubin, was the highest in the NP culture in all four conditions. Sults (Sulfotransferases) and Gsts (glutathione S-transferases) are also predominant phase II metabolic enzymes. In the present study we investigated the Sult1c1 and Ste (Sult1e1) genes as Sult genes, and Gstm1 (glutathione S-transferase M1) as Gst gene. The expressions of Sult1c1 and Ste in NP-cultured 3-D spheroids were both higher than those in monolayered ML and SW although they were less than freshly isolated hepatocytes (Figure 3.4). The expression of Gstm1 was increased more in the NP-cultured 3-D spheroid than in the 2-D tissues by the conventional ML and SW cultures. As a result, the expressions of genes not only Ugts but also Sults and Gsts in NP-cultured 3-D spheroids were higher than those in monolayered ML and SW.

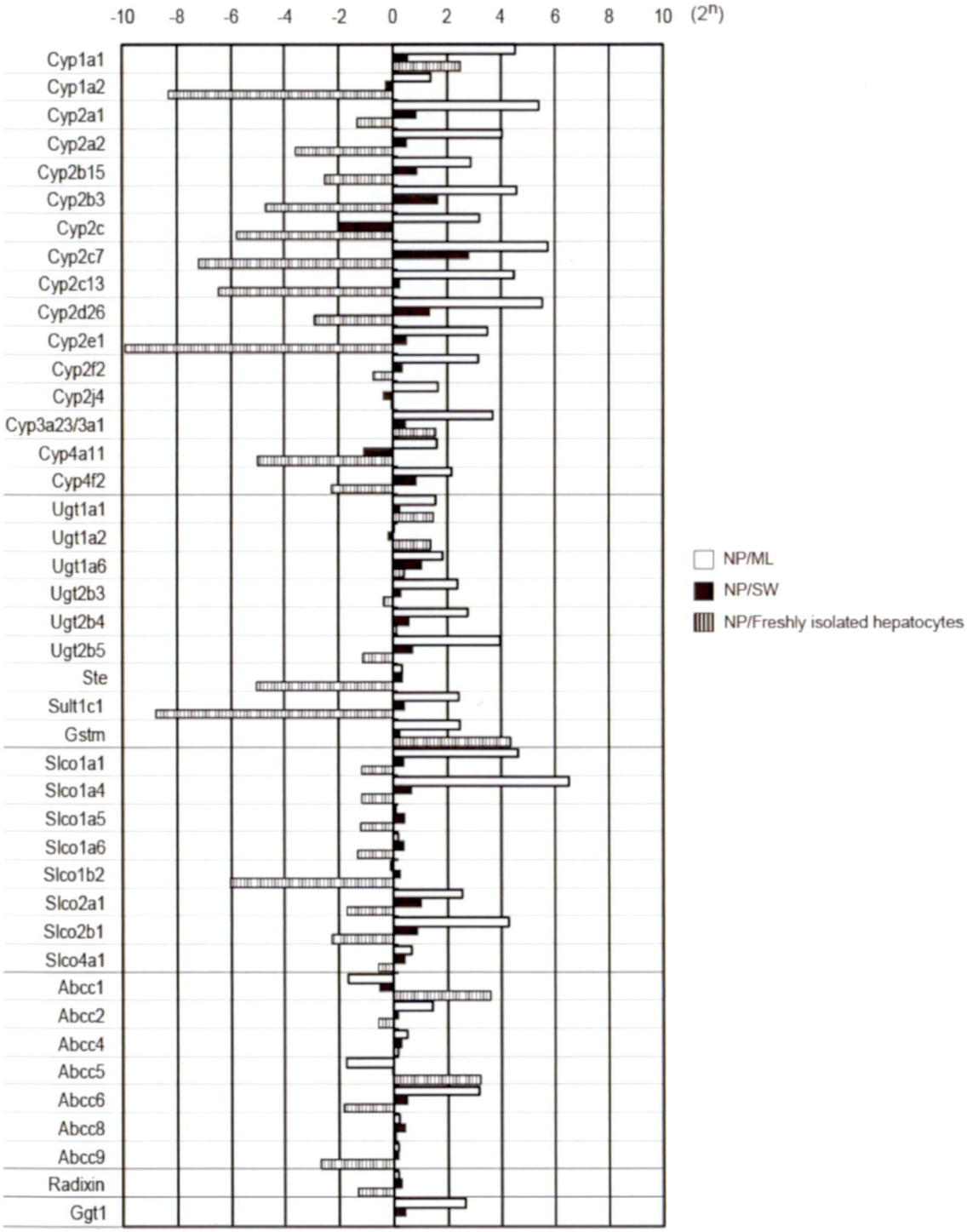

Figure 3.4 Quantitative comparison of phase-I (i.e., Cyp), phase II (i.e., Ugt), uptake (i.e., Slco), excretion transporter (i.e., Abcc) and Radixin mRNA in hepatocytes from NP culture with mRNA in hepatocytes from ML culture (NP/ML), mRNA in hepatocytes from NP culture with mRNA in hepatocytes from SW culture (NP/SW), and mRNA in hepatocytes from NP culture with mRNA in freshly isolated hepatocytes (NP/freshly isolated hepatocytes).

Table 3.1 Genes investigated in this study

Probe name	Accession ID	Gene symbol	Major GO term biological process
A_43_P15534	NM_017111	Slco1a1	GO:0006811(ion transport)
A_42_P708480	NM_131906	Slco1a4	GO:0006811(ion transport)
A_44_P203532	NM_131906	Slco1a4	GO:0006811(ion transport)
A_44_P113879	NM_030838	Slco1a5	GO:0006811(ion transport)
A_44_P320677	NM_130736	Slco1a6	GO:0006811(ion transport)
A_44_P328097	NM_031650	Slco1b2	GO:0006811(ion transport)
A_44_P373483	NM_022667	Slco2a1	GO:0006810(transport)
A_44_P491450	NM_080786	Slco2b1	GO:0006810(transport)
A_44_P128007	NM_080786	Slco2b1	GO:0006810(transport)
A_44_P337125	NM_133608	Slco4a1	GO:0006810(transport)
A_44_P321009	NM_012540	Cyp1a1	GO:0006118(electron transport)
A_44_P142025	NM_012541	Cyp1a2	GO:0006118(electron transport)
A_42_P654578	NM_012692	Cyp2a1	GO:0006118(electron transport)
A_44_P356143	NM_012693	Cyp2a2	GO:0006118(electron transport)
A_44_P316194	NM_017156	Cyp2b15	GO:0006118(electron transport)
A_44_P205599	NM_173294	Cyp2b3	GO:0006118(electron transport)
A_44_P280786	NM_019184	Cyp2c	GO:0006118(electron transport).
A_43_P13939	NM_017158	Cyp2c7	GO:0006118(electron transport)
A_44_P327817	NM_138514	Cyp2c13	GO:0006118(electron transport)
A_44_P325666	NM_012730	Cyp2d26	GO:0006118(electron transport)
A_44_P409232	NM_031543	Cyp2e1	GO:0006118(electron transport)
A_42_P678870	NM_019303	Cyp2f2	GO:0006118(electron transport)
A_42_P792497	NM_023025	Cyp2j4	GO:0006118(electron transport)
A_42_P785801	NM_173144	Cyp3a23/3a1	GO:0006118(electron transport)
A_44_P147020	NM_001044770	Cyp4a11	GO:0006118(electron transport)
A_43_P12051	NM_019623	Cyp4f2	GO:0006118(electron transport)
A_44_P446578	NM_012683	Ugt1a1	GO:0006789(bilirubin conjugation)
A_44_P432355	NM_201423	Ugt1a2	GO:0008152(metabolic process)
A_44_P402641	NM_201423	Ugt1a2	GO:0008152(metabolic process)
A_44_P432358	NM_057105	Ugt1a6	GO:0006805(xenobiotic metabolic process)
A_44_P247784	NM_153314	Ugt2b3	GO:0006805(xenobiotic metabolic process)
A_44_P236068	NM_001004271	Ugt2b4	GO:0008152(metabolic process)
A_42_P670179	NM_001007264	Ugt2b5	GO:0008152(metabolic process)
A_44_P405190	NM_031732	Sult1c1	GO:0006790(sulfur metabolic process)
A_44_P359759	NM_012883	Ste	GO:0008202(steroid metabolic process)
A_43_P11776	NM_017014	Gstm1	GO:0008152(metabolic process)
A_44_P252417	NM_022281	Abcc1	GO:0006810(transport)
A_43_P11580	NM_012833	Abcc2	GO:0006810(transport)
A_44_P344679	NM_133411	Abcc4	GO:0006811(ion transport)
A_44_P257526	NM_133411	Abcc4	GO:0006811(ion transport)
A_42_P568172	NM_053924	Abcc5	GO:0006810(transport)
A_42_P463998	NM_031013	Abcc6	GO:0006200(ATP catabolic process)
A_43_P11674	NM_013039	Abcc8	GO:0005975(carbohydrate metabolic process)
A_44_P455479	NM_013040	Abcc9	GO:0006810(transport)
A_44_P219628	NM_053840	Ggt1	GO:0006520(amino acid metabolic process)
A_44_P385117	NM_001005889	Rdx	GO:0045176(apical protein localization)

Third, the expressions of transporter genes whose translation products have the significant role of taking substrate into hepatocyte and excreting bile acid or metabolites into bile canaliculi were analyzed (Table 3.1). As in the current pre-clinical *in vivo* trials using animals, quantitative assessment of uptake and excretion will be predominant, which will be similar for *in vitro* assays using cells in the future (73). A number of uptake transporters are expressed on the hepatocellular membrane. In particular, OATPs that are the translation products of Slco genes perform a crucial role in the uptake of bile acids or one of the primary pharmaceutical agents of HMG-CoA reductase inhibitor such as pravastatin, pitavastatin, atorvastatin, and fluvastatin (74). Then, we analyzed the expressions of the Slco genes. The result showed that the expression level of almost all the Slco transporter genes from the 3-D NP culture tended to be higher than that from the conventional 2-D ML or SW cultures (Figure 3.4). In contrast, the expression levels of all the Slco genes investigated in this study from the NP culture were lower than that from freshly isolated hepatocytes (Figure 3.4). This result indicates that establishing an *in vitro* culture system that reconstructs the expression level of uptake transporter genes similar to the native liver is difficult even if the formation of 3-D tissue by the NP culture was achieved. From the viewpoint of drug metabolism, Slco1a1 is a key molecule whose substrates are bile acids and the cholesterol-lowering pravastatin (75). The expression level of this gene extracted from the 3-D NP culture was 24 times higher than that from the 2-D ML culture (Figure 3.4). Although the absolute values of expressional ratios determined by the current microarray analysis are different from those determined by previous real-time PCR analysis (data not shown), the expressional trend of Slco1a1 was reproduced. The expression trend of Abcc genes is different for each individual gene. The expression of Abcc2, whose main function is to excrete glucuronidated bilirubin to bile acid (48,49), and that of Abcc6, whose function is unknown so far (53), were both higher in the NP-cultured 3-D spheroid than in the ML-cultured 2-D tissue. In contrast, the expression of Abcc1, whose function is to excrete glutathione conjugate or leukotriene (76,77), and that of Abcc5, whose main function is to excrete cyclic nucleotide (78), were both higher in the ML-cultured 2-D tissue than in the NP-cultured 3-D spheroid (Figure 3.4). Abcc2 plays a significant role in the excretion of metabolized bile acids in hepatocyte to bile canaliculi, and this is the gene that we have ever been focusing on. We previously reported that the gene expression level of the Abcc2 gene in the NP-cultured 3-D spheroid was determined to be about five times higher than in the ML-cultured 2-D tissue by using real-time PCR analysis (64). In comparison, it was three times higher according to the results of the

present study using microarray analysis. As a result, the 3-D spheroid culture using the NP plate was endorsed to be a more effective method for Abcc2 expression. Furthermore, we specified Ggt1 (gamma-glutamyltransferase 1) whose molecular function is gamma-glutamyl transpeptidase (γGTP) activity, which is the major enzyme in liver (79,80). γGTP is present in the cell membranes of many tissues, including the bile duct, and involved in amino acids transfer and metabolism. This means γGTP is the primary indicator of hepatic function such as biliary excretion that we have been focusing on. Although we could not obtain the data of freshly isolated hepatocyte, the expression of Ggt1 in cells cultured by NP was higher than that by monolayer and SW. This is the important finding to upgrade the value of the NP culture.

Pathway analyses were introduced to characterize the expressional profile obtained under different culture conditions (Table 3.2). In order to investigate the metabolic ability of 3-D spheroids formed by the NP plate, we focused on the Irinotecan pathway (http://www.pharmgkb.org/pathway/PA2001). As a result, the pathway was more activated in the NP-cultured 3-D spheroids than in the ML- or SW-cultured 2-D tissue under the assumed criterion of -4.0 < [ML/NP] < -2.0 and -4.0 < [SW/NP] < -2.0. The dynamics of ADME-related molecules in liver cells such as Oatps, Cyps, Ugts, and Abccs, which are the molecules we specified in this study, are depicted in this Irinotecan pathway and are also involved in the pharmacokinetics of other common drugs and xenobiotics. The result indicates that 3-D spheroids formed by the NP culture possessed higher metabolic ability than did those formed by the conventional 2-D monolayer culture.

Table 3.2 Pathway analysis

MAPP name	Criteria	Z score	Permute P-value
Regularion of actin cytoskeleton	2.0<[ML/NP]<=4.0	4.577	0
Alpha6-beta4-integrin	2.0<[ML/NP]<=4.0	3.032	0
Alpha6-beta4-integrin	2.0<[SW/NP]<=4.0	3.614	0.005
Focal adhesion	2.0<[SW/NP]<=4.0	2.452	0.02
Irinotecan pathway	-4.0<[ML/NP]<=-2.0	3.688	0.006
Irinotecan pathway	-4.0<[SW/NP]<=-2.0	3.576	0.03

Finally, we investigated the correlation between tissue structure and gene expressions. We previously reported that decreased expression of cell-matrix adhesion-related gene such as talin correlates with the increased that of hepatic function such as Abcc2 on the process of 3-D structure formation (64). Then, we examined the pathway related to cell-matrix adhesions. As a result, Actin Cytoskeleton and Alpha6-Beta4-integrin pathways were both found to be more activated in the ML-cultured tissue than in the NP-cultured one under the assumed criterion of 2.0 < [ML/NP] < 4.0 (Table 3.2). In a similar fashion, Alpha6-Beta4-integrin and Focal Adhesion pathways were both found to be more activated in the SW-cultured tissue than in the NP-cultured one under the assumed criterion of 2.0 < [SW/NP] < 4.0 (Table 3.2). These results mean that the pathway related to cell-matrix adhesion is more activated in the ML- or SW-cultured 2-D cultures than in the NP-cultured 3-D spheroids. Hepatocellular polarity is also one of the primary factors that fulfill the hepatocellular function. Then, we focused on the expression of radixin, the dominant ERM protein. As a result, the expression of radixin in NP-cultured 3-D spheroid was higher than that in ML- and SW-cultured monolayer tissue (Figure 3.4). This result means that the structural polarity of NP-cultured spheroid is better organized than the conventional 2-D culture.

3.4 Discussion

The Agilent Whole Rat Genome Microarray was used to comprehensively examine the hepatocellular functions related to DMPK and compare the expressional profiles obtained from the 3-D NP culture with those from the 2-D SW and ML cultures and the freshly isolated hepatocytes. It was found that the expressions of DMPK-related genes of the 3-D tissue from the NP culture were globally increased more than those of the conventional 2-D tissue from the SW or ML cultures.

HCA showed that NP and SW belonged to the same cluster (Figure 3.2). This result indicates that the NP-cultured 3-D tissue was closer to the freshly isolated hepatocytes than was the ML-cultured 2-D tissue because the SW culture possesses differentiated functions and a polarity similar to native hepatocytes than does the conventional simple monolayer culture as formerly reported (31). Our finding and the indication here are consistent with the previous report that the structure and function of the 3-D spheroids formed by the NP culture was closer to that of the native tissue than that of the

conventional 2-D tissue (64). Next, PCA was carried out. The result showed that the expressional profile of the NP culture was closer to that of the freshly isolated hepatocytes than that of the SW culture (Figure 3.3). These results of the HCA and PCA suggest that the global expressional trend acquired from the NP culture was the closest to the freshly isolated hepatocytes under the three culture conditions conducted in this study. As the result of PCA, the freshly isolated hepatocytes and ML were plotted widely apart, and NP and SW were plotted closely between the two groups in PC1 (63.3%) (Figure 3.3). It is considered that PC1 reflects the difference of the culture condition. In comparison, a contributory factor of PC2, in which case the group of NP/SW and that of the freshly isolated hepatocytes/ML are plotted clearly wide apart (Figure 3.3), remains to be accounted for.

The expression levels of Cyp1a1 and 3a23/3a1 in the NP culture were significantly higher than that of the freshly isolated hepatocytes. The expressions of these two genes were reported to be induced by dexamethasone, a steroidal anti-inflammatory drug (81-83). We considered that the effect was due to dexamethasone that was included in all the culture media used in this study. Abcc genes constitute a family, and their substrates differ according to each gene. In this study, we reported that the expression trend of Abcc genes differed from one gene to another unlike the molecules such as phase-I and phase-II or uptake transporter genes. This finding was likely to be because several phase-I and -II metabolic enzymes produced a wide variety of metabolites due to the differences in culture conditions, and consequently variations of up-regulated or down-regulated excretion transporters were observed. Glucuronic-conjugated bilirubin generated by UGT1A1 was reported to be excreted into bile canaliculi by MRP2 that is a translation product of Abcc2 gene (48,49). The present study showed the gene expressions of Ugt1a1 and Abcc2 were both up-regulated in the 3-D spheroids by the NP culture (Figure 3.4). This result suggests that the up-regulation of the conjugation enzyme occurred in conjunction with that of the excretion transporter in the 3-D NP culture. Therefore, it is proposed that the metabolic process by which hepatocytes configure the 3-D spheroids in the NP culture metabolizes more bilirubin (B) into conjugated bilirubin (B*) than does that by conventional 2-D-cultured hepatocytes (Figure 3.5A, B). Accordingly, more conjugated bilirubin (B*) is speculated to be excreted by MRP2. Enhanced expression of the Abcc2 gene related to biliary excretion in conjunction with Ugt1a1 strongly indicates that the NP-cultured 3-D spheroid has the potential to fulfill a higher hepatocellular metabolic function than does 2-D tissue formed by conventional monolayer culture.

A Hepatocytes of the 3-D spheroid by the NP culture

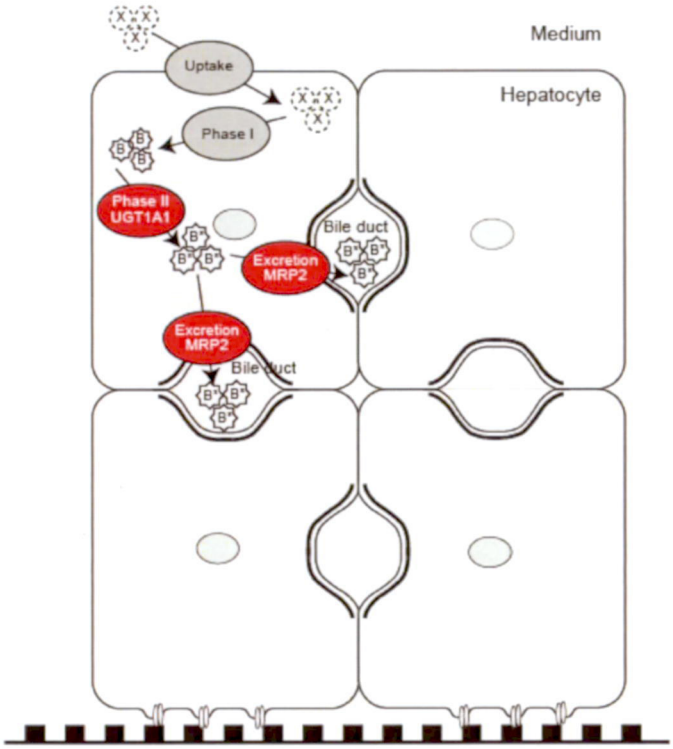

B Hepatocytes by the conventional 2-D monolayer culture

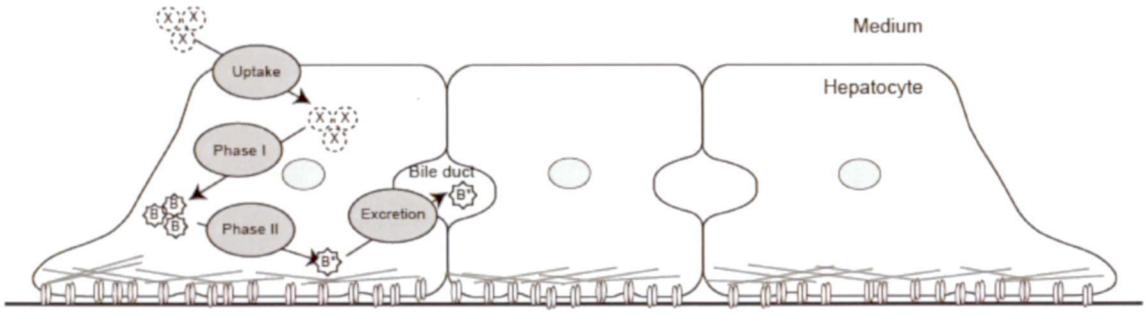

: Substrate to be metabolized

: Bilirubin

: Glucuronic-conjugated bilirubin

: Cell-matrix adhesion molecule (e.g., alpha6 beta4 integrin)

: Radixin

: Actin stress fibers

Figure 3.5 Proposed metabolic process of bilirubin. (A) Hepatocytes of the 3-D spheroids by the NP culture. (B) Hepatocytes of the conventional 2-D monolayer culture. Up-regulated genes are highlighted in red.

In the pathway analyses, the Irinotecan pathway, which is related to the metabolic process in hepatocytes, was activated more in the NP-cultured 3-D spheroid than in the ML- or SW-cultured 2-D tissue (Table 3.2). PCA showed that the gene expression profile obtained from the NP-cultured 3-D spheroids was closer to that from the freshly isolated hepatocytes than that from the SW-cultured 2-D tissue (Figure 3.3). These findings, along with the results of expressional analyses of DMPK-related genes (Figure 3.4), account for the fact that the 3-D spheroids formed by the NP culture possesses higher metabolic ability and function closer to that of the native liver, which also support our hypothesis presented in Figure 3.5. This would be because the 3-D spheroid has more bile canaliculi that were brought by a number of cell-cell adhesion sites of the 3-D spheroid than that of 2-D tissue. Consequently, hepatocytes came to possess a structural polarity and tended to recover the primary functions of the liver by establishing a 3-D structure (12,13,18).

Finally, we discuss the correlation of tissue structure and hepatic function. The pathway related to cell-matrix adhesion was more activated in the ML- or SW-cultured 2-D tissues than in the NP-cultured 3-D spheroids. In other words, the number of the expressed molecules of talin of the NP spheroid is smaller than that of the ML culture. Our previous study in chapter 2 showed the correlation between decreased expression of talin and formation of 3-D structure (64), which was consistent with the result of the present microarray study. This indicates that the growing number of cell-cell adhesion site were formed in the NP-cultured 3-D spheroid under the culture condition using pillar structure, consequently the spheroid exhibited better structure closer to an *in vivo* native environment and functional Abcc2 expression than did the conventional 2-D culture (Figure 3.5). Moreover, the expression of radixin in the NP-cultured 3-D spheroid was higher than that in ML- and SW-cultured monolayer tissue (Figure 3.4). Radixin has been reported to selectively tether MRP2 to the apical canalicular membrane (84), and is required to maintain epithelial polarity and the membrane structure in hepatocytes (85). Radixin protein can act downstream of Rho GTPases such as Rac1, Cdc42 or RhoA, which are key regulators of cell polarity. However, the detailed mechanism that describes the relation between the physical architecture of culture substratum and radixin activation by way of small GTPases has not been elucidated. Although this is the future issue to be solved, our result suggests that higher expression of radixin in the NP-cultured spheroid lead MRP2 to be retained on the membrane. Accordingly, more conjugated bilirubin (B*), as an example, is speculated to have been excreted (Figure 3.5).

3.5 Conclusion

In conclusion, the DNA microarray analysis showed that the expressions of cytochrome P450, UDP-glucuronosyltransferase, and transporter genes in the NP-cultured 3-D spheroids were globally more enhanced than those in the conventional ML- or SW-cultured 2-D tissue. Comprehensive increase in the expression of the DMPK-related genes of the NP-cultured 3-D spheroids is a definitive confirmation that the NP spheroid has specific functions near a native liver. This means NP spheroid culture has a potential to be a culturing technique for predicting DMPK in native environment.

Chapter 4

Respiratory Activity Measurement of Nanopillar-Cultured Spheroids

4.1 Introduction

Existing methodologies for evaluating drug metabolism and toxicity in the development of new drugs are performed using animals. However, testing in animals does not always predict drug metabolism in humans because of species differences, which often results in unacceptable clinical efficacy and poor pharmacokinetics (1,5). An alternative *in vitro* screening system that uses human hepatocytes is required instead of the conventional *in vivo* study (6,86). In order to establish an *in vitro* screening system, we need hepatocytes that possess a polarized structure and differentiated functions close to those of the native liver which was described in chapter 2 and 3. Moreover, when using the cells in a drug screening, we also need to develop a method that can measure the cellular activity and quality noninvasively, which provides a benefit that the viability of the spheroid can be evaluates prior to the nonclinical call-based test and the drug response can be monitored continuously at single spheroid level. To resolve these two issues would surely become a great advantage for establishing an *in vitro* system.

In order to obtain the hepatocytes as above, we have developed a culture device for forming 3-D spheroids, the NP plate (64). 3-D hepatocyte spheroids sustain viability for extended culture periods and enhance high levels of liver specific functions, such as albumin secretion, urea synthesis, or Cyp (cytochrome P450) activity, better than does conventional 2-D monolayer tissue (10-12,14-17,35,64). Accordingly, spheroid culture is an alternative culturing technique for predicting the metabolic process in all native

environments (12,13). We previously reported that the spheroid formation of rat primary hepatocytes was able to be controlled by optimizing the pillar diameter and the pillar pitch (pillar center-to-center distance) of the NP plate and that the spheroids possessed higher viability and polarity (64). The functions of hepatocytes were enhanced by combining spheroid formation and Matrigel overlaying (64).

For measuring the cellular activity, we have been interested in scanning electrochemical microscopy (SECM). SECM is a technology for measuring the local distribution of electroactive species by scanning with the tip of a microelectrode used as a probe with higher spatial resolution (29,87-90). Application to a biological environment at the single-cell level is a promising field for SECM to quantitatively characterize various biological functions under physiological conditions (89-94). Oxygen consumption around the cells measured by SECM directly reflects the cellular respiratory activity. In the previous study, SECM was applied to measure the oxygen consumption of single bovine embryos (28,29). Since the SECM method is ideally noninvasive, the dose effect can be monitored continuously (87,88,95). Furthermore, SECM can measure very low concentration of dissolved oxygen derived from very small amount of cells or single cell (28,29,95). This means the SECM is highly-sensitive measuring device.

When we apply a spheroid for preclinical testing in the drug development process, we need a spheroid with higher cellular activity or viability. For this purpose, we need to obtain knowledge of the relation between the spheroid size and the cellular activity. Based on this background, the objective of this study is to determine the valid diameter of hepatocyte spheroids by establishing a method for measuring cellular activity of single spheroid using the SECM. First, we attempted to make spheroids of various sizes by using hollow and non-hollow NP plates (Figure 4.1). Second, we measured the respiratory activity of each single spheroid of rat primary hepatocytes to elucidate the valid diameter in terms of high respiratory activity and its small variation by using the SECM. We report here that a spheroid of 70 μm in diameter is adequate and that the noninvasive SECM method had the potential to evaluate the activity of a single spheroid.

4.2 Materials and Methods

4.2.1 Preparation of the NP plate

NP plate preparation was described in the previous report (64). One was a new designed hollow NP plate, in which each macroscopic culture well had microscopic hollows with a diameter of 200 μm and a depth of 80 μm and each microscopic hollow had a round nanopillar area with a diameter of 80 μm in the middle (Figure 4.1A); the other was a non-hollow NP plate (Figure 4.1B, same plate used in chapter 2 and 3). The pillar diameter and pillar pitch were commonly 2.0 μm and 4.0 μm (twice the pillar diameter), respectively. Photograph of 24-well culture plate was shown in figure 4.1A and B.

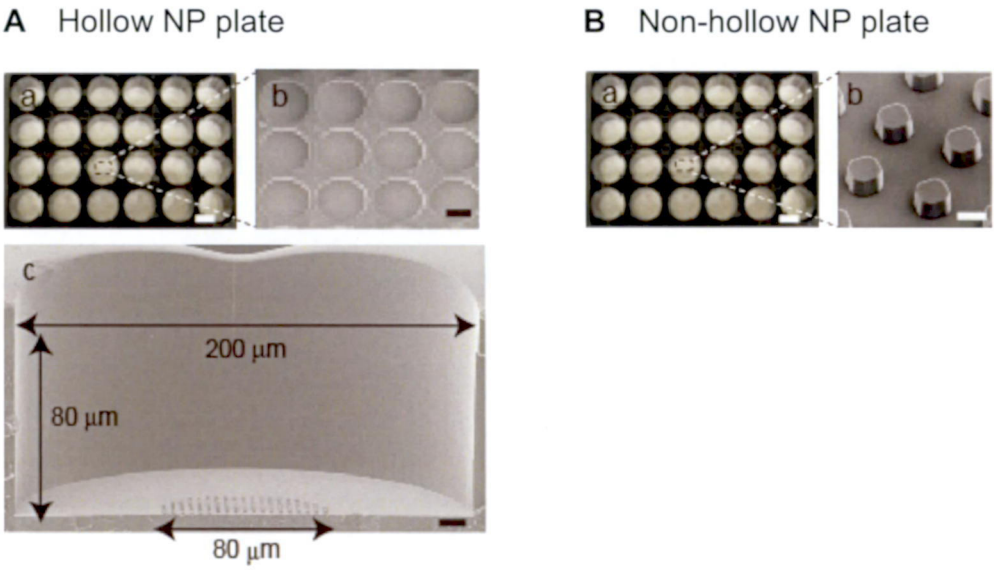

Figure 4.1 (A) Hollow NP plate. (a) Photograph of 24-well NP culture plate. Bar, 1 cm. (b) Scanning electron microscopy (SEM) image of structure of hollows. Bar, 100 μm. (c) SEM image of single hollow with localized pillars. Bar, 10 μm. (B) Non-hollow NP plate; same plate used in chapter 2 and 3. (a) Photograph of 24-well NP culture plate. Bar, 1 cm. (b) SEM image of pillars. Bar, 2 μm.

4.2.2 Hepatocyte culture

Hepatocytes were isolated from 6- to 8-week-old male specific viral-pathogen-free Fischer rats (Charles River Japan Inc., Japan) weighing about 150-250 g by using a modified two-step *in situ* collagenase perfusion method (42) and purified by isodensity Percoll centrifugation (43). The viability of the hepatocytes was determined by trypan blue exclusion, and hepatocytes with over 85% viability were used for culturing.

The hepatocytes were resuspended in William's E medium, which contained 10% fetal bovine serum and was supplemented with 8.6 nM of insulin (Sigma-Aldrich Corp., MO), 255 nM of dexamethasone (Nacalai Tesque, Inc., Japan), 50 ng/ml of epidermal growth factor (Sigma-Aldrich Corp.), and 5 Kallikrein Inactivator Units (KIU)/ml of aprotinin (Wako Pure Chemical Industries, Ltd., Japan). The hepatocytes were seeded at a density of 1×10^5 cells/cm^2 onto prepared NP plates. One was a hollow NP plate; the other was a non-hollow NP plate (Figure 4.1). Both NP plates were precoated with a solution containing 100 ng/ml of type I collagen. The seeded hepatocytes were incubated in a humidified chamber with 5% CO_2 at 37°C. The culture medium was replaced 24 h after seeding with serum-free William's E medium containing the same supplements described above. Afterward, the culture medium was changed daily. Forty-eight hours post-seeding, the medium for the NP plate culture was replaced with a serum-free medium containing 250 μg/ml of Matrigel (BD Bioscience, MA) with the same supplements. Rat primary hepatocytes were cultured for a total of 96 hours.

4.2.3 Statistical analysis

The spheroid diameter was measured from phase-contrast 2-D micrographs. Then, the spheroid volume was calculated by using the spheroid diameter. The F test was used to determine specific differences in spheroid diameter between the hollow and non-hollow NP plates. A p value less than 0.05 was considered significant.

4.2.4 Respiratory activity measurement by SECM (29,95)

Figure 4.2A schematically shows the measuring procedure for a spheroid sample in a cone-shaped microwell. A sample is located at the bottom of a cone-shaped microwell (Figure 4.2B). The height of the center of the sample from the peak of the cone-shaped microwell (h) is determined by the degree of the microwell cone (θ) and the sample

radius (r_s) as:

$$h = (1/\sin\theta)\cdot r_s \qquad [1].$$

The area ($S_{z=z_0}$, see Figure 4.2A. z_0 is a certain point on the z-axis.) of a part cut out by the cone-shaped microwell from the sphere with the radius of $(h+z_0)$ is expressed as:

$$S_{z=z_0} = 2\pi(1-\cos\theta)(h+z_0)^2 \qquad [2]$$

When $\theta = 45°$ and $h = \sqrt{2}\cdot r_s$,

$$S_{z=z_0} = 2\pi(1-1/\sqrt{2})Lp^2 \qquad [3],$$

where Lp is the distance from the top of the cone (point P in Fig. 1D) to the tip of the microelectrode. Lp is expressed as $[(h+z)^2 + r_s^2]^{0.5}$. The oxygen concentration profile according to Lp [C(Lp)] is expressed as:

$$C(Lp) = [C(L_A = h + r_s) - C^*](h + r_s)/[(h+z)^2 + r_s^2]^{0.5} + C^* \qquad [4],$$

where $C(L_A = h + r_s)$ and C^* are the oxygen concentration at sample surface at point A (0, 0, r_s) and in bulk, respectively, in Figure 4.2A. Equation [4] is allowed only when the concentration at the sample surface is uniform and the mass transfer rate through the sample surface is steady. In this study, the oxygen concentration profile of the rat hepatocyte spheroids located in the cone-shaped microwell was measured directly by scanning a Pt-microelectrode (tip radius, 5.0 μm) at 20 μm/s from point B to the point at z=300 μm for three times along the z-axis to monitor the oxygen reduction current at a tip potential of -0.6 V versus Ag/AgCl. The concentration difference (ΔC) between these points is appropriate to use to estimate the oxygen consumption rate, which is given as the slope of the C versus r_s/Lp plots. The ΔC value obtained by the method above is defined as ΔC^{well} in the present study. The flux density f^{well} [mol cm^{-2} s^{-1}] at $S_{z=r_s}$ and the total oxygen consumption rate of the hepatocyte spheroid F^{well} [mol s^{-1}] are given by the following equations.

$$f^{well}_{z=r_s} = D\Delta C^{well}/(h + r_s) \qquad [5]$$

$$F^{well}_{z=r_s} = S_{z=r_s}\cdot f^{well}_{z=r_s} = 2\pi(1-1/\sqrt{2})(h+r_s)D\Delta C^{well} \qquad [6]$$

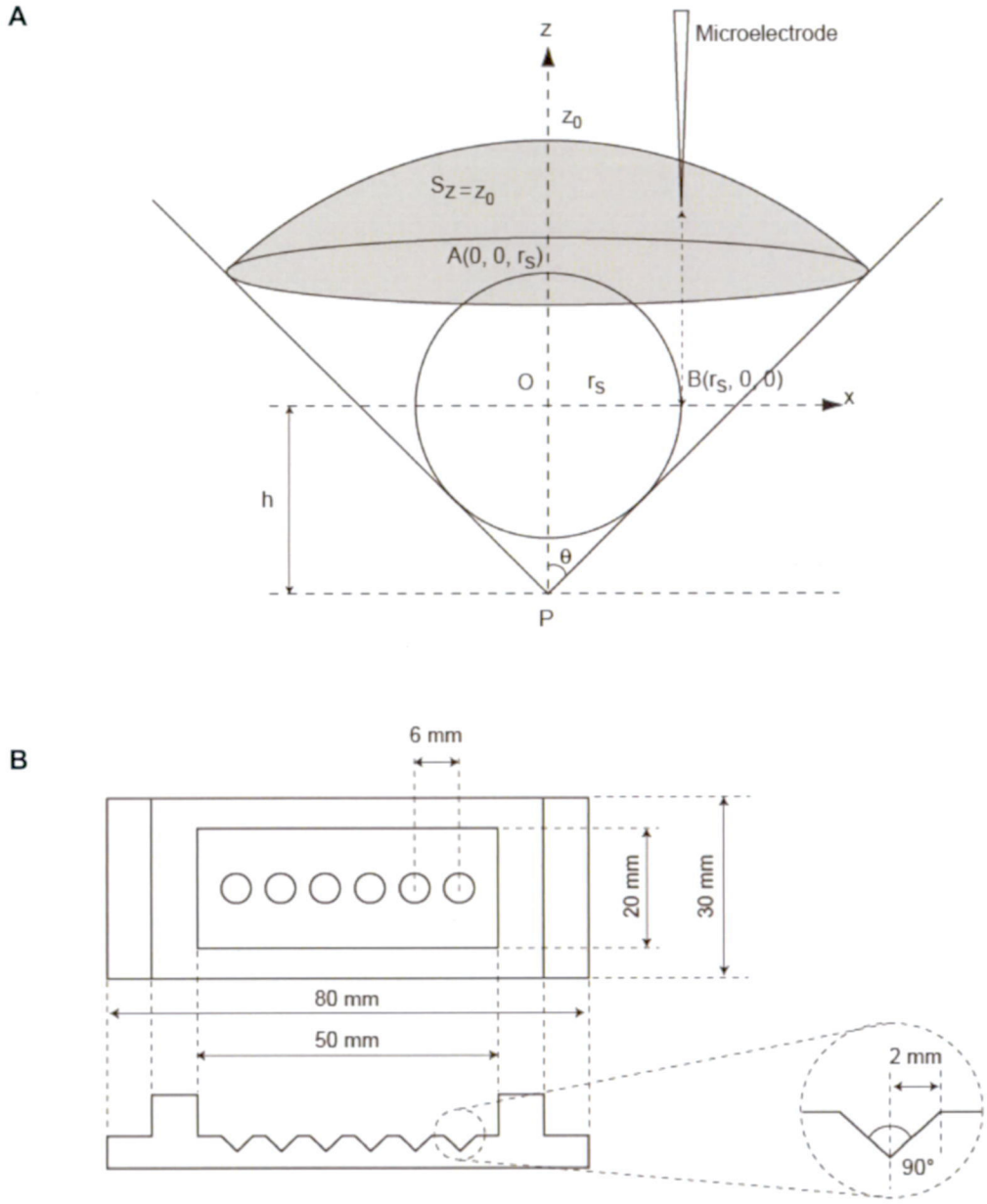

Figure 4.2 (A) Schematic view of SECM measurement for a spheroid sample located in a cone-shaped microwell. Points O and P indicate the center of the spheroid sample and the tip of the cone-shaped microwell, respectively. Point B indicates the starting point for the oxygen concentration profile measurements. r_s, sample radius; q, the degree of the microwell cone; h, the height of the center of the sample from the peak of the cone-microwell; $Sz=r_s$, the spherical section area at $z=z_0$. (B) A plan for measuring the spheroid equipped with six cone-shaped microwells. The bottom angle of the microwell (2θ) is 90°.

4.2.5 Semi-quantitative gene expression analysis

Total RNA was extracted from a single spheroid by using the RNeasy Plus Micro Kit (Qiagen GmbH, Germany). The total RNA was reverse transcribed, and quantitative real-time PCR was conducted in the Thermal Cycler Dice Real Time System (TaKaRa Bio Inc., Japan) with a final reaction mixture of the RT product, TaqMan Gene Expression Assay (Applied Biosystems, CA), Premix Ex Taq™ (TaKaRa Bio Inc.), and DW. Glyceraldehyde 3-phosphate dehydrogenase (Gapdh) was used as an endogenous control and for calibrating the cell number of a single spheroid between various samples. The relative changes in expression were determined toward a control sample.

4.3 Results

4.3.1 Formation of rat hepatocyte spheroids with various diameters by using the hollow and non-hollow NP plates

In order to make various sizes of spheroids, we first tried to seed hepatocytes onto the hollow and non-hollow NP plates (Figure 4.1A, B). The hollow NP plate, a new design plate, was used with the aim of making smaller sized spheroids; the non-hollow NP plate was used with the aim of making larger sized spheroids. After seeding hepatocytes onto each NP plate, phase-contrast micrographs were taken every 24 h. On the hollow NP plate, we observed that individual cells began to aggregate to form spheroids 24 h post-seeding and a single spheroid started to be formed per hollow 48 h post-seeding. During this time, individual cells migrated only inside the hollow and cells did not interact by climbing over the hollow wall. We successfully inhibited aggregations from being bigger spheroids by using the hollow structure. Finally, spheroid formation with a compact morphology that adhered to the substratum was almost totally completed in all the hollows 96 h post-seeding (Figure 4.3A, upper). The mean spheroid diameter and the standard deviation (SD) were 71.3±19.8 μm (Table 4.1). Primary hepatocytes seeded onto the non-hollow NP plate equally started to form spheroids 24 h post-seeding as well as the hollow NP plate. However, each adjacent spheroid was aggregated together time dependently, and bigger-sized spheroids were formed 96 h post-seeding on the non-hollow NP plate accordingly (Figure 4.3A, lower). The mean spheroid diameter and the SD were 113.7±44.8 μm (Table 4.1). As a result, we obtained spheroids with a wider

size of diameters ranging from 32.8 to 166.6 μm by using two kinds of NP plates. Then, we analyzed the variance of spheroid size between spheroids formed by two kinds of NP plate. Statistical analysis by the *F* test revealed that the variance of the spheroids diameter by the hollow NP plate was significantly smaller than that by the non-hollow NP plate (Figure 4.3B*, *F*: 5.08 > critical value: 1.49, $p < 0.01$). Therefore, the hollow NP plate was effective in reducing the variance of the spheroid diameter compared to the non-hollow NP plate.

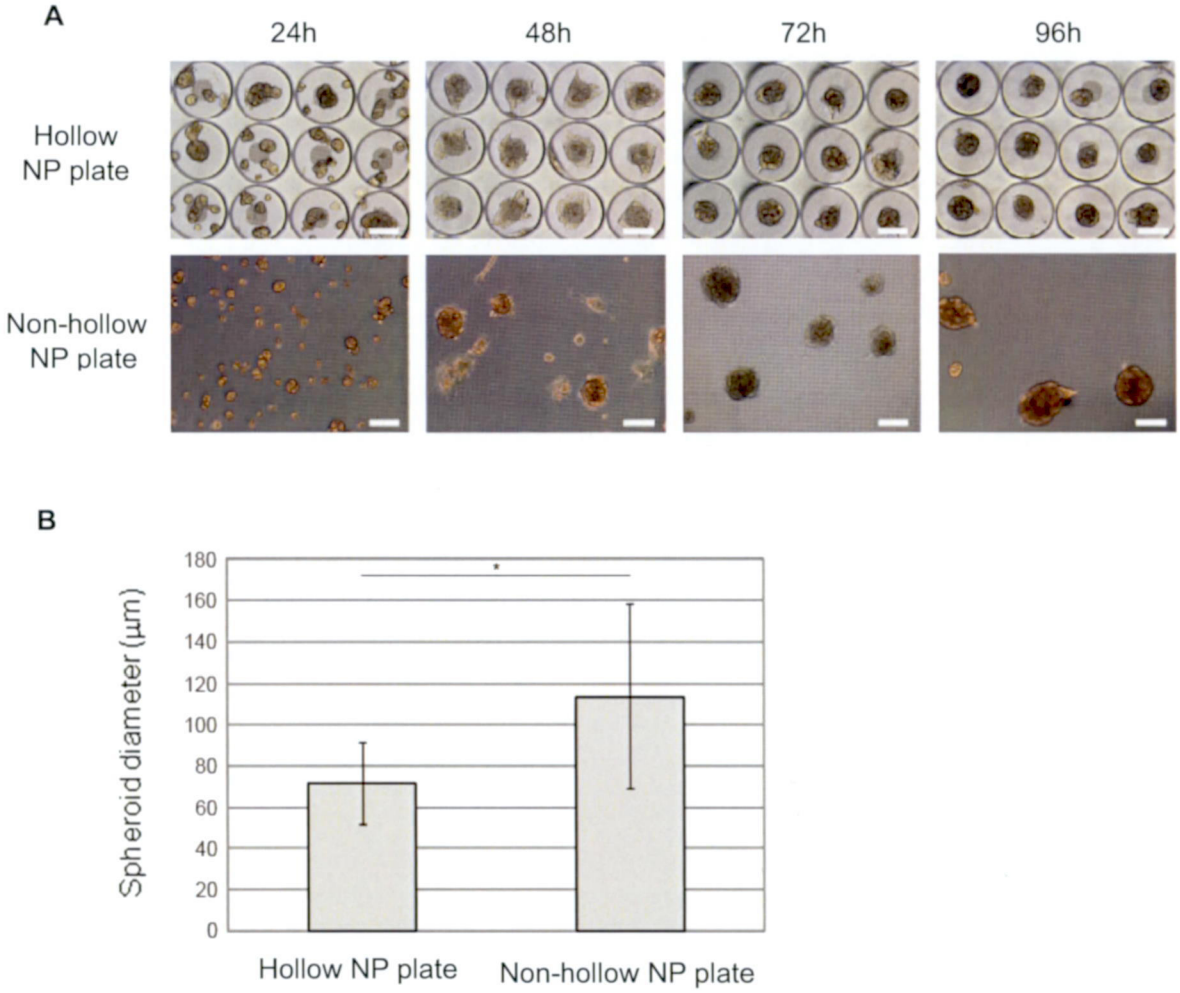

Figure 4.3 (A) Phase-contrast micrographs of hepatocyte spheroids on the NP plates. Hepatocytes were cultured on hollow NP plate (upper) and non-hollow NP plate (lower). The view field of the upper panels is the same as that in Figure 4.1A (b). Phase-contrast micrographs were taken every 24 h. Matrigel was overlaid 48 h post-seeding. Bars, 100 μm. (B) Size distributions of hepatocyte spheroids. Hepatocytes were cultured on the hollow NP plate (left) and non-hollow NP plate (right) coated with a solution containing 100 ng/ml of type I collagen solution. Spheroid diameters were measured 96 h post-seeding. *$p < 0.01$ (*F*-test)

Table 4.1 Mean spheroid diameter±SD.

Hollow NP plate	Non-hollow NP plate
71.3±19.8	113.7±44.8

4.3.2 Measuring respiratory activity by SECM

In order to evaluate the small difference of the cellular activity depending on spheroid sizes by means of oxygen consumption and determine the valid diameter in terms of high respiratory activity and its small variation, we employed the SECM and measured the respiratory activity. A total of 57 spheroids (Table 4.2) were transferred to the cone-shaped microwell, and the oxygen concentration profiles of the spheroids were measured by SECM. As a result, F^{well} increased as the spheroid diameter increased (Table 4.2, Figure 4.4A). While the F^{well} of spheroids smaller than 70 μm in diameter were nearly constant, those of spheroids larger than 70 μm in diameter seemed to vary a great deal in accordance with the spheroid size (Figure 4.4B). Statistical analysis by the *F* test revealed that the variance of the F^{well} of spheroids smaller than 70 μm in diameter was significantly smaller than that of those larger than 70 μm in diameter (Figure 4.4B**, *F*: 25.0 > critical value: 2.98, $p < 0.05$). These results revealed that the diameter of the spheroid with the highest F^{well} and the smallest deviation was around 70 μm.

Next, we examined the respiratory activity of each cell constituting the spheroid between various samples. Although evaluating by using the F^{well} divided by the number of cells of a spheroid is reasonable, it is difficult to measure the cell number. We therefore applied the F^{well} divided by the spheroid volume that was described in this study as the F^{well} per unit volume: $F^{well,\ unit}$ (fmol s^{-1} μm^{-3}). As a result, $F^{well,\ unit}$ decreased as the spheroid size increased: inverse correlation (Table 4.2, Figure 4.4C). The variation of $F^{well,\ unit}$ remarkably increased more among spheroids larger than 70 μm in diameter than it did for the spheroids smaller than 70 μm in diameter (Figure 4.4C). These results revealed that the diameter of the spheroid with the highest $F^{well,\ unit}$ and the smallest deviation was less than 70 μm.

When we apply the spheroids for preclinical testing in the drug development process, those with higher F^{well} and $F^{well,\ unit}$ are required as the indicators of higher cellular activity or viability. From this point of view, our results showed that the size of the

Table 4.2 Total oxygen consumption rate of the hepatocyte spheroid (F^{well}), the F^{well} per unit volume ($F^{well, unit}$), and relative gene expressions of 57 spheroids.

Spheroid	Diameter (≅m)	Volume ($x10^3$ ≅m^3)	F^{well} (mol s^{-1})	$F^{well, unit}$ ($x10^{-5}$ mol s^{-1} ≅m^{-3})	Relative gene expression				
					Hnf4≅	Abcc2	P450-3a23/3a1	Albumin	Ldha
1	43.4	42.9	4.4	10.3	1	1	-	1	-
2	46.2	51.5	10.0	19.3	-	-	-	-	-
3	49.3	62.8	14.1	22.5	-	-	-	-	-
4	56.7	95.4	12.3	12.9	1.40	0.73	1	1.40	-
5	41.6	37.6	7.8	20.7	-	-	-	-	-
6	40.0	33.4	4.6	13.8	-	-	-	-	-
7	32.9	18.6	2.4	12.8	1.25	0.29	-	1.74	-
8	44.6	46.5	6.7	14.5	-	-	-	-	-
9	40.8	35.4	5.3	14.8	-	-	-	-	-
10	119.3	890	27.1	3.0	0.52	1.61	0.17	2.23	-
11	109.1	680	16.3	2.4	0.67	1.18	-	1.90	-
12	121.4	936	22.5	2.4	0.43	0.60	0.64	1.44	-
13	110.5	707	75.4	10.7	0.23	0.62	1.27	1.37	-
14	111.8	732	34.4	4.7	0.18	0.80	0.41	2.08	-
15	153.2	1880	240	12.7	0.14	0.29	1.78	1.16	-
16	103.1	573	93.8	16.4	0.23	0.66	2.53	2.87	-
17	124.6	1010	123	12.2	0.24	0.99	1.91	1.98	-
18	120.8	924	109	11.8	0.12	0.42	1.53	1.71	-
19	124.7	1015	135	13.3	0.13	0.73	0.87	2.44	-
20	67.9	164	20.0	12.2	0.39	0.25	0.24	1.25	-
21	58.7	106	17.2	16.3	0.69	0.47	1.55	3.20	-
22	77.5	244	10.3	4.2	0.80	0.56	2.72	3.92	-
23	54.2	83	11.0	13.1	0.17	0.58	1.40	2.56	-
24	78.2	250	30.6	12.2	-	-	-	-	-
25	83.4	304	41.3	13.6	-	-	-	-	-
26	81.7	285	34.9	12.2	-	-	-	-	-
27	93.6	430	39.7	9.2	-	-	-	-	-
28	74.0	213	25.6	12.1	-	-	-	-	-
29	95.4	455	26.3	5.8	0.30	0.50	1.64	1.86	1
30	76.6	235	38.9	16.5	0.36	-	-	3.24	-
31	82.8	297	25.9	8.7	1.11	-	-	2.49	-
32	77.6	245	16.4	6.7	-	-	-	-	-
33	81.5	284	18.1	6.4	-	-	-	-	-
34	65.6	148	12.7	8.6	0.26	0.43	-	1.11	0.26
35	69.8	178	15.4	8.7	0.94	-	-	2.07	-
36	73.8	211	6.2	2.9	0.17	-	1.14	1.74	0.77
37	75.9	229	12.0	5.2	0.25	-	-	1.72	1.64
38	81.8	286	20.1	7.0	0.56	-	-	1.24	-
39	83.0	300	25.2	8.4	0.27	0.60	1.40	1.78	0.55
40	166.6	2420	109	4.5	0.24	0.90	-	3.20	0.64
41	106.7	637	27.3	4.3	-	-	-	-	-
42	129.4	1140	61.7	5.4	0.16	0.28	-	1.03	0.73
43	86.3	336	29.1	8.7	0.09	0.71	0.96	1.84	0.50
44	87.0	345	19.7	5.7	0.67	-	1.90	1.45	-
45	77.6	244	27.5	11.3	-	-	-	-	-
46	107.4	649	11.4	1.8	0.86	-	-	1.23	-
47	97.5	486	23.6	4.9	0.86	-	-	5.55	1.20
48	99.7	519	19.7	3.8	0.29	-	1.18	0.51	-
49	84.4	315	10.1	3.2	0.51	-	-	2.65	-
50	83.8	308	21.4	7.0	-	-	-	-	-
51	102.7	567	76.4	13.5	0.36	-	2.63	2.08	-
52	97.3	483	22.4	4.6	0.87	1.66	-	3.26	1.98
53	100.5	532	33.0	6.2	0.70	-	-	2.46	-
54	109.6	689	16.1	2.3	-	-	-	2.09	-
55	90.6	389	34.1	8.8	0.41	0.80	-	0.99	0.83
56	148.2	1710	67.9	4.0	-	-	-	-	-
57	104.4	595	22.2	3.7	-	-	-	-	-

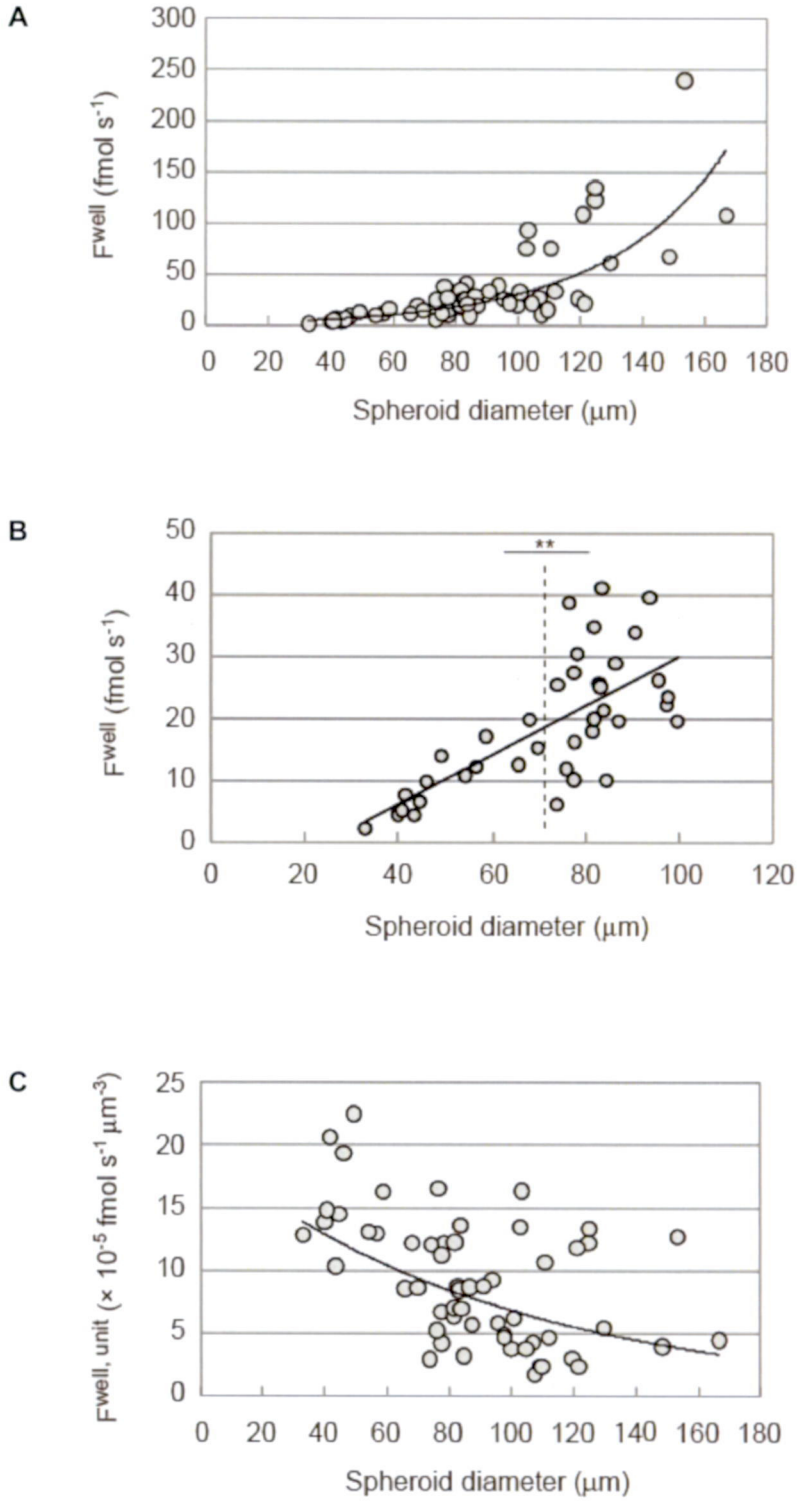

Figure 4.4 (A) Relationship between spheroid diameter and F^{well} (n = 57). (B) Enlargement of (A) up to 100 μm in diameter. Solid line indicates fitted curves. *$p < 0.05$ (*F*-test) (C) Relationship between spheroid diameter $F^{well, unit}$ (n = 57). Solid line indicates fitted curves.

spheroid with a diameter of 70 μm was adequate (Figure 4.4). In the meantime, obtaining more highly reproducible test results for cell-based assays can also be considered critical. Since higher reproducibility requires a small deviation of both F^{well} and $F^{well, unit}$, our results also showed that the spheroids smaller than 70 μm in diameter were optimal (Figure 4.4). Taken together, we determined that spheroids with 70 μm in diameter were valid in terms of high respiratory activity and its small variation by using the SECM measurement system.

4.3.3 Respiratory activity and gene expression analysis

We performed a gene expression analysis by using a real-time PCR to evaluate quantitatively the respiratory action, hepatocellular function or differentiation of a single spheroid on the molecular level.

First, we examined the expressions of Gck (glucokinase), Pdha1 (pyruvate dehydrogenase alpha 1), Cs (citrate synthase), Sdha (succinate dehydrogenase complex, subunit A), which are all aerobic respiration-related genes that follow the glycolysis to the electron transport system by way of the Krebs cycle, and Ldha (lactate dehydrogenase A), as the gene related to anaerobic respiration that utilizes pyruvate metabolized by glycolysis. Among these respiratory metabolism-related genes, only the expression of Ldha was detected (Figure 4.5A). In contrast, other four genes, all of which were aerobic respiration-related genes, were below the detectable limit. The correlation factor between gene expression of Ldha and spheroid size was 0.0017.

Next, we examined the expression of Hnf4α (hepatocyte nuclear factor 4α), Abcc2, Cyp3a23/3a1, albumin, which are all the indicators of hepatocellular differentiation or function. The results showed that the expression of Hnf4α, which is essential for hepatocytes to fulfill many liver functions and is the indicator of well-differentiated hepatocytes (96,97), decreased as the spheroid size increased (Figure 4.5B). The correlation factor of Hnf4α was 0.246. The other three genes related to hepatocellular functions such as Abcc2, Cyp3a23/3a1, and Albumin had much less correlation between the gene expression and the spheroid size. The correlation factors were 0.0302, 0.0002, and 0.0001, respectively (Figure 4.5C, D and E). As a result, the correlation factor of Hnf4α was the highest among four genes. Hnf4α is the transcription factor expressed in the liver and kidneys, and regulates the expression level of the genes related to the several kinds of hepatic metabolism (98-100). It was already revealed that the $F^{well, unit}$ of smaller spheroids was high (Figure 4.4C). We also revealed that the smaller

spheroids had a higher level of Hnf4α expression (Figure 4.5B). Thus, we analyzed the relationship between the $F^{well,\ unit}$ and the Hnf4α expression. As a result, the five spheroids that had relatively higher expression levels of Hnf4α (Figure 4.5B, dashed-line box) showed a higher $F^{well,\ unit}$ (Figure 4.5G, dashed-line box).

4.4 Discussion

We first elucidated that a spheroid with a diameter of 70 μm was adequate in terms of high respiratory activity and its small deviation from the result of SECM measurement (Figure 4.4A, B). We also showed that a hollow structure can be considered to contribute to limiting the cellular interaction over the hollow, resulting in reducing the variance of the spheroid diameter (Table 4.1, Figure 4.3B). The homogeneous spheroid contributes to acquiring highly reproducible measurement results, which will be one of the features of future preclinical application with the NP plate. From this point of view, it is decisively important to keep spheroid size around 70-80 μm with little variation. For this purpose, we did some calculations and concluded that, assuming that the rat single hepatocyte is a sphere of 25 μm diameters, 22-33 cells should be seeded at a density of 1×10^5 cells/cm^2 into 200 μm hollow to make spheroid with 70-80 μm in diameters. This will be a valuable suggestion toward a future *in vitro* preclinical test in the course of new drug screening.

Among the respiration-related genes examined in this study, the genes related to aerobic respiration were under the detectable limit although the reason remains to be identified. The expression level of the respiration-related genes of a spheroid cultured by using the NP plate had already been revealed to be globally low by our previously examined DNA microarray analysis (Chapter 2). While the expressions of aerobic respiration-related genes were not detected, the expression of anaerobic one of Ldha was detected, especially in the spheroids larger than 70 μm in diameter (Figure 4.5A). Furthermore, the result of SECM measurement showed that the respiratory activity (F^{well}) increased as the spheroid diameter increased up to 70 μm (Figure 4.4A, B). These results suggest that each cell constituting the spheroid less than 70 μm acquire energy as ATPs by normal aerobic respiration. Then, we re-analyzed the expression data of Ldha and lined out the fitting curve except for the samples of 129.4 and 166.6 μm in diameters. As a result, the expression of Ldha increased proportionally as the spheroid size increase from 70 up to 100 μm (Figure 4.5F, correlation factor: 0.2428). This result

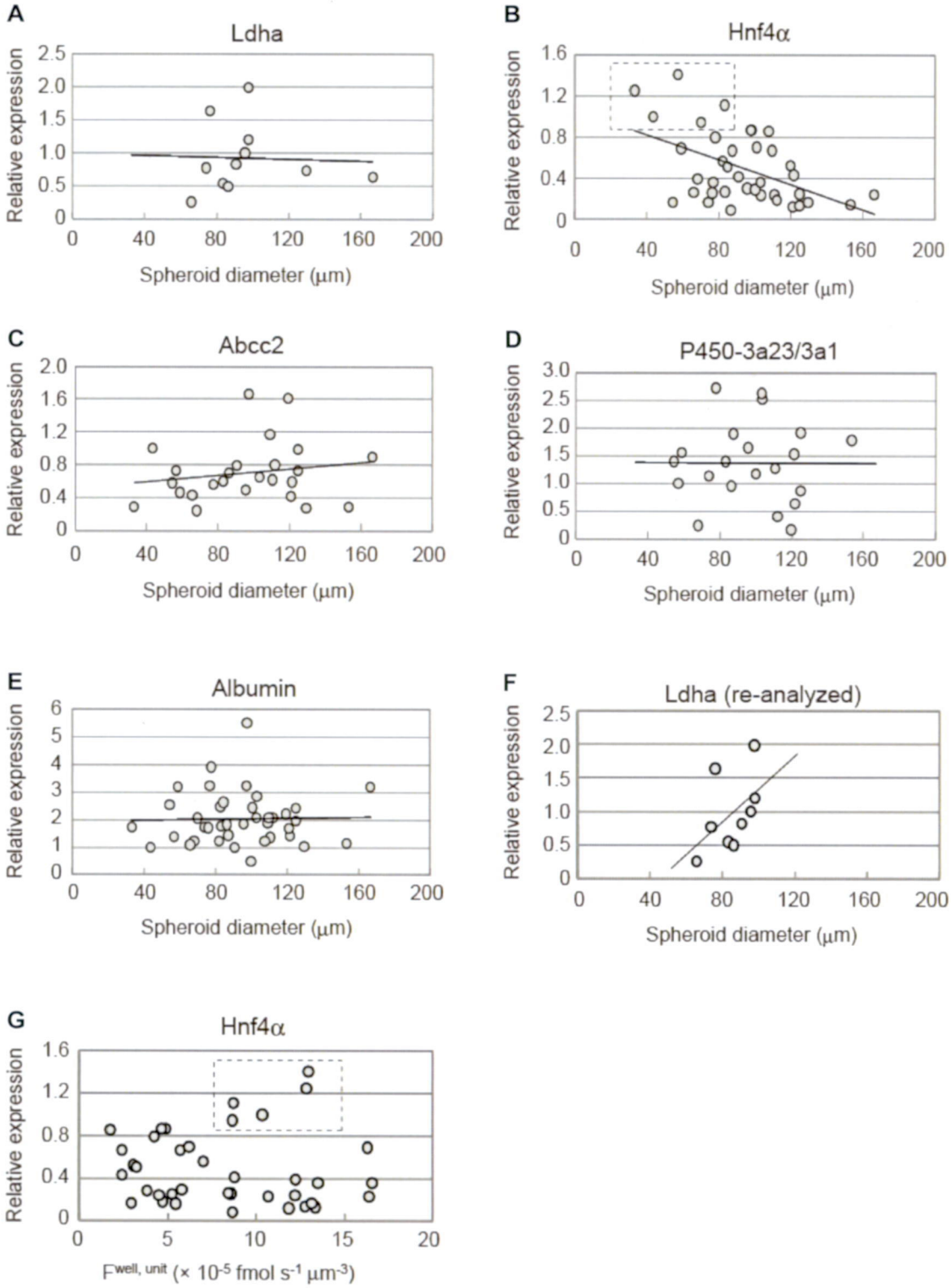

Figure 4.5 Semi-quantitative real-time PCR. Relative amounts of mRNA expression were measured 96 h post-seeding. Expression values of each gene of 57 spheroids were measured (Table 4.2). (A) Ldha (Correlation factor, 0.0017). (B) Hnf4α (0.2465). (C) Abcc2 (0.0302). (D) P450-3a23/3a1 (0.0002). (E) Albumin (0.0001). (F) Re-analyzed Ldha (0.2428). Assays were performed in triplicate in each gene. Solid lines indicate fitted curves. (G) Relationship between $F^{well,\ unit}$ and gene expression of Hnf4α.

indicates that the cells that were located at the region of 35 to 50 μm from the spheroid surface were survived by using energy acquired by the anaerobic respiration. Although it remains to be understood why the expression of Gck that catalyzes the initial step in glycolysis was undetected in this experiment, the detection of the Ldha expression could account for the fact that the metabolized pyruvate of internally-located cells did not enter the Krebs cycle but rather the lactate generation process under the hypoxic condition, which is an anaerobic metabolic pathway. Based on these remarks, we here offer new numerical insight into the way of cellular respiration of 3-D spheroid and more detailed knowledge is added to the previous report that no oxygen limitation will take place in spheroids up to 100 μm in diameter (45,101). In proposed model here, cells of spheroids up to 70 μm in diameter acquire energy by aerobic respiration (Figure 4.6A) and those of spheroids of 70-100 μm in diameter acquire the one by both aerobic and anaerobic respiration (Figure 4.6B). As for the spheroids over 100 μm, it was inferred that some cells located centrally were necrotic (Figure 4.6C) due to the fact that the variance of the F^{well} significantly increased (Figure 4.4A). This might be because cells cannot contact with the culture medium and accordingly were led to a deficiency in oxygen supply. In summary, cells that located in the region of up to 35 μm from spheroid surface are speculated to be under moderate condition in which they can respire aerobically, cells that located in the region of 35 up to 50 μm from spheroid surface are speculated to be under hypoxic condition in which they can respire anaerobically, and cells that located in the region of more than 50 μm are speculated to be necrotic (Figure 4.6).

We specified the Hnf4α that expresses mainly in the liver and kidney, and its translated protein HNF4 binds to a specific DNA element as a homodimer (102). The role of HNF4 is not only essential for maintaining hepatocellular differentiation and fulfilling hepatic functions (96,97) but also for glucose (98), lipid (99), and xenobiotic (100) metabolism. In this study, we showed the correlation between the respiratory activity observed by SECM and Hnf4α expression, which means smaller sized spheroids that have high respiration activity possess high Hnf4α expression (Figure 4.5B). Translated HNF4 protein was indicated to regulate the opposite metabolisms: both gluconeogenesis and glycolysis, which depend on fasted/fed conditions (103). While HNF4 induces gluconeogenesis synergistically with FOXO1, a member of the FOXO family of forkhead transcription factor, in the fasted condition, it also induces glycolysis with FOXO1 inactivation by phosphorylation due to insulin signaling in the fed condition (103). The culture medium that we used in this study includes insulin.

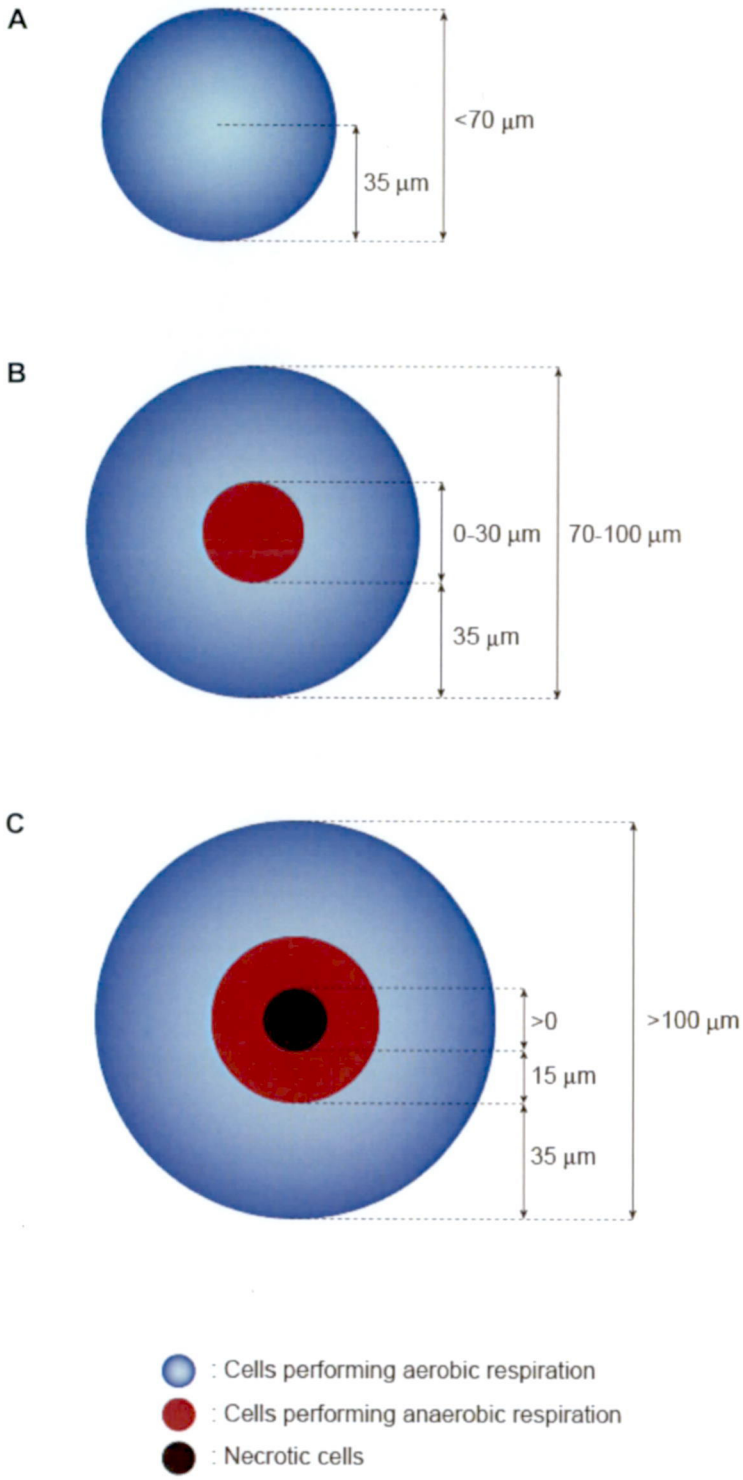

Figure 4.6 Respiration models of three different sized spheroids. (A) Hepatocytes constituting spheroid less than 70 μm in diameter perform aerobic respiration. (B) Hepatocytes constituting spheroid ranging from 70 to 100 μm in diameter perform aerobic and anaerobic respiration. (C) Hepatocytes constituting spheroid larger than 100 mm in diameter perform aerobic, anaerobic respiration and part of which are necrotic.

In addition, almost all of the cells constituting smaller sized spheroids less than 70-80 μm in diameters could be easily considered to access the culture medium because cells must be only at most two or three layers in spheroid of such size, assuming that the rat hepatocyte is a sphere of 25 μm diameters. Taken together, it is argued to be the fed condition for the smaller spheroids. Our result proposes that the smaller sized spheroids utilize the latter metabolic process, although we cannot speculate on the FOXO1 regulation mechanism from the results of this study.

4.5 Conclusion

In conclusion, we constructed the method that can evaluate the small difference of the cellular activity depending on spheroid sizes by means of oxygen consumption by employing the SECM. As we investigate the correlation between spheroid size and respiratory activity, we elucidated that a spheroid with 70 μm in diameter was adequate in terms of high respiratory activity and its small deviation, and that the noninvasive SECM method had the potential to evaluate the activity of a single spheroid. This study made a great advance towards the establishment of a noninvasive assessment system for single spheroids that will be the future cell sources for *in vitro* drug screening and toxicity assays. Noninvasively measuring cellular activity by SECM makes it possible to evaluate the respiratory activity of spheroids prior to a nonclinical test and enables the continued monitoring of the drug response by using single spheroid. These advantages of SECM suggest accordingly the possibility that the validation carried out by the conventional animal experiments will be possible by the *in vitro* monitoring system. Therefore, SECM becomes a powerful tool in this field to satisfying the increasing demand for an *in vitro* system.

Chapter 5

Concluding remarks and future prospect

In the present thesis, we studied novel 3-D culturing method with aiming at utilization in the course of new drug development. The animal study in the preclinical phase may not be sufficient for predicting the fate of drug candidates in human. This means that great number of attrition of pre-clinical and clinical test has been conducted. In order to eliminate this attrition, we need the alternative *in vitro* cell-based assay models that better reflect native environment. The objective of this study is to establish a culturing method for liver-mimicking 3-D spheroid formation using NP plate and a non-invasive cellular activity measuring method by applying the scanning electrochemical microscopy.

First of all, we developed a culture device, NP plate, and challenged 3-D culture for making spheroid using adult rat primary hepatocytes. In the result, spheroids with a compact morphology that were adhesive to the substratum and had an optimal size (50 to 100 μm) were obtained using the plate with a pillar diameter of 2.0 μm. Immunohistochemistry revealed that the spheroids had a structure similar to that of native liver tissue. Transmission electron microscopy showed that the spheroids had bile canaliculi, some with well-developed microvilli. We then revealed the hepatic functions of NP-cultured spheroid was significantly higher than those of hepatocytes cultured using a conventional two-dimensional method by measuring the amount of expressed genes of Abcc2, albumin, and Cyp3a23/3a1 using semi-quantitative real-time PCR. In contrast, the expression level of talin was the highest for the monolayer-cultured hepatocytes. The mechanism of spheroid formation on the NP plate was speculated to

be correlated with less-expression of cell-matrix related protein such as Talin by immunohistochemical and gene expression analysis. The functionality of the bile canaliculi such as biliary excretion was confirmed microscopically with CDFDA in the spheroid. The spheroids obtained exhibited higher structural polarity and functional bile canaliculi compared with hepatocytes cultured using a conventional two-dimensional method. The present study demonstrates that it is practically possible to control the formation of spheroid simply by optimizing the physical property of substrate surface.

Second, we performed genome-wide gene-expression analysis using a DNA microarray. The DNA microarray analysis showed that the expressions of Cyps, Ugts, and transporter genes in the NP-cultured 3-D spheroids were globally more enhanced than those in the conventional ML- or SW-cultured 2-D tissue. Principal component analysis showed that the global gene expression profile in sample from NP culture is closer to that from freshly isolated hepatocytes than that from SW culture. The expressions of almost all Cyp 1 to 3 and Ugt genes of NP-cultured 3-D spheroid were higher than those of ML and SW. The expression of Abcc2 gene whose translation product has a critical role in excretion of metabolized bile acids in hepatocyte to bile canaliculi was three times higher in NP than in ML. From these results, 3-D spheroid formed by the NP culture was suggested to possess higher ability of metabolism and excretion than 2-D tissue by conventional monolayer culture which was consistent with the previous study. Comprehensive increase in the expression of the DMPK-related genes of the NP-cultured 3-D spheroids is a definitive confirmation that the NP spheroid has specific functions near a native liver. This means NP spheroid culture has a potential to be a culturing technique for predicting DMPK in native environment.

Finally, we constructed the method that can evaluate the small difference of the cellular activity noninvasively depending on spheroid sizes by means of oxygen consumption. In order to measure the respiratory activity of NP-cultured hepatocyte spheroid, we applied the SECM. Moreover, in order to obtain homogeneous spheroids for this purpose, nanopillar culture plates of a new design were tested. As we investigate the correlation between spheroid size and respiratory activity, we elucidated that a spheroid with 70 μm in diameter was adequate in terms of high respiratory activity and its small deviation, and that the noninvasive SECM method had the potential to evaluate the activity of a single spheroid. We next performed the gene expression analysis using the real-time PCR method to evaluate the correlation with respiratory activity. In the result, spheroids with higher expression level of Hnf4α that is essential for hepatocyte to fulfill a number of liver functions and is the indicator of well-differentiated

hepatocyte showed relatively higher respiratory activity. We concluded the non-invasive SECM technique could evaluate the cellular activity of a single spheroid constituted by rat primary hepatocytes. Furthermore, we offered new numerical insight into the way of cellular respiration of 3-D spheroid by interpretation of the result that the expression of the gene for Ldha, an indicator of anaerobic respiration, was higher in larger spheroids. In this model, cells that located in the region of up to 35 μm from spheroid surface are speculated to be under moderate condition in which they can respire aerobically, cells that located in the region of 35 up to 50 μm from spheroid surface are speculated to be under hypoxic condition in which they can respire anaerobically, and cells that located in the region of more than 50 μm are speculated to be necrotic. Noninvasive SECM system would contribute the establishment of *in vitro* assay system in the course of drug development.

In conclusion, we showed novel 3-D culturing method that relatively sustained differentiated hepatic function by developing NP plate. In addition, we constructed the method that can evaluate the cellular activity of single spheroid by means of oxygen consumption rate by employing the SECM. In the light of present thesis, we hope these two achievements will pave the way for the establishment of a practical *in vitro* cell-based drug screening and toxicity assay, and also for the well-controlled culture system for cell biology in general.

References

1. Paul, S.M., Mytelka, D.S., Dunwiddie, C.T., Persinger, C.C., Munos, B.H., Lindborg, S.R., and Schacht, A.L.: How to improve R&D productivity: the pharmaceutical industry's grand challenge, *Nat Rev Drug Discov*, **9**, 203-214 (2010).
2. Ashburn, T.T.Thor, K.B.: Drug repositioning: identifying and developing new uses for existing drugs, *Nat Rev Drug Discov*, **3**, 673-683 (2004).
3. Kola, I.Landis, J.: Can the pharmaceutical industry reduce attrition rates?, *Nat Rev Drug Discov*, **3**, 711-715 (2004).
4. Arrowsmith, J.Miller, P.: Trial Watch: Phase II and Phase III attrition rates 2011-2012, *Nat Rev Drug Discov*, **12**, 569 (2013).
5. Roberts, S.A.: Drug metabolism and pharmacokinetics in drug discovery, *Curr Opin Drug Discov Devel*, **6**, 66-80 (2003).
6. Lau, Y.Y., Chen, Y.H., Liu, T.T., Li, C., Cui, X., White, R.E., and Cheng, K.C.: Evaluation of a novel in vitro Caco-2 hepatocyte hybrid system for predicting in vivo oral bioavailability, *Drug Metab Dispos*, **32**, 937-942 (2004).
7. Kunz-Schughart, L.A., Freyer, J.P., Hofstaedter, F., and Ebner, R.: The use of 3-D cultures for high-throughput screening: the multicellular spheroid model, *J Biomol Screen*, **9**, 273-285 (2004).
8. Enat, R., Jefferson, D.M., Ruiz-Opazo, N., Gatmaitan, Z., Leinwand, L.A., and Reid, L.M.: Hepatocyte proliferation in vitro: its dependence on the use of serum-free hormonally defined medium and substrata of extracellular matrix, *Proc Natl Acad Sci U S A*, **81**, 1411-1415 (1984).
9. Moscona, A.: Rotation-mediated histogenetic aggregation of dissociated cells. A quantifiable approach to cell interactions in vitro, *Exp Cell Res*, **22**, 455-475 (1961).

10. Landry, J., Bernier, D., Ouellet, C., Goyette, R., and Marceau, N.: Spheroidal aggregate culture of rat liver cells: histotypic reorganization, biomatrix deposition, and maintenance of functional activities, *J Cell Biol*, **101**, 914-923 (1985).

11. Koide, N., Sakaguchi, K., Koide, Y., Asano, K., Kawaguchi, M., Matsushima, H., Takenami, T., Shinji, T., Mori, M., and Tsuji, T.: Formation of multicellular spheroids composed of adult rat hepatocytes in dishes with positively charged surfaces and under other nonadherent environments, *Exp Cell Res*, **186**, 227-235 (1990).

12. Dvir-Ginzberg, M., Elkayam, T., Aflalo, E.D., Agbaria, R., and Cohen, S.: Ultrastructural and functional investigations of adult hepatocyte spheroids during in vitro cultivation, *Tissue Eng*, **10**, 1806-1817 (2004).

13. Elkayam, T., Amitay-Shaprut, S., Dvir-Ginzberg, M., Harel, T., and Cohen, S.: Enhancing the drug metabolism activities of C3A--a human hepatocyte cell line--by tissue engineering within alginate scaffolds, *Tissue Eng*, **12**, 1357-1368 (2006).

14. Nakazawa, K., Lee, S.W., Fukuda, J., Yang, D.H., and Kunitake, T.: Hepatocyte spheroid formation on a titanium dioxide gel surface and hepatocyte long-term culture, *J Mater Sci Mater Med*, **17**, 359-364 (2006).

15. Meng, Q., Wu, D., Zhang, G., and Qiu, H.: Direct self-assembly of hepatocytes spheroids within hollow fibers in presence of collagen, *Biotechnol Lett*, **28**, 279-284 (2006).

16. Matsushita, T., Ijima, H., Koide, N., and Funatsu, K.: High albumin production by multicellular spheroids of adult rat hepatocytes formed in the pores of polyurethane foam, *Appl Microbiol Biotechnol*, **36**, 324-326 (1991).

17. Abu-Absi, S.F., Friend, J.R., Hansen, L.K., and Hu, W.S.: Structural polarity and functional bile canaliculi in rat hepatocyte spheroids, *Exp Cell Res*, **274**, 56-67 (2002).

18. Hamilton, G.A., Westmorel, C., and George, A.E.: Effects of medium composition on the morphology and function of rat hepatocytes cultured as spheroids and monolayers, *In Vitro Cell Dev Biol Anim*, **37**, 656-667 (2001).

19. Ingber, D.: Integrins as mechanochemical transducers, *Curr Opin Cell Biol*, **3**, 841-848 (1991).

20. Ingber, D.E.: Mechanobiology and diseases of mechanotransduction, *Ann Med*, **35**, 564-577 (2003).

21. Chou, S.Y., Krauss, P.R., and Renstrom, P.J.: Imprint of sub-25 nm vias and trenches in polymers, *Appl. Phys. Lett.*, **67**, 3114-3116 (1995).

22. Kuwabara, K., Ogino, M., Morowaki, S., and Miyauchi, A.: Fluorecence measurements of nanopillars fablicated by high-aspect-ratio nanoprint technology, *Microelectronic Eng.*, **73-74**, 752-756 (2004).

23. Balaban, N.Q., Schwarz, U.S., Riveline, D., Goichberg, P., Tzur, G., Sabanay, I., Mahalu, D., Safran, S., Bershadsky, A., Addadi, L., and Geiger, B.: Force and focal adhesion assembly: a close relationship studied using elastic micropatterned substrates, *Nat Cell Biol*, **3**, 466-472 (2001).

24. Nomura, S., Kojima, H., Ohyabu, Y., Kuwabara, K., Miyauchi, A., and Uemura, T.: Nanopillar sheets as a new type of cell culture dish: detailed study of HeLa cells cultured on nanopillar sheets, *J Artif Organs*, **9**, 90-96 (2006).

25. Liu, H.Y., Fan, F.F., Lin, C.W., and Bard, A.J.: Scanning Electrochemical and Tunneling Ultramicroelectrode Microscope for High-Resolution Examination of Electrode Surfaces in Solution, *J. Am. Chem. SOC*, **108**, 3838-3839 (1986).

26. Bard, A.J., Fan, F.F., Kwak, J., and Lev, O.: Scanning electrochemical microscopy. Introduction and principles, *Anal Chem*, **61**, 132-138 (1989).

27. Lee, C., Kwak, J., and Bard, A.J.: Application of scanning electrochemical microscopy to biological samples, *Proc Natl Acad Sci U S A*, **87**, 1740-1743 (1990).

28. Shiku, H., Shiraishi, T., Ohya, H., Matsue, T., Abe, H., Hoshi, H., and Kobayashi, M.: Oxygen Consumption of Single Bovine Embryos Probed by Scanning Electrochemical Microscopy, *Anal Chem*, **73**, 3751-3758 (2001).

29. Shiku, H., Shiraishi, T., Aoyagi, S., Utsumi, Y., Matsudaira, M., Abe, H., Hoshi, H., Kasai, S., Ohya, H., and Matsue, T.: Respiration activity of single bovine embryos entrapped in a cone-shaped microwell monitored by scanning electrochemical microscopy *Analytica Chimica Acta*, **522**, 51-58 (2004).

30. Bissell, D.M., Stamatoglou, S.C., Nermut, M.V., and Hughes, R.C.: Interactions of rat hepatocytes with type IV collagen, fibronectin and laminin matrices. Distinct matrix-controlled modes of attachment and spreading, *Eur J Cell Biol*, **40**, 72-78 (1986).

31. Caron, J.M.: Induction of albumin gene transcription in hepatocytes by extracellular matrix proteins, *Mol Cell Biol*, **10**, 1239-1243 (1990).

32. Dunn, J.C., Yarmush, M.L., Koebe, H.G., and Tompkins, R.G.: Hepatocyte function and extracellular matrix geometry: long-term culture in a sandwich

configuration, *Faseb J*, **3**, 174-177 (1989).

33. Moghe, P.V., Berthiaume, F., Ezzell, R.M., Toner, M., Tompkins, R.G., and Yarmush, M.L.: Culture matrix configuration and composition in the maintenance of hepatocyte polarity and function, *Biomaterials*, **17**, 373-385 (1996).

34. Liu, X., Chism, J.P., LeCluyse, E.L., Brouwer, K.R., and Brouwer, K.L.: Correlation of biliary excretion in sandwich-cultured rat hepatocytes and in vivo in rats, *Drug Metab Dispos*, **27**, 637-644 (1999).

35. LaRue, K.E., Bradbury, E.M., and Freyer, J.P.: Differential regulation of cyclin-dependent kinase inhibitors in monolayer and spheroid cultures of tumorigenic and nontumorigenic fibroblasts, *Cancer Res*, **58**, 1305-1314 (1998).

36. Otsuka, H., Hirano, A., Nagasaki, Y., Okano, T., Horiike, Y., and Kataoka, K.: Two-dimensional multiarray formation of hepatocyte spheroids on a microfabricated PEG-brush surface, *Chembiochem*, **5**, 850-855 (2004).

37. Satoh, M., Ando, S., Shinoda, T., and Yamazaki, M.: Clearance of bacterial lipopolysaccharides and lipid A by the liver and the role of argininosuccinate synthase, *Innate Immun*, **14**, 51-60 (2008).

38. Fukuda, J., Sakai, Y., and Nakazawa, K.: Novel hepatocyte culture system developed using microfabrication and collagen/polyethylene glycol microcontact printing, *Biomaterials*, **27**, 1061-1070 (2006).

39. Chen, C.S., Mrksich, M., Huang, S., Whitesides, G.M., and Ingber, D.E.: Geometric control of cell life and death, *Science*, **276**, 1425-1428 (1997).

40. Ingber, D.E., Madri, J.A., and Jamieson, J.D.: Role of basal lamina in neoplastic disorganization of tissue architecture, *Proc Natl Acad Sci U S A*, **78**, 3901-3905 (1981).

41. Lehnert, D., Wehrle-Haller, B., David, C., Weiland, U., Ballestrem, C., Imhof, B.A., and Bastmeyer, M.: Cell behaviour on micropatterned substrata: limits of extracellular matrix geometry for spreading and adhesion, *J Cell Sci*, **117**, 41-52 (2004).

42. Seglen, P.O.: Preparation of isolated rat liver cells, *Methods Cell Biol*, **13**, 29-83 (1976).

43. Kreamer, B.L., Staecker, J.L., Sawada, N., Sattler, G.L., Hsia, M.T., and Pitot, H.C.: Use of a low-speed, iso-density percoll centrifugation method to increase the viability of isolated rat hepatocyte preparations, *In Vitro Cell Dev Biol*, **22**, 201-211 (1986).

44. Yalcin, A.: Quantification of thioredoxin mRNA expression in the rat hippocampus by real-time PCR following oxidative stress, *Acta Biochim Pol*, **51**, 1059-1065 (2004).

45. Glicklis, R., Merchuk, J.C., and Cohen, S.: Modeling mass transfer in hepatocyte spheroids via cell viability, spheroid size, and hepatocellular functions, *Biotechnol Bioeng*, **86**, 672-680 (2004).

46. Chu, Y.S., Thomas, W.A., Eder, O., Pincet, F., Perez, E., Thiery, J.P., and Dufour, S.: Force measurements in E-cadherin-mediated cell doublets reveal rapid adhesion strengthened by actin cytoskeleton remodeling through Rac and Cdc42, *J Cell Biol*, **167**, 1183-1194 (2004).

47. Bissell, D.M., Arenson, D.M., Maher, J.J., and Roll, F.J.: Support of cultured hepatocytes by a laminin-rich gel. Evidence for a functionally significant subendothelial matrix in normal rat liver, *J Clin Invest*, **79**, 801-812 (1987).

48. Suzuki, H.Sugiyama, Y.: Single nucleotide polymorphisms in multidrug resistance associated protein 2 (MRP2/ABCC2): its impact on drug disposition, *Adv Drug Deliv Rev*, **54**, 1311-1331 (2002).

49. Nies, A.T.Keppler, D.: The apical conjugate efflux pump ABCC2 (MRP2), *Pflugers Arch*, **453**, 643-659 (2007).

50. Zamek-Gliszczynski, M.J., Xiong, H., Patel, N.J., Turncliff, R.Z., Pollack, G.M., and Brouwer, K.L.: Pharmacokinetics of 5 (and 6)-carboxy-2',7'-dichlorofluorescein and its diacetate promoiety in the liver, *J Pharmacol Exp Ther*, **304**, 801-809 (2003).

51. Burridge, K.Connell, L.: A new protein of adhesion plaques and ruffling membranes, *J Cell Biol*, **97**, 359-367 (1983).

52. Dohda, T., Nakamura, Y., Kamihira, M., and Iijima, S.: Functional role of RhoA in growth regulation of primary hepatocytes, *J Biochem*, **135**, 631-637 (2004).

53. Zhang, P., Tian, X., Chandra, P., and Brouwer, K.L.: Role of glycosylation in trafficking of Mrp2 in sandwich-cultured rat hepatocytes, *Mol Pharmacol*, **67**, 1334-1341 (2005).

54. Schmucker, D.L., Ohta, M., Kanai, S., Sato, Y., and Kitani, K.: Hepatic injury induced by bile salts: correlation between biochemical and morphological events, *Hepatology*, **12**, 1216-1221 (1990).

55. Nelson, D.R., Koymans, L., Kamataki, T., Stegeman, J.J., Feyereisen, R., Waxman, D.J., Waterman, M.R., Gotoh, O., Coon, M.J., Estabrook, R.W.,

Gunsalus, I.C., and Nebert, D.W.: P450 superfamily: update on new sequences, gene mapping, accession numbers and nomenclature, *Pharmacogenetics*, **6**, 1-42 (1996).

56. Baldwin, S.J., Bramhall, J.L., Ashby, C.A., Yue, L., Murdock, P.R., Hood, S.R., Ayrton, A.D., and Clarke, S.E.: Cytochrome P450 gene induction in rats ex vivo assessed by quantitative real-time reverse transcriptase-polymerase chain reaction (TaqMan), *Drug Metab Dispos*, **34**, 1063-1069 (2006).

57. Hu, J.M., Camper, S.A., Tilghman, S.M., Miller, T., Georgoff, I., Serra, R., and Isom, H.C.: Functional analyses of albumin expression in a series of hepatocyte cell lines and in primary hepatocytes, *Cell Growth Differ*, **3**, 577-588 (1992).

58. Humphries, J.D., Wang, P., Streuli, C., Geiger, B., Humphries, M.J., and Ballestrem, C.: Vinculin controls focal adhesion formation by direct interactions with talin and actin, *J Cell Biol*, **179**, 1043-1057 (2007).

59. Takei, R., Suzuki, D., Hoshiba, T., Nagaoka, M., Seo, S.J., Cho, C.S., and Akaike, T.: Role of E-cadherin molecules in spheroid formation of hepatocytes adhered on galactose-carrying polymer as an artificial asialoglycoprotein model, *Biotechnol Lett*, **27**, 1149-1156 (2005).

60. Minami, K., Okano, H., Okumachi, A., and Seino, S.: Role of cadherin-mediated cell-cell adhesion in pancreatic exocrine-to-endocrine transdifferentiation, *J Biol Chem*, **283**, 13753-13761 (2008).

61. Smith, N.F., Raynaud, F.I., and Workman, P.: The application of cassette dosing for pharmacokinetic screening in small-molecule cancer drug discovery, *Mol Cancer Ther*, **6**, 428-440 (2007).

62. Bissell, D.M.Guzelian, P.S.: Phenotypic stability of adult rat hepatocytes in primary monolayer culture, *Ann N Y Acad Sci*, **349**, 85-98 (1980).

63. Hamamoto, R., Yamada, K., Kamihira, M., and Iijima, S.: Differentiation and proliferation of primary rat hepatocytes cultured as spheroids, *J Biochem*, **124**, 972-979 (1998).

64. Takahashi, R., Sonoda, H., Tabata, Y., and Hisada, A.: Formation of hepatocyte spheroids with structural polarity and functional bile canaliculi using nanopillar sheets, *Tissue Eng Part A*, **16**, 1983-1995 (2010).

65. Tong, J.Z., Sarrazin, S., Cassio, D., Gauthier, F., and Alvarez, F.: Application of spheroid culture to human hepatocytes and maintenance of their differentiation, *Biol Cell*, **81**, 77-81 (1994).

66. Fukuda, J.Nakazawa, K.: Orderly arrangement of hepatocyte spheroids on a

microfabricated chip, *Tissue Eng*, **11**, 1254-1262 (2005).

67. Tanaka, H., Shimazawa, M., Kimura, M., Takata, M., Tsuruma, K., Yamada, M., Takahashi, H., Hozumi, I., Niwa, J., Iguchi, Y., Nikawa, T., Sobue, G., Inuzuka, T., and Hara, H.: The potential of GPNMB as novel neuroprotective factor in amyotrophic lateral sclerosis, *Sci Rep*, **2**, 573 (2012).

68. Mathijs, K., Brauers, K.J., Jennen, D.G., Lizarraga, D., Kleinjans, J.C., and van Delft, J.H.: Gene expression profiling in primary mouse hepatocytes discriminates true from false-positive genotoxic compounds, *Mutagenesis*, **25**, 561-568 (2010).

69. de Haan, J.R., Wehrens, R., Bauerschmidt, S., Piek, E., van Schaik, R.C., and Buydens, L.M.: Interpretation of ANOVA models for microarray data using PCA, *Bioinformatics*, **23**, 184-190 (2007).

70. Tukey, R.H.Strassburg, C.P.: Human UDP-glucuronosyltransferases: metabolism, expression, and disease, *Annu Rev Pharmacol Toxicol*, **40**, 581-616 (2000).

71. Dawson, P.A., Lan, T., and Rao, A.: Bile acid transporters, *J Lipid Res*, **50**, 2340-2357 (2009).

72. Williams, J.A., Hyland, R., Jones, B.C., Smith, D.A., Hurst, S., Goosen, T.C., Peterkin, V., Koup, J.R., and Ball, S.E.: Drug-drug interactions for UDP-glucuronosyltransferase substrates: a pharmacokinetic explanation for typically observed low exposure (AUCi/AUC) ratios, *Drug Metab Dispos*, **32**, 1201-1208 (2004).

73. Nakakariya, M., Ono, M., Amano, N., Moriwaki, T., Maeda, K., and Sugiyama, Y.: In vivo biliary clearance should be predicted by intrinsic biliary clearance in sandwich-cultured hepatocytes, *Drug Metab Dispos*, **40**, 206-209 (2012).

74. Watanabe, T., Kusuhara, H., Maeda, K., Kanamaru, H., Saito, Y., Hu, Z., and Sugiyama, Y.: Investigation of the rate-determining process in the hepatic elimination of HMG-CoA reductase inhibitors in rats and humans, *Drug Metab Dispos*, **38**, 215-222 (2010).

75. Jigorel, E., Le Vee, M., Boursier-Neyret, C., Bertrand, M., and Fardel, O.: Functional expression of sinusoidal drug transporters in primary human and rat hepatocytes, *Drug Metab Dispos*, **33**, 1418-1422 (2005).

76. Leier, I., Jedlitschky, G., Buchholz, U., Cole, S.P., Deeley, R.G., and Keppler, D.: The MRP gene encodes an ATP-dependent export pump for leukotriene C4 and structurally related conjugates, *J Biol Chem*, **269**, 27807-27810 (1994).

77. Muller, M., Meijer, C., Zaman, G.J., Borst, P., Scheper, R.J., Mulder, N.H., de Vries, E.G., and Jansen, P.L.: Overexpression of the gene encoding the multidrug resistance-associated protein results in increased ATP-dependent glutathione S-conjugate transport, *Proc Natl Acad Sci U S A*, **91**, 13033-13037 (1994).

78. Jedlitschky, G., Burchell, B., and Keppler, D.: The multidrug resistance protein 5 functions as an ATP-dependent export pump for cyclic nucleotides, *J Biol Chem*, **275**, 30069-30074 (2000).

79. Nemesanszky, E.Lott, J.A.: Gamma-glutamyltransferase and its isoenzymes: progress and problems, *Clin Chem*, **31**, 797-803 (1985).

80. Clark, S.P., Davis, M.A., Ryan, T.P., Searfoss, G.H., and Hooser, S.B.: Hepatic gene expression changes in mice associated with prolonged sublethal microcystin exposure, *Toxicol Pathol*, **35**, 594-605 (2007).

81. Backman, J.T., Olkkola, K.T., and Neuvonen, P.J.: Rifampin drastically reduces plasma concentrations and effects of oral midazolam, *Clin Pharmacol Ther*, **59**, 7-13 (1996).

82. Pichard, L., Fabre, I., Daujat, M., Domergue, J., Joyeux, H., and Maurel, P.: Effect of corticosteroids on the expression of cytochromes P450 and on cyclosporin A oxidase activity in primary cultures of human hepatocytes, *Mol Pharmacol*, **41**, 1047-1055 (1992).

83. Lai, K.P., Wong, M.H., and Wong, C.K.: Modulation of AhR-mediated CYP1A1 mRNA and EROD activities by 17beta-estradiol and dexamethasone in TCDD-induced H411E cells, *Toxicol Sci*, **78**, 41-49 (2004).

84. Kikuchi, S., Hata, M., Fukumoto, K., Yamane, Y., Matsui, T., Tamura, A., Yonemura, S., Yamagishi, H., Keppler, D., Tsukita, S., and Tsukita, S.: Radixin deficiency causes conjugated hyperbilirubinemia with loss of Mrp2 from bile canalicular membranes, *Nat Genet*, **31**, 320-325 (2002).

85. Wang, W., Soroka, C.J., Mennone, A., Rahner, C., Harry, K., Pypaert, M., and Boyer, J.L.: Radixin is required to maintain apical canalicular membrane structure and function in rat hepatocytes, *Gastroenterology*, **131**, 878-884 (2006).

86. Lin, J.H.Lu, A.Y.: Role of pharmacokinetics and metabolism in drug discovery and development, *Pharmacol Rev*, **49**, 403-449 (1997).

87. Royce, C.E.Christine, M.P.: Scanning electrochemical microscopy, *Anal Chem*, **61**, 1099A-1104A (1989).

88. Bard, A.J., Fan, F.F., Kwak, J., and Lev, O.: Scanning electrochemical

microscopy. Introduction and principles, *Anal Chem*, **61**, 132-138 (1989).

89. *Scanning Electrochemical Microscope* Marcel-Dekker Inc., New York (2001).

90. Liu, B.Mirkin, M.V.: Charge transfer reactions at the liquid/liquid interface, *Anal Chem*, **73**, 670A-677A (2001).

91. Yasukawa, T., Kaya, T., and Matsue, T.: Characterization and Imaging of Single Cells with Scanning Electrochemical Microscopy, *Electroanalysis*, **12**, 653-659 (2000).

92. Yasukawa, T., Uchida, I., and Matsue, T.: Permeation of redox species through a cell membrane of a single, living algal protoplast studied by microamperometry, *Biochim Biophys Acta*, **1369**, 152-158 (1998).

93. Liu, B., Rotenberg, S.A., and Mirkin, M.V.: Scanning electrochemical microscopy of living cells: different redox activities of nonmetastatic and metastatic human breast cells, *Proc Natl Acad Sci U S A*, **97**, 9855-9860 (2000).

94. Barker, A.L., Gonsalves, M., Macpherson, J.V., Slevin, C.J., and Unwin, P.R.: Scanning electrochemical microscopy: beyond the solid/liquid interface *Analytica Chimica Acta*, **385**, 225-240 (1999).

95. Torisawa, Y.S., Kaya, T., Takii, Y., Oyamatsu, D., Nishizawa, M., and Matsue, T.: Scanning electrochemical microscopy-based drug sensitivity test for a cell culture integrated in silicon microstructures, *Anal Chem*, **75**, 2154-2158 (2003).

96. Luebke-Wheeler, J., Zhang, K., Battle, M., Si-Tayeb, K., Garrison, W., Chhinder, S., Li, J., Kaufman, R.J., and Duncan, S.A.: Hepatocyte nuclear factor 4alpha is implicated in endoplasmic reticulum stress-induced acute phase response by regulating expression of cyclic adenosine monophosphate responsive element binding protein H, *Hepatology*, **48**, 1242-1250 (2008).

97. Li, J., Ning, G., and Duncan, S.A.: Mammalian hepatocyte differentiation requires the transcription factor HNF-4alpha, *Genes Dev*, **14**, 464-474 (2000).

98. Stoffel, M.Duncan, S.A.: The maturity-onset diabetes of the young (MODY1) transcription factor HNF4alpha regulates expression of genes required for glucose transport and metabolism, *Proc Natl Acad Sci U S A*, **94**, 13209-13214 (1997).

99. Hayhurst, G.P., Lee, Y.H., Lambert, G., Ward, J.M., and Gonzalez, F.J.: Hepatocyte nuclear factor 4alpha (nuclear receptor 2A1) is essential for maintenance of hepatic gene expression and lipid homeostasis, *Mol Cell Biol*, **21**, 1393-1403 (2001).

100. Tirona, R.G., Lee, W., Leake, B.F., Lan, L.B., Cline, C.B., Lamba, V., Parviz,

F., Duncan, S.A., Inoue, Y., Gonzalez, F.J., Schuetz, E.G., and Kim, R.B.: The orphan nuclear receptor HNF4alpha determines PXR- and CAR-mediated xenobiotic induction of CYP3A4, *Nat Med*, **9**, 220-224 (2003).

101. Ijima, H., Matsushita, T., Nakazawa, K., Fujii, Y., and Funatsu, K.: Hepatocyte Spheroids in Polyurethane Foams: Functional Analysis and Application for a Hybrid Artificial Liver, *Tissue Engineering*, **4**, 213-226 (1998).

102. Sladek, F.M., Zhong, W.M., Lai, E., and Darnell, J.E., Jr.: Liver-enriched transcription factor HNF-4 is a novel member of the steroid hormone receptor superfamily, *Genes Dev*, **4**, 2353-2365 (1990).

103. Hirota, K., Sakamaki, J., Ishida, J., Shimamoto, Y., Nishihara, S., Kodama, N., Ohta, K., Yamamoto, M., Tanimoto, K., and Fukamizu, A.: A combination of HNF-4 and Foxo1 is required for reciprocal transcriptional regulation of glucokinase and glucose-6-phosphatase genes in response to fasting and feeding, *J Biol Chem*, **283**, 32432-32441 (2008).

Acknowledgements

First and foremost, I would like to express my deepest appreciation to Ms. Akiko Hisada of Hitachi, Ltd., Central Research Laboratory, for her continuous guidance, invaluable discussions, and considerable encouragement. I would also like to acknowledge Mr. Hiroshi Sonoda of Hitachi, Ltd., Social Innovation Business Project Division, for his technical support and helpful discussions.

I am pleased to acknowledge Professor Yasuhiko Tabata of Kyoto University for helpful suggestions and discussions about Nanopillar Cull Culture Device. I would also like to acknowledge Professor Tomokazu Matsue, Associate Professor Hitoshi Shiku, Ms. Yoshiko Horiguchi and Mr. Yuanshu Zhou, for their helpful suggestion and technical advice about scanning electrochemical microscopy.

I am deeply grateful to my colleagues at Hitachi, Ltd. I would like to acknowledge Mr. Shigeharu Nishiuchi, Mr. Masabumi Nemoto, Mr. Taku Saito, and Dr. Akihiro Miyauchi, for giving me the opportunity to start this research and continuous support. Moreover, I would like to acknowledge Mr. Kazutoshi Kan, Dr. Shizu Takeda, for giving me invaluable advice and complete support during this research. I thank Dr. Ryota Nakajima, Dr. Naoshi Itabashi and Mr. Jiro Yamamoto, for their kind support, helpful suggestions, and technical advice. I also thank Dr. Hiroki Sato, Dr. Takushige Katsura, Dr. Yusuke Seki, and Dr. Hirokazu Atsumori for their kind support while I was writing this thesis. I thank Dr. Toyoshige Kobayashi, Dr. Takayuki Nozaki, Dr. Erino Matsumoto, Dr. Guangbin Zhou, Dr. Naoko Senda, and Ms. Yumiko Igarashi, for their general support. I am also grateful to Mr. Kenko Uchida, Dr. Kazuo Saito, Dr. Minoru Sakairi, Dr. Toru Hisamitsu, Dr. Haruo Takeda, and Dr. Nobuyuki Osakabe, for organizing this research and their considerable encouragement. I further thank Ms. Kimie Mase, Ms. Yumi Mizunuma, Ms. Chiemi Hoshina, for their technical support.

I would like to express my sincere gratitude to members of Rikkyo University for reviewing this thesis and continued encouragement.

Last but not least, I would like to thank my family. I thank Kaori, my wife, for her understanding, continuous encouragement, and invaluable help. I especially thank Akinaga and Tadahiro, our sons.